# Improving Traffic Safety through Better Snow Fences: Image-Based Methods to Measure Trapped Snow Volume and the Snow Relocation Coefficient

**Final Report
August 2017**

MIDWEST
TRANSPORTATION
CENTER **MTC**

IOWA STATE UNIVERSITY
Institute for Transportation

Technical Report Documentation Page

1. Report No.	2. Government Accession No.	3. Recipient's Catalog No.	
4. Title and Subtitle		**5. Report Date**	
Improving Traffic Safety through Better Snow Fences: Image-Based Methods to Measure Trapped Snow Volume and the Snow Relocation Coefficient		August 2017	
		6. Performing Organization Code	
7. Author(s)		**8. Performing Organization Report No.**	
Heng-Wei Tsai, Marian Muste, George Constantinescu, and Chris Rehmann			
9. Performing Organization Name and Address		**10. Work Unit No. (TRAIS)**	
IIHR – Hydroscience and Engineering University of Iowa 100 C. Maxwell Stanley Hydraulics Laboratory Iowa City, IA 52242-1585	Department of Civil, Construction, and Environmental Engineering Iowa State University 813 Bissell Road Ames, IA 50011-1066		
		11. Contract or Grant No.	
		Part of DTRT13-G-UTC37	
12. Sponsoring Organization Name and Address		**13. Type of Report and Period Covered**	
Midwest Transportation Center Institute for Transportation 2711 S. Loop Drive, Suite 4700 Ames, IA 50010-8664 U.S. Department of Transportation Office of the Assistant Secretary for Research and Technology 1200 New Jersey Avenue, SE Washington, DC 20590	IIHR – Hydroscience and Engineering University of Iowa 100 C. Maxwell Stanley Hydraulics Laboratory Iowa City, IA 52242-1585	Final Report	
		14. Sponsoring Agency Code	

15. Supplementary Notes

Visit www.intrans.iastate.edu for color pdfs of this and other research reports.

16. Abstract

Blowing and drifting snow is a major concern in terms of safety, transportation efficiency, and road maintenance and repair. One common way to mitigate snow drift on roadways is to install structural or living snow fences, but the design of snow fences relies on empirical relationships—in particular, for estimating the snow relocation coefficient (SRC)—that do not necessarily apply to the US Midwest. Therefore, the use of these relationships at sites with different meteorological conditions is problematic.

Moreover, the SRC is a function of the site terrain and ground surface characteristics. Estimating the SRC requires quantification of the snowfall and snow drift fluxes at the site where the snow fence is to be installed. Without being able to estimate the local value of the SRC, an efficient design for the snow fence is practically impossible.

The research described in this report addressed three critical aspects of snow fence design: estimation of the snowfall and snow drift fluxes and mapping of the snow volumes accumulated at the snow fence after its deployment at the site. This report describes the protocols developed for documentation of snowfall, snow drift, and snow deposit mapping as well as a set of laboratory and field experiments performed to validate these new techniques and protocols. This report also describes the actual implementation of the developed protocols as applied to event-based monitoring at various locations exposed to snow drift.

A set of non-intrusive measurement techniques were innovatively assembled to document snowfall and snow drifting over roads protected by snow fences. The present research proposes the use of particle tracking velocimetry (PTV) and large-scale particle image velocimetry (LSPIV) coupled with three-dimensional (3D) photogrammetry to quantify, through direct measurements, the snowfall and snow drift fluxes. The report proposes strategies for providing adequate illumination, setting camera parameters, and processing the raw information with commercially available software to obtain accurate and robust estimations of the main variables of interest.

Snow drift measurements were demonstrated in laboratory conditions with modeled snow particles. Additionally, the present research refines previously proposed methods to determine the volume of snow retained by the fence. The approach is based on close-range 3D photogrammetry and provides a general methodology for non-intrusive remote estimation of the snow deposit volume using automated data acquisition protocols.

17. Key Words		**18. Distribution Statement**	
3D photogrammetry—particle tracking velocimetry—snow drifting—snowfall—snow fence design—snow relocation coefficient		No restrictions.	
19. Security Classification (of this report)	**20. Security Classification (of this page)**	**21. No. of Pages**	**22. Price**
Unclassified.	Unclassified.	147	NA

Form DOT F 1700.7 (8-72)   **Reproduction of completed page authorized**

IMPROVING TRAFFIC SAFETY THROUGH BETTER SNOW FENCES: IMAGE-BASED METHODS TO MEASURE TRAPPED SNOW VOLUME AND THE SNOW RELOCATION COEFFICIENT

Final Report
August 2017

Principal Investigator
George Constantinescu, Professor and Research Engineer
IIHR – Hydroscience and Engineering, University of Iowa

Co-Principal Investigators
Marian Muste, Adjunct Professor and Research Engineer
IIHR – Hydroscience and Engineering, University of Iowa

Chris Rehmann, Professor
Civil, Construction, and Environmental Engineering, Iowa State University

Research Assistant
Heng-Wei Tsai

Authors
Heng-Wei Tsai, Marian Muste, George Constantinescu, and Chris Rehmann

TABLE OF CONTENTS

LIST OF FIGURES

viii

LIST OF TABLES

ACKNOWLEDGMENTS

EXECUTIVE SUMMARY

Blowing and drifting of snow is a major concern in terms of safety, transportation efficiency, and road maintenance and repair in regions subject to intense snowfalls and winds during the winter season. Snow blowing across the road and accumulating (or drifting) on the roadway induces ice formation on roads, reduces drivers' visibility and safety, and ultimately increases the number of accidents.

One common way to mitigate snow drift on roadways is to install structural or living snow fences. Unfortunately, the design of snow fences relies on empirical relationships. In particular, this is the case for the snow relocation coefficient (SRC), which is the percentage of fallen snow relocated from the upwind fetch area and is one of the main variables on which snow fence design relies. Empirical relationships have been proposed to evaluate the SRC. These empirical relationships are typically site-dependent and strongly correlated with the local meteorological and topological conditions. No corrections have been proposed to easily adapt these relationships for use at sites with different conditions. Therefore, the use of these relationships at sites with different meteorological conditions is problematic. Moreover, the SRC is a function of the site terrain and ground surface characteristics. Estimation of the SRC requires quantification of the snowfall and snow drift fluxes at the site where the snow fence is installed. Without being able to estimate the local value of the SRC, an efficient design for the snow fence is practically impossible because snow drifting is a process that is highly variable from location to location, even within the same climatological area, and is highly variable across time, even at the same location.

The main objective of the present study was to prove and test a set of new technologies that efficiently support the design and evaluation of snow fence performance by taking advantage of new, non-intrusive measurement technologies (image-based methods). The research discussed in this report addressed three critical aspects of snow fence design: estimation of the snowfall and snow drift fluxes and mapping of the snow volumes accumulated at the snow fence after its deployment at the site.

The present research for the first time advocates measuring the snowfall and snowdrift fluxes directly at the site. A set of non-intrusive measurement techniques were innovatively assembled to document snowfall and snow drifting over roads protected by snow fences. The proposed measurement methods do not require permanent installation, are mobile, and can be quickly performed to produce a wealth of qualitative and quantitative information readily usable for the design of snow fences. Specifically, the present research proposes the use of particle tracking velocimetry (PTV) and large-scale particle image velocimetry (LSPIV) coupled with three-dimensional (3D) photogrammetry to quantify snowfall and snow drift fluxes through direct measurements. Measurements can be obtained during both daytime and nighttime. By quantifying the snow budget near snow fences, critical parameters needed for snow fence design can be measured directly rather than estimated using empirical formulas.

This report proposes strategies needed to provide adequate illumination, set camera parameters, and process raw information with commercially available software to obtain accurate and robust

estimations of the main variables of interest (e.g., snowflake velocity and size, from which the horizontal and vertical snow fluxes can be estimated). Snow drift measurements were demonstrated in laboratory conditions with modeled snow particles. Moreover, the new methodologies and protocols assembled for characterizing the snow drift at a site provide multiple variables, i.e., velocity of snow sheet ripples moving along the bed (top of the fixed layer of snow), mean direction of motion over short and long time intervals, and estimations of the wind-fetch distance.

Additionally, the present research refines previously proposed methods to determine the volume of snow retained by the fence. Quantification of snow accumulation at the fence site over long periods (e.g., a winter season) is the ultimate qualifier that determines the performance of the snow fence design. The availability of robust and accurate techniques to monitor snow deposits at a snow fence site is critical for the post-construction efficiency assessment of snow fences. In particular, the present research further refines the use of close-range photogrammetry, developed through previous research work sponsored by the Iowa Department of Transportation (DOT), for providing a general methodology for non-intrusive remote estimation of the snow deposit volume using automated data acquisition protocols.

The present report describes the protocols developed for the documentation of snowfall, snow drift, and snow deposit mapping as well as a set of laboratory and field experiments performed to validate these new techniques and protocols. The report also describes the actual implementation of the developed protocols as applied to event-based monitoring at various locations exposed to snow drift. The tested techniques to measure snow fluxes and snow deposits are more accurate than previously developed methods, very efficient in data acquisition, portable, and safe to operate. An important advantage that these new methods have over classic methods is that they reduce the exposure of the individual performing the measurements to an adverse, often harsh, environment. Finally, the set of instruments, measurement protocols, and processing procedures developed through this research create a reliable measurement infrastructure for advancing the research in snow fence engineering and possibly other aspects of winter road maintenance and safety.

CHAPTER 1: INTRODUCTION

1.1 Research Background

Drifting and blowing snow is an extremely problematic and dangerous aspect of roadway travel in four-season areas subject to intense snowfalls and winds during the winter season. Snow drift occurs when a sufficient quantity of loose snow is present on the ground and the wind velocity, magnitude, and temperature exceed critical values. In this research, the main concern is blowing and drifting snow up to 5 m from the road surface. Snow blowing across the road and accumulating (or drifting) on the roadway reduces drivers' visibility and safety (Figure 1.1[a]) and ultimately increases accidents during the winter season (Figure 1.1[b]). The US Midwest, and especially northern Iowa, is often exposed to strong winds and large quantities of snow. Blowing and drifting snow is also the main cause for ice cover formation on roads and can reduce the effective road width (Figure 1.1[c]).

(a)   (b)   (c)

Heng-Wei Tsai, IIHR – Hydroscience and Engineering

Figure 1.1. Effects of snow blowing on I-35 in Iowa: (a) reduced visibility, (b) accidents, (c) reduction of the effective road width

Several studies, such as Andrey and Olley (1990), concluded that the combined effect of the snowfall-induced hazards can lead to an increase in traffic accidents by 100% or more compared with normal weather conditions. Most of the studies, however, found more moderate (but statistically still significant) increases in the number of traffic accidents during adverse weather conditions (Andreescu and Frost 1998).

The unquestionably detrimental impacts of snowfall and snow drift on highway traffic are mitigated with a plethora of methods and activities implemented before, during, and after snow storms. Reducing the impacts of drifting snow on highway operations can primarily be accomplished through two approaches (Perchanok 1998):

1. Controlling how the snow moves across the road
2. Preventing the snow from reaching the road

To control snow movement over the road, road design should include provisions to facilitate the accumulation of snow in ditches and to prevent the snow from moving onto or accumulating on the road. Alternatively, the road cross-section should be streamlined to maintain a smooth wind flow across the driving surface so that drifting snow coming from adjacent areas continues to

move over the road without stopping. However, designing roads so that snow drifts never accumulate on the roadways is not always possible, especially when the local topography is prone to snow accumulation and/or the rights-of-way are narrow.

Most often, the preferred approach to reducing the impact of snow drifting on highways is to prevent the snow from reaching the road. The present study focuses on some of the measures and activities designed to prevent such drifting. Preventive actions are included both during the road design stage and after road construction through road maintenance activities. Development of an effective snow-retention solution is preferred to maintenance activities because the latter can become a large component of winter maintenance costs for states or local agencies. Removing snow mechanically from roadways is costly due to equipment expenses and salaries for the snow removal crews. Moreover, snow removal results in less usage of the roads between the time the snow deposits and the time the snow is removed (e.g., Tabler 1991, Tabler 2003, Iowa DOT 2005, Sañudo-Fontaned et al. 2011). According to Perchanok (1998), blowing and drifting snow (as opposed to falling snow and frost) is responsible for about 30% of the plowing, salting, and sanding activities used to maintain roadways at operational status.

The most frequently used blowing snow prevention measure has been and continues to be the deployment of snow fences. The fences can either be constructed at the site or set in the form of living fences (e.g., shrubs, trees, or local grasses) planted along the road. For constructed snow fences, the typical materials used to build the fences include wood, metal rails, plastic nets, polymer rails, and woven fabric. Fence materials are attached to supporting structures (e.g., posts) made of steel or wood or to truss-type custom-designed frames set in the ground. Living fences are increasingly used as alternatives to constructed snow fences because they are beneficial not only for protecting the road against snow drifting and accumulation (Nixon et al. 2006), but also for providing important ecological and aesthetic benefits.

Constructed snow fences are generally installed perpendicular to the prevailing wind direction in the vicinity of the roadway, as illustrated in Figure 1.2(a).

(a)

I-20, Iowa (Heng-Wei Tsai, IIHR – Hydroscience and Engineering)

(b)

(c)
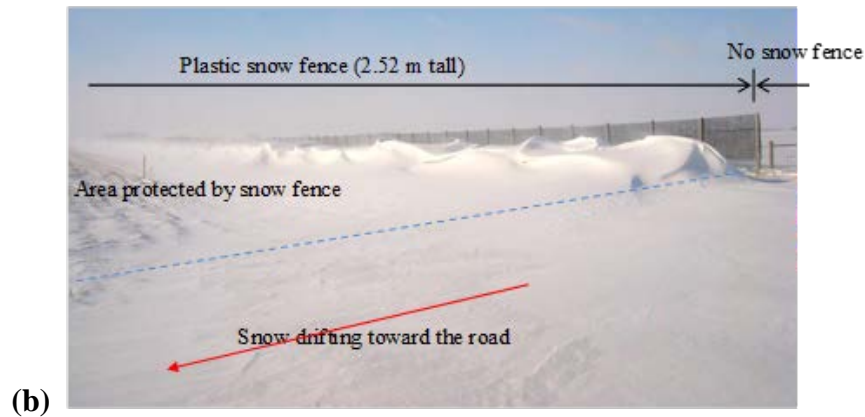
I-20, Iowa (Heng-Wei Tsai, IIHR – Hydroscience and Engineering)

Figure 1.2 Effect of snow fence presence

Drifting snow particles approaching a fence tend to deposit on the downwind side of the snow fence, where the velocity magnitude is smaller than the velocity on the upwind side. By slowing the speed of the snow particles and promoting snow deposition downwind of the fence, snow fences can result in a dramatic decrease in the problems related to snow blowing and drifting, as illustrated in Figures 1.2(b) and 1.2(c). The efficiency of snow fences differs depending on the position and orientation of the fences with respect to the road as well as on snow fence construction details such as height, orientation, porosity, and bottom gap (Basnet et al. 2016). Constantinescu and Muste (2015) found that snow fence efficiency is mainly a function of the fence porosity and the size of the bottom gap. Fences can be fit with additional hydrodynamic features (e.g., adjustable blades and variable opening geometries) to improve their operational

efficiency (Kaneko et al. 2012). However, the simple snow fence designs continue to be widely used because they are easy to install and do not require adjustments. Moreover, they have proven to be highly economical when compared to alternative snow mitigation techniques and practices (Basnet et al. 2016).

Several states (e.g., Minnesota, Utah) have established a clear link between the deployment of snow fences in critical areas of highways and a significant decrease (about 50%) in the number of serious accidents that result in human injuries. These deployments have also been linked to a major drop in winter maintenance costs, as seen in Figure 1.3.
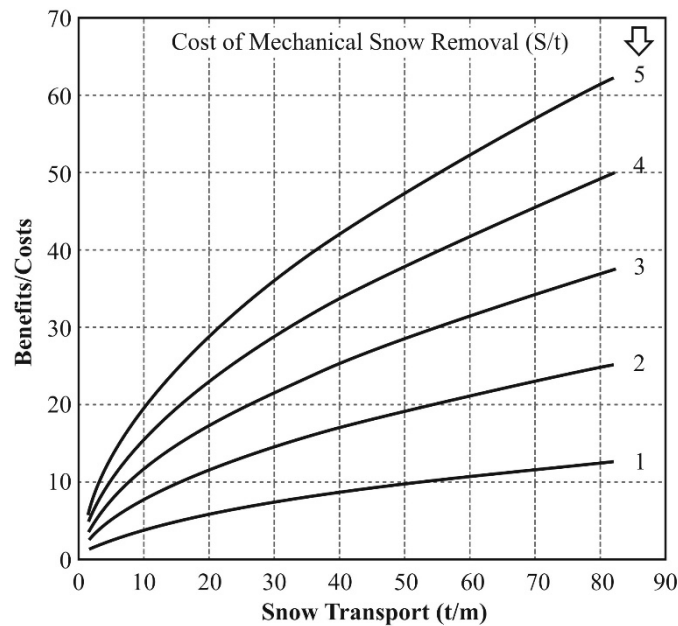
Tabler 2003, Copyright © 2003 by Ronald D. Tabler

Figure 1.3. Benefit-cost ratios for permanent snow fences in relation to seasonal snow transport and costs for mechanical snow removal

A more recent study conducted in Wyoming, a state that deals with an extremely high number of winter weather–related crashes, showed that up to 25% of the crashes that took place on Interstate 80 occurred in areas without snow fences, whereas a mere 11% of crashes occurred in areas protected by fences (Peel et al. 2017). The cost of snow fences and their installation is one to two orders of magnitude lower than the cost of mechanical snow removal. Tabler (2003) states that mechanical snow removal typically costs about $3 per 2,205 lbs. For comparison, a snow fence 4 ft tall can retain 4.2 tons of snow/ft.

The design of snow fences is based on a set of local or regional weather conditions estimated over the long term and taking into consideration the topography of the site. In general, the design of snow fences for prevention of snow drift entails the following steps (Kaneko et al. 2012):

1. Site characterization (i.e., collection of meteorological and snow drift information on past snow storms) and selection of a road route based on local topological conditions

2. Site survey and analysis (i.e., collection of additional topographic and meteorological information and quantification of snow drift features for the selected route)

3. Establishment of the orientation, geometry, and specifications for the snow fence's structural characteristics (i.e., overall geometry, materials, and hydrodynamic aspects)

4. Evaluation of the snow fence's performance (i.e., a survey of all aspects of the operational performance, from retention efficiency to maintenance costs)

The design activities described above require technical expertise from various road operation domains (i.e., planning, meteorology, structural design, and maintenance). Irrespective of the agency scale, designing snow fences requires sound engineering judgment in two main areas: (a) evaluating the potential for snow blowing and drifting at the construction site (Step 2 in the design process) and (b) providing specifications regarding the snow fence orientation and construction details commensurate with the estimation obtained through activity (a) above (Step 3 in the design process). The layout and dimensions of the fence are determined using formulae related to the annual quantities of drifting snow expected at the site, the road alignment, the surrounding terrain features, and the desired efficiency. The design equations can be simple analytical formulae, graphical solutions based on empirical and semi-empirical equations, or (increasingly) more complex numerical models (Liang et al. 2010, Naaim et al. 1998). The methodology implemented in the snow fence design is reviewed in Chapter 2.

1.2 Research Goals and Motivation

The overall goal of the proposed research is to prove and test a set of new technologies that efficiently support the design and evaluation of snow fence performance by taking advantage of new non-intrusive measurement technologies. Specifically, the present research contributes elements necessary to Steps 1, 2, and 3 of the design process outlined above by prototyping new or emerging measurement techniques for the following:

- Quantifying the snowfall and snow drift required in Steps 1 and 2 of the design process
- Supporting the evaluation conducted in Step 3 of the design process

The current measurement protocols used for snowfall and snow drift quantification and the evaluation of design efficiency are outdated, costly, and of unknown (presumably quite low) accuracy. Most of the current instrumentation pitfalls are related to the fact that the measurements are acquired using intrusive instruments. Data acquisition performed with these types of instruments also requires extended exposure to adverse, frigid, and windy conditions that pose a significant risk to the safety and health of personnel.

To be able to efficiently design a snow fence, it is necessary to obtain detailed information on the record of snowfall, the temperature, and the length of the snow seasons, as well as local data on the intensity and direction of the wind. This information is needed to estimate the storage capacity of the snow fence (failure to design for the correct snow capacity required in a certain region is a common mistake), its extent (e.g., the fence should be about 20 fence heights longer on each side of the region to be protected), its direction (in general, fences should be placed perpendicular to the dominant winter wind direction), and its position with respect to the road (e.g., fences positioned too close to the road can result in increased snow drifts on the roadways) and to design for the fence's height. The information on wind and temperature is well documented by meteorological observations on a national scale (e.g., the National Oceanic and Atmospheric Administration's Local Climatological Data provides summary data for about 1,600 US locations) and is complemented by other federal and state wind data repositories (e.g., the National Renewable Energy Laboratory [www.nrel.gov/gis/data_wind.html] and the Iowa Energy Center [http://www.iowaenergycenter.org]). Similarly, data on precipitation (including snow) are available from national and local observations (e.g., National Centers for Environmental Information [https://www.ncei.noaa.gov/] and the Community Collaborative Rain, Hail, and Snow Network [https://www.cocorahs.org], respectively). The above data are readily processed to enable access to annual and seasonal summaries of the observed data for practically any location on the map in the US.

While accurate data for rain, temperature, and wind can be easily acquired, snowfall data are acquired at 90% of the stations using intrusive methods, such as direct tape measurements of snow deposited on (white) boards over a certain time span (NOAA 2013). Most precipitation gauges operated by the US National Weather Service are situated in exposed locations (such as airports), and not all are equipped with wind shields; therefore, they underestimate the actual precipitation when wind is blowing. At windy sites, where the gauge is not equipped with a wind shield, the true precipitation can be as much as twice that collected by the gauge. When using precipitation data, it is wise to visit the weather stations involved to determine whether some allowance should be made for gauge-catch error (Tabler et al. 1990).

There are few research-grade snowfall measurement stations that are designed to eliminate the effect of wind on the snowfall estimation (personal communication with J. Angel, Illinois State Climatologist). Moreover, even if the duration of the measurements is relatively short (e.g., 10 minutes), a certain degree of compactness of the accumulated snow layer affects the accuracy of the snowfall quantification. For the particular case of snow fence design, the use of correct raw snowfall data is critical, because this quantity is used for estimation of the snow relocation coefficient (SRC), a critical input for snow fence design (Tabler 1994). The measurement method proposed in this research is non-intrusive (image-based), portable (can be easily deployed at the snow fence site), and direct (does not involve a board). Data on snowfall density and wind-resolved fluxes are readily available through the processing of the collected images of the snowflakes moving within a control area, as described in Chapter 3.

Obtaining quantitative information on snow drift is even more challenging because currently this parameter is rarely directly measured. Snow drift is a complex type of particulate transport. To form, snow drift requires several conditions to be met. Specifically, when the horizontal wind velocity is above a given threshold (i.e., about 5 m/s) there are two other factors that decide the

severity of the snow drift: (a) the snow pack characteristics (e.g., snow pack surface tension, snow pack temperature, snow depth, snow age, and others) and (b) the characteristics of the roadway (i.e., local topography and land cover) surrounding the fence location within the snow fetch distance (Osborne et al. 2012). When all the conditions are met, the physical process, collectively labeled as snow drifting, is quite involved because it results from several near-bed interactions, as described in Chapter 2. Given the complexity of the in situ measurement of snow drifts, several empirical and semi-empirical relationships have been developed to quantify drifting snow based on independent process parameters (e.g., Tabler 1991, Pomeroy and Gray 1995, Baker and Williams 1990, Perchanok et al. 1993). The empirical relationships are typically site-dependent; therefore, their accuracy might be low when applied to other geo-climatological areas. The measurement method proposed in this research is non-intrusive, applicable to the site of snow fence construction, and proof-tested for other similar bed-transport processes (Muste et al. 2016). Details on the measurement method are provided in Chapter 3.

Given the current limitations in the estimation of such critical design elements as snowfall and snow drift, the assessment of the post-construction efficiency of snow fences is critical, not only because the design typically assumes a one-storm event at the fence site, but also because multiple thermal processes are acting on the snow trapped at the fences during and between successive storms that are not accounted for in the design. Moreover, the variability of weather conditions from storm to storm is not a parameter considered in the standard snow fence design procedure. Based on the above considerations, one can conclude that the quantification of snow accumulation at a fence site is the ultimate qualifier that determines the performance of snow fence design. Direct observations of a post-construction snow fence provide useful feedback for continually improving the design guidelines. Conventional methods for quantification of snow accumulation are tedious, expensive, and, given the harsh winter weather environment, risky at times. The present research further refines the use of close-range photogrammetry developed through previous work (Basnet et al. 2016) to provide a general methodology for non-intrusive remote estimation of snow deposit volume using automated data acquisition protocols.

1.3 Contributions of the Present Research Study

Given the limitations of the current measurement technologies as applied to snow transport measurement and the gaps in our analytical capabilities to describe them, the research described in this report is based on a purely experimental approach for obtaining direct measurements of critical process variables. The main contribution of the present research stems from the assemblage of a set of measurement techniques that uniquely leverage advancements made in other areas of research. This set of techniques and methodologies is applied in the present study to a problem that impacts a socio-economic activity that is critical for communities located in regions with large amounts of snow precipitation during the winter season. To the knowledge of the authors, the application of particle tracking velocimetry and large-scale image velocimetry coupled with photogrammetry is a first attempt to quantify through direct measurements, rather than through inference, critical weather parameters such as snowfall and snow drift. Not only are the tested techniques more accurate than previously developed methods, but they are also efficient in terms of data acquisition, portable, and safe to operate because they reduce the exposure of the individual performing the measurements to an adverse, often harsh, environment.

These technologies rely on image-based techniques that are easy to use and widely available as off-the-shelf products, making the access to and transfer of technology faster. The raw data provided by the instruments are processed with customized or commercial software that offers opportunities to extract additional information following the measurement process. Collectively, the set of instruments, measurement protocols, and processing procedures developed through this research creates a reliable measurement infrastructure for advancing the research in snow fence engineering and possibly in other aspects of winter road maintenance and safety. The development of the measurement techniques described in this research is also relevant to the broader area of hydrometeorology.

The report is organized as follows. Chapter 1 outlines the context of the research and the motivation for developing the proposed measurement methodologies. Chapter 2 reviews the theoretical background of snow transport in the lower region of the atmospheric boundary layer and conceptualizes the transport modes relevant to snow fence design. Chapter 2 also reviews the current semi-empirical approaches to estimating snow drifting and the design software available to transportation design units. Chapter 3 reviews the fundamental and essential elements of the measurement techniques utilized in the present research (image velocimetry, large-scale particle image velocimetry, and photogrammetry) and extends the application areas of these techniques to the measurement of critical snow-related variables. Also described is the ancillary software used in conjunction with the processing of the final results of the measurement protocols. Chapter 4 describes the protocols developed for the documentation of snowfall, snow drift, and snow deposit mapping. Given that the experimental sites used to develop the various protocols were different, the sites are described and placed in the wider context of the investigated subject. Chapter 5 presents the actual implementation of the developed protocols as applied to event-based monitoring at various locations exposed to snow drift. Chapter 6 presents the main conclusions and discusses ideas for further research based on this study.

CHAPTER 2: BACKGROUND ON RELEVANT PHYSICAL PROCESSES AND VARIABLES

This chapter reviews some important aspects of the physical processes related to air and snow transport at sites where important snow precipitation occurs during the winter. Of particular interest is to describe how snow transport occurs over the ground and how this transport is affected by the presence of a snow fence. Given that the main role of snow fences is to diminish the adverse effects of snow drifting, the focus is on snow transport via drifting. Additionally, some of the main variables used in snow fence design are introduced (e.g., snow relocation coefficient) and their significance is discussed.

2.1 Snow Transport via Drifting

Snow transport via drifting, also called snow drift, is formed when small granular snow particles from the layer of snow deposited on the ground surface are re-entrained by the wind. Surface snow particles already deposited on the ground are entrained when the wind velocity over the layer of snow covering the ground is large and/or turbulence in the airflow over the snow layer is large. The threshold for particles to be entrained is a function of snow surface properties and flow conditions. In most cases, a wind velocity higher than 5 m/s is needed for the snow crystals to be entrained into the air flow over the top of the snow layer (Kathlein 2009). The snow drift dies when one or more of these conditions occurs:

- Wind velocity decays below the threshold value required for particles to move either via saltation or in suspension

- Temperature is high enough to produce the melting of the snow particulates portion of the snow drift

- Particles become so sticky that they remain attached when they interact with the top of the snow layer

The amount of snow carried over the layer of snow deposited on the ground surface is mainly dependent on the snowfall flux and wind velocity. The main modes of movement of the loose snow particles forming the snow drift are saltation and suspended transport (particles moving in suspension). The total flux of the snow drift is the sum of the flux associated with the movement of snow particles via saltation and the movement associated with particles moving in suspension. Because most of the snow portion of the snow drift is transported in a layer of less than 2 m thickness, the total flux is calculated by measuring from the top of the snow layer to about 2 m over it (Kathlein 2009). The maximum volumetric flux of snow within the snow drift (0 m $<$ z $<$ 2 m) that can be carried at a certain mean wind velocity is proportional to the mean velocity at power α, where α is close to 4 based on a regression analysis applied to field measurements (Kathlein 2009).

Particles moving via saltation are moving in "bounces" or "jumps" over the top of the layer of snow and are in periodic contact with it. For sufficiently high velocities, once particles are entrained from the top of the snow layer, they move in suspension within what can be called a suspension layer and have negligible interaction with the top surface. So the flow over the top of the layer of deposited snow is a two-phase flow containing snow particles. A two-way coupling occurs between the carrying air phase and the snow particles. Kathlein (2009) mentions that in most cases the height of the saltation layer is limited to couple tens of centimeters and that the average distance of the saltation jumps is less than 1 m. In fact, in a good approximation, the height of the saltation layer is proportional to the square of the bed friction velocity.

Given that the energy required for the snow particles to be entrained from the top of the snow layer and to move over it is provided by the wind, the characteristics of the flow inside the layer containing most of the snow drift are somewhat different than those observed under similar geometrical and flow conditions but without the presence of snow particles over the top of the layer of deposited snow. For example, the collision of the particles moving via saltation with the top of the snow layer results in an increase in friction with flow strength compared to the corresponding one-phase flow, a phenomenon called saltation-induced friction (Dyer 1986, Schmidt 1986, Bintaja 2001). The turbulent eddies present in the flow over the top of the snow layer provide most of the energy for the snow particles moving in suspension (Adams and Weatherly 1981, Bintanja 2001). Bintanja (2001) also showed that particle buoyancy effects can also have an important effect on the snow drift. The effects of saltation decrease in high winds, where most of the particles inside the snow drift move in suspension. In these cases, saltation typically accounts for only 10% of the total snow drift flux (Kathlein 2009). For wind velocities higher than 12 m/s, most of the particles within the snow drift move in suspension. Though the turbulent eddies can lift some of these snow particles to significant heights over the top of the snow layer, about 90% of these particles do not move more than 2 m away from the top of the snow layer (Kathlein 2009).

Snowflake crystals have different forms and characteristics (e.g., dendritic flakes, icy pellets). As snowflake crystals fall, they tend to become more rounded in shape. They have a different density than that of the air, and this density difference is a function of the snow's characteristics. Though a detailed description of the different types of snow and their characteristics is beyond the purpose of the present study, such descriptions can be found in the comprehensive book by McClung and Schaerer (1993), which describes three snow classification systems. The first system is the simplest. It introduces only three categories of snow based on the degree of riming to distinguish between fresh, new snow crystals and older, more compacted, graupel-type snow crystals whose branches have been filled in by riming. The second classification system, adopted by the International Commission on Snow and Ice, identifies eight categories and the temperature ranges associated with some of these categories of snow particles. Finally, the third system contains about 80 snow categories.

Once the snowflakes deposit on the ground or at the top of the snow layer, they become interlocked. Typically, after several hours the top of the snow layer forms a bonded crust, and drifting is possible as long as the wind is strong enough to entrain snow particles from the crust. The stress needed to entrain snow particles from the top of the snow layer and the flow of these particles inside the suspension/saltation layer depends on the snowflake characteristics. It should

also be noted that snow particles become smaller and rounder as they move with the snow drift due to abrasion and particle-particle interactions. In terms of particle entrainment from the snow layer, it typically takes about 250 m for the snow transport above a certain surface to reach equilibrium conditions (Takeuchi 1980, Bintanja 2001). So the flux of snow produced by entrainment at the top of the snow layer increases nonlinearly with the wind direction until about 250 m, when it becomes constant.

However, the snow particles extract energy from the mean wind flow. Moreover, as the density of the snow particles decreases with increasing distance from the top of the snow layer, the airflow over the top of the snow layer becomes slightly stably stratified. Bintanja (2001) showed that stratification effects on snow drifts can be relatively important very close to the top of the snow layer. For example, he observed a reduction of up to 40% in the turbulent kinetic energy in a strong wind flow carrying snow particles compared to the same flow with no snow particles. Kobayashi (1978) also found that shear-induced turbulence production is higher in cases where the flow carries snow particles.

When the flow contains particles in suspension, the turbulent kinetic energy dissipation is larger. Assuming large particles or weak flow, this extra dissipation term describing density drifting effects (Elgobashi and Abou-Arab 1983) is proportional to the velocity difference between the particle and the carrying (air) flow at that location and to the mean vertical (z) gradient of the particle volume concentration C. If one approximates this velocity difference to be of the order of the terminal fall velocity and assumes that Stokes' law applies (this strictly applies for snowflakes with a diameter less than 400 μm), then this extra dissipation term, which is generally referred to as the particle-induced buoyancy destruction component, can be written as Bintanja (2001):

$$B_p = -((\rho_p \div \rho_f) - 1)) g \times K \times dC \div dz \tag{2.1}$$

Where ρ_p is the density of the particles in suspension (e.g., snowflakes), ρ_f is the density of the carrying fluid (e.g., air), g is the gravitational acceleration, and K is the turbulent diffusivity.

In principle, the extra dissipation term also has a contribution that is unrelated to the presence of density stratification effects ($dC \div dz$ not equal to zero). However, this term is hard to quantify and is usually neglected when estimating the total extra dissipation term. Bintanja (2001) discusses the reasons why, for snowflakes moving in suspension, the particle-induced buoyancy destruction term is the main contributor to the total extra dissipation term.

The effect of saltation on increasing the effective bed roughness in a flow with snow particles moving via saltation is discussed next based on the work of Bintanja (2001). He proposed an empirical relationship to account for the actual roughness length (z'_0) that incorporates effects induced by snow drift. The actual roughness length is always larger than the standard roughness length, z_0, due only to friction at the top of the snow layer in the absence of snow particulates moving via saltation. This relationship is calculated with the following equation:

$z'_0=0.0029u_*^{2.48}$ (2.2)

Figure 2.1 shows a plot of equation (2.2) together with the experimental data used to generate the best fit.
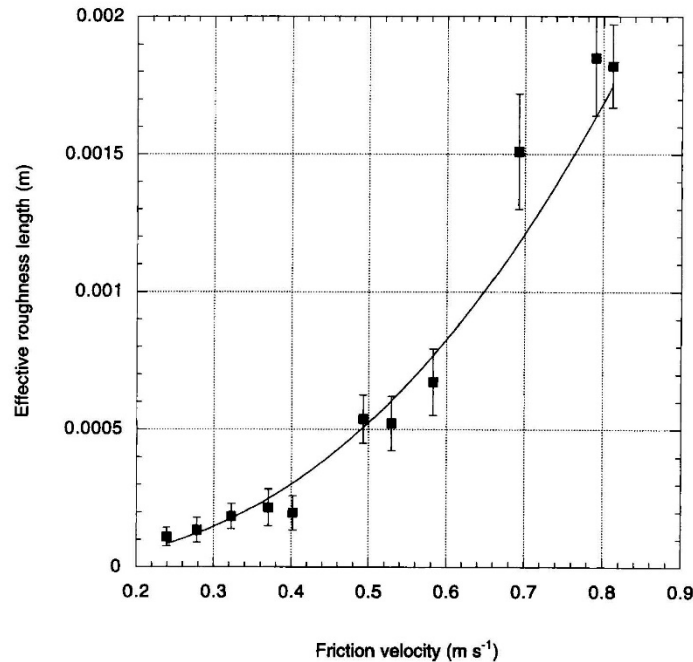
Bintanja 2001, © Royal Meteorological Society 2001, used with WILEY permission

Figure 2.1. Dependence of the effective (or apparent) roughness length, as determined from the wind speed profile, on friction velocity

The increase of z'_0 with u_* occurs because more snow particles are entrained from the top of the snow layer as the wind velocity, and thus u_*, increases. In the experiments by Bintanja (2001), z_0 = 0.0001 m. So for friction velocity values of close to 0.6 m, the effective roughness length to be used in log-law wind velocity profiles over the top of the snow layer is about one order of magnitude larger than the corresponding case with no snowdrift. Moreover, Bintanja (2001) showed that the mean fall velocity of the snow particles increases with u_* and thus with the mean wind velocity (e.g., the mean fall velocity increases by more than 50% as the friction velocity increases from 0.3 m/s to 0.5 m/s). A stronger flow can entrain larger snow particulates from the top of the snow layer. Larger particles have larger fall velocities and generate more turbulence as they interact with the carrying flow.

As previously mentioned, the differential concentration of the snow particles entrained from the top of the snow layer creates a mild stably stratified flow inside the saltation/suspension layer (snow drift). For the heavier snow particles to remain above the top of the snow layer, they have to extract turbulent kinetic energy from the carrying (air) flow. The immediate consequence is that the mean vertical wind velocity profiles are different from those observed in a flow with no

12

particulates. Bintanja (2001) proposed a modified wind vertical profile, U(z), for such cases using the following form:

$$U(z)=(u_*/k)(ln(z/z_0')+Az/L_{tot}) \tag{2.3}$$

Where k is the von Karman constant, $A = 5$, and L_{tot} is the Obukhov length that accounts for particle buoyancy effects.

The variation of z/L_{tot} with the friction velocity was determined experimentally by Bintanja (2001) and is included in Figure 2.2, which also shows the length scales associated with thermal effects (z/L_θ) and buoyancy effects (z/L_η) separately. The figure shows that particle buoyancy effects are important, especially for high wind conditions.
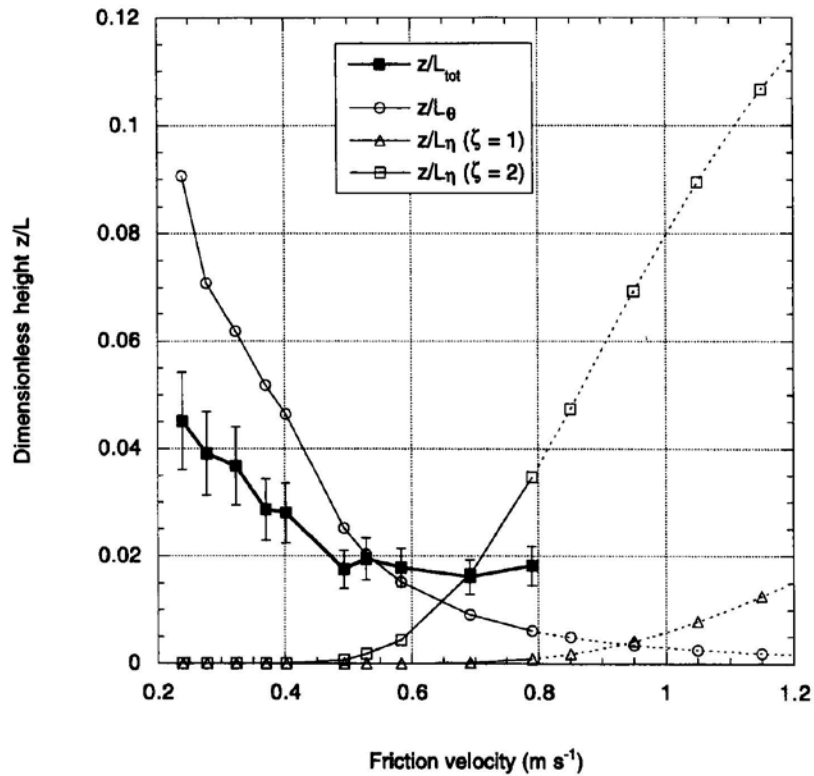
Bintanja 2001, © Royal Meteorological Society 2001, used with WILEY permission

Figure 2.2. Dependence of stability parameter z/L_{tot} on friction velocity at z=2 m from the top of the snow layer based on log-linear fitting of measured wind velocity profiles

In a one-phase flow, the mean velocity is linearly related to the bed friction velocity. As noted by Bintanja (2001), the fact that snow particles moving via saltation or in suspension in the snow drift affect the wind velocity profiles also means that friction velocity is a non-linear function of the mean wind speed and particle buoyancy. This is especially the case at high wind speeds, where buoyancy effects become important. Bintanja's (2001) experimental data confirmed that for wind speeds higher than 10 m/s in a flow with snow particles, the friction velocity increases

13

faster with increasing wind speed compared to the same flow with no snow particles. This effect was attributed to the fact that stable stratification reduces turbulent fluctuations and thus the bed friction velocity values increase for the same mean wind velocity. As previously discussed, saltation effects also increase the bed friction velocity and thus the vertical gradient of the wind velocity profile near the top of the snow layer. This effect is especially important in moderate wind conditions. Another effect is that the production of turbulent kinetic energy also increases in cases where snow particulates are present over the top of the snow layer. For example, Bintanja (2001) showed that the turbulence production for a wind speed of about 12 m/s increases by more than 100% when a strong snow drift is present. Saltation is the main reason for the increase of turbulence production, while stable stratification tends to slightly reduce the turbulence production when no snow particulates are transported.

2.2 Physical Factors Affecting Snow Drifting

Snow drifting generally cannot be avoided in open areas, but the snow drifts at a certain location can be minimized using snow fences whose role is to collect snow in between their locations and the road or to help the snow blow away (blowing snow fences). The intensity of the snow drift is a function of the wind-fetch and, as previously discussed, of the roughness of the top layer of deposited snow on the ground. A larger fetch means that snow particles can be entrained over a larger surface; thus the total flux of snow increases with the fetch distance until equilibrium conditions occur (typically for distances along the wind direction that are larger than 250 m), and the total flux becomes constant and independent of the fetch distance. Tabler (1994) and Pomeroy and Gray (1990) present empirical relationships relating the total flux of snow to the fetch distance and the roughness of the top of the snow layer.

The exact shape of the ground surface can also significantly affect where erosion and deposition take place and determine how severe erosion or deposition is at a certain location. The presence of an obstruction (e.g., snow fence) can greatly alter the snow deposition/erosion processes around the obstruction during the times when wind velocity parallel to the ground is significant. As mentioned by Schaerer (1972), "the critical task in planning protection against snow drifting is to predict the direction of drift-producing winds." This means that, in principle, wind should be measured locally and that its interaction with the three-dimensional (3D) ground surface and large-scale obstructions situated in the region where snow drifting has to be characterized should be taken into account.

As discussed by Schaerer (1972), the presence of hills, trees, or valleys along with man-made obstructions (e.g., buildings, fences) can greatly alter the snow erosion and deposition pattern in a certain region. Of particular interest for the present study are regions where highways are present and need to be protected against the adverse effects of snow drifting. For example, snow drifts are smallest at the tops of hills, assuming that the hill is not situated in the wake of another large terrain obstruction. However, the lee sides of hills are regions where snow deposition is the largest. In general, isolated obstructions (e.g., buildings, trees, fences) on the upwind side of the highway slow the wind and cause some of the snow particles to deposit on the downwind side of the obstruction. Ideally, this distance should be smaller than the distance between the obstruction

and the highway so that snow does not deposit on the road. Tabler (1994) gives a procedure for determining the approximate distance over which snow deposits downstream of an obstruction.

The presence of vegetation is especially important when the ground is not covered by snow or is covered by a thin layer of snow such that protruding vegetation increases the roughness at the top of the ground or the snow layer. This affects the threshold mean wind velocity at which snow particles can be entrained into the snow drift. Moreover, when melting occurs or the wind velocity is very high such that entrainment causes a significant reduction in the thickness of the layer of deposited snow, vegetation can again protrude over the top of the layer of snow and the roughness can increase, which then affects the conditions for further entrainment of snow particles into the snow drift current. Moreover, when installing snow fences to protect against snow drifting in the direction of the predominant wind at a location, one should be careful not to produce adverse effects when the wind direction changes, because at many sites wind direction during the winter season is not stable. These geometrical features of the terrain can be used to predict and control drifting on the highways.

2.3 Snow Transport Modes Relevant to Snow Fence Design

Different snow events have different snow transport modes. Three such transport modes are introduced and discussed below. At any site, part of the snow movement can be described as snowfalling. Most of the snowflake movement can be described as snowfalling under very low wind conditions such that the snowflakes move, in the mean, along a vertical direction. Snow drifting is formally defined as snow moving fairly parallel to the ground surface in between this surface and a height of 2 m (approximately 6 ft) above the ground. The horizontal movement of snow transported above this height is typically called snow blowing.

Under negligible wind, where most of the snow movement can be described as snowfalling, the deposition of snow at a site where a snow fence is present is basically the same as at a site where a snow fence is not present, as shown in Figure 2.3.
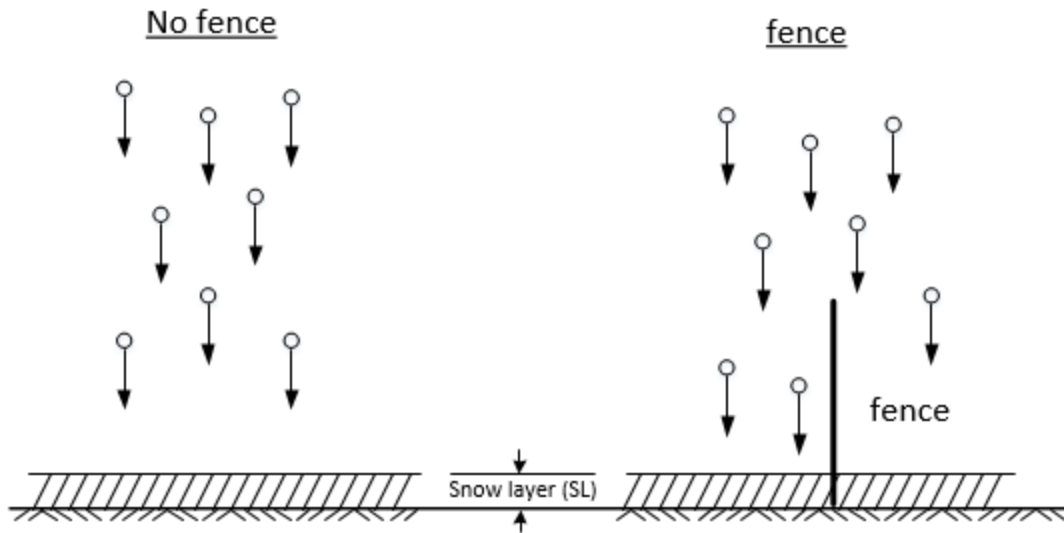
Figure 2.3. Movement of snowflakes at a site with no snow fence (left) and at a site where a snow fence is present (right) for the case where the first snow transport mode (snowfalling under negligible lateral wind) is dominant

In both cases, snow particles fall straight down to the ground. This is the first mode of snow transport that can be observed at a site where a snow fence is present.

The second transport mode observed during a snow event at a site where a snow fence is present occurs when the wind component parallel to the ground is not negligible, but the wind velocity does not exceed the threshold value, called drift velocity. At this point, snowflakes deposited on the ground are entrained into the boundary layer developing over the snow-covered ground, move via saltation, and are eventually relocated further downstream along the horizontal wind component direction (snow drifting is not active). Several studies (e.g., Kobayashi 1979, Pomeroy and Gray 1990, Schaerer 1972) have proven that the threshold value for the wind velocity to produce snow drifting is close to 5 m/s or about 10 miles/hr. When this transport mode is dominant, the snowflakes do not follow vertical trajectories. Figure 2.4 illustrates in a graphical way the second transport mode, where V is the mean horizontal wind velocity and V_D is the drift velocity.
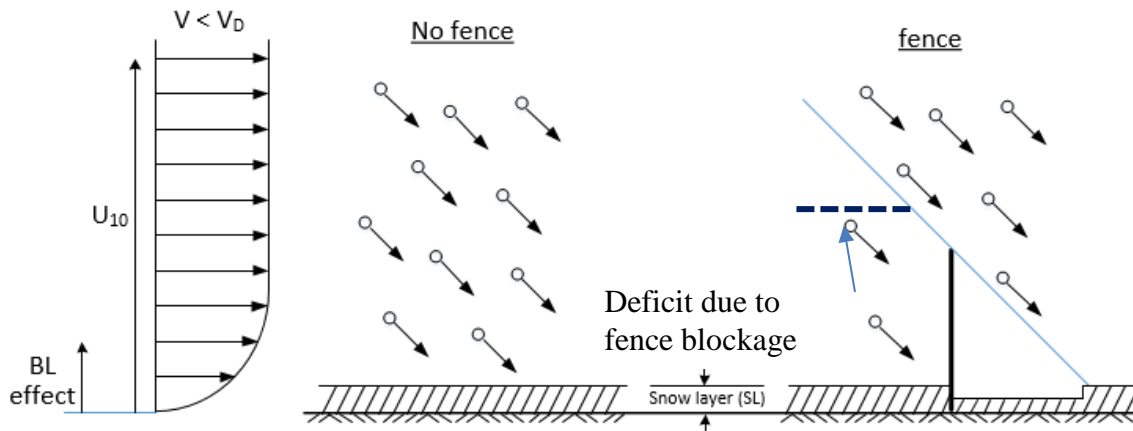
Figure 2.4. Movement of snowflakes at a site with no snow fence (left) and at a site where a snow fence is present (right) for the case where the second snow transport mode (lateral wind is present but its velocity is not sufficiently large to induce significant snow drifting in the vicinity of the ground surface) is dominant

Another relevant velocity is the snow drift velocity, V_{SD}, which is the actual velocity of the moving layer of (high-concentration) snow close to the bed. For this mode of transport, V is smaller than V_D and $V_{SD} = 0$. At sites not equipped with a fence, snow particles approach the ground at a non-zero angle relative to the vertical direction. If a snow fence is present at the site, due to the blockage induced by the fence, snow deposition in the vicinity of the fence is affected by the presence of the fence.

The third snow transport mode occurs when the wind velocity component parallel to the ground exceeds the threshold value ($V > V_D$). This mode of transport is dominated by snow drifting, which is the focus of the present study. Figure 2.5 presents three different possible situations: no snow fence is present at the site, a snow fence is present at the site during the snow event (snowfall is non-negligible), and a snow fence is present at the site after a snow event that generated a snow layer over the ground from which snow can be entrained and carried by the wind via drifting.
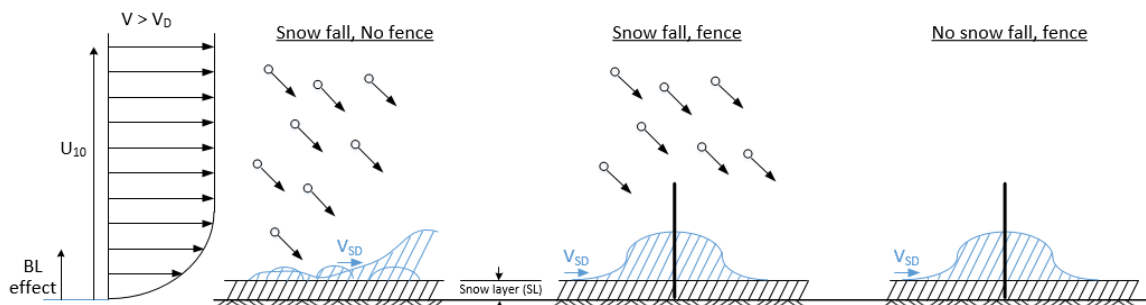
Figure 2.5. Movement of snowflakes at a site with no snow fence (left) and at a site where a snow fence is present (center and right) for the case where the third transport mode (wind parallel to the ground surface is present and its velocity is sufficiently high to induce snow drifting in the vicinity of the ground surface) is dominant

In the case where snowfall and wind are strong and no snow fence is present, the snow particles pile up and generate larger deposition. However, if a snow fence is deployed at the site, the snow fence is expected to significantly reduce snow accumulation on the downwind side of the fence by trapping snow particles.

Also associated with drifting is the snow drift velocity, V_{SD}. Note that once snow accumulates on the ground, this mode of transport can occur even outside of snowfalling events when a strong wind is present at the site.

In summary, several types of snow transport modes can be present at a site where snow precipitation occurs. For the snow drift to be significant, the wind velocity should exceed a threshold value. Snow drift can occur even in the absence of significant snowfalling.

2.4. Estimation of Snow Transport and Snow Relocation Coefficient

When estimating snow drift at a site where snow accumulation on a road situated at the site is of concern, several variables need to be estimated in order to be able to correctly design the snow fence to be deployed at the site. Of particular interest is the estimation of the mean annual snow transport at the site and the snow storage capacity of the fence. Though several approaches have been proposed in the literature, in this section we review only the procedure proposed by Tabler (1994, 2003), which is the procedure used by most state DOTs in the US to design snow fences. The empirical formulae are determined based on experiments conducted in Wyoming. A major unknown factor is the extent to which formulae calibrated for Wyoming can be used to obtain accurate predictions in other regions where heavy snow precipitation occurs during the winter season. Also, the empirical formulae are based on mean annual estimates of the relevant fluxes and thus are not site-specific. As discussed in the previous subsection, the geometrical characteristics of the site can greatly affect the flux of drifted snow. Similar to other researchers, Tabler assumed that most of the snow transport occurs up to 5 m above the top of the layer of deposited snow.

The mean annual snow transport (in Kg/m) is calculated as follows:

$$Q_t=500 \times T \times S_{rwe}(1-0.14^{F/T}) \tag{2.4}$$

Where S_{rwe} is the mean monthly relocated snowfall water equivalent in meters, F is the fetch distance in meters, and T is the maximum transport distance in meters.

The maximum transport distance varies greatly from one storm to the next (depending on relative humidity, air temperature, and wind speed), but season-long averages appear to be relatively stable. The mean value estimated for Wyoming conditions by Tabler (2003) was T = 3,000 m. Generally, the fetch can be determined from aerial photographs after the direction of the mean dominant wind is determined. The fetch is defined as the distance between the location to be protected and the nearest location on the upwind side where snow particles from the top of the snow layer moving toward the protected location are entrained. If the fetch cannot be clearly

determined from photographs, it can be assumed that it is so large that the second term in equation (2.4) is equal to zero.

The other important flux is the evaporation loss, Q_e, in Kg/m of width across the wind. Its expression given by Tabler (2003) is as follows:

$$Q_e=1000 \times S_{rwe}F\text{-}500 \times T \times S_{rwe}(1\text{-}0.14^{F/T}) \qquad (2.5)$$

The main fluxes of snow at a site where a snow fence is present are represented in Figure 2.6.
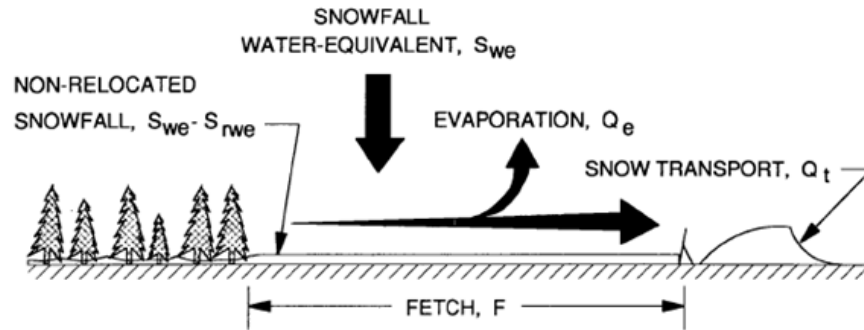
Tabler 1994, © 1994 Ronald D. Tabler

Figure 2.6. Diagram of snow transport in the vicinity of a snow fence

Tabler's procedure to estimate S_{rwe} (1994) is based first on an estimation of the total mass horizontal snow transport by the wind over a distance of 5 m from the top of the snow layer, Q_{0-5}. This discharge in units of kg/s per meter of width across the wind is estimated as follows:

$$Q_{0-5} = \frac{U_{10}^{3.8}}{233847} \qquad (2.6)$$

Where U_{10} is the wind velocity in meter/second measured 10 meters up from the bed. Then S_{rwe} is obtained from the following equation:

$$S_{rwe} = \frac{Q_{0-5}}{500\ T} \qquad (2.7)$$

As noted by Tabler (1994), S_{rwe} is the part of the snowfall relocated by the wind and excludes snow retained by vegetation and topographic features and snow that hardens or melts in place. Equations (2.6) and (2.7) were derived from a regression equation relating mass flux to wind, speed, and height above the surface (Mellor and Fellers 1986). The regression equation shows that the rate of snow transport is a strong function of the wind speed. For example, increasing wind speed by a factor of two results in a nearly 15-fold increase of snow transport. This reduction of the snow transport rate due to a local reduction of wind speed due to the presence of an obstruction is the main effect on which the design of snow fences relies.

The total amount of winter snow precipitation is generally expressed as a water-equivalent snow depth from records of monthly snow precipitation at the nearest meteorological stations. In principle, this value obtained from meteorological measurements has to be corrected for wind blowing effects even when the gauges collecting the snow precipitation are shielded. If possible, snow precipitation should be estimated based on measurements of peak snowpack water equivalent following the procedures employed by the U.S. National Resources Conservation Service (Tabler 2003). A reasonable estimate for the snowfall water equivalent is $S_{we}=$ (snowfall depth) / 10, where the mean snowfall depth should be estimated based on records obtained as close as possible to the site. The non-relocated snowfall is then estimated as S_{we} - S_{rwe} (see also Figure 2.6).

Finally, once S_{rwe} and S_{we} are estimated, the snow relocation coefficient can be calculated as follows:

$$\theta = \frac{S_{rwe}}{S_{we}}$$
(2.8)

This equation represents the fraction of the winter snowfall water equivalent relocated by the wind. Generally, the values of θ are less than 0.7 (Tabler 2003). Smaller values ($\theta = 0.2$ to 0.3) were estimated in the northeastern part of the US. It is important to determine this variable accurately because it is a main design variable. For example, the predictions of the Wyoming Department of Transportation (WYDOT) Snow Drift Profiler software used to design snow fences are strongly dependent on the value of the snow relocation coefficient. This value has to be provided as an input parameter. Better estimates of the snow relocation coefficient improve predictions of the volume of snow to be stored, and the snow fence is designed based on these predictions to carry a certain risk of being overtopped by the stored snow. The value of the snow relocation coefficient is subject to significant uncertainties. Generally, a conservative value of close to 0.5 is used by the Iowa Department of Transportation (DOT) for the design of snow fences, but this is simply because there are no easy ways to get a more accurate estimate at a given site. The other two variables that greatly affect the design solution are the snow-water equivalent and the fetch distance. Even if it were possible to develop a better mean estimate of snow relocation coefficient for Iowa, this would not be an acceptable solution given the fact that this variable is strongly dependent on local conditions at the site. For example, the presence of high vegetation at a site can greatly reduce the amount of relocated snow compared to a case with similar meteorological conditions but with a smooth ground surface.

In the following chapters, a procedure for directly estimating the snow relocation coefficient at any given site using a set of state-of-the-art experimental techniques is outlined. This procedure eliminates the need to estimate some variables for which accurate estimates are hard to obtain (e.g., the fetch distance). The horizontal snow movement and the average snow drift velocity close to the top of the snow layer are estimated using large-scale particle image velocimetry (LSPIV) measurements conducted at the site. The snowfall precipitation depth is also directly determined based on measurements of the vertical snow particle fall velocity using particle tracking velocimetry (PTV).

CHAPTER 3: MEASUREMENT TECHNIQUES AND INSTRUMENTS USED FOR IN SITU SNOW DRIFT ESTIMATION

3.1 Introduction

Conventional methods for estimating snow drifting are still under development. Most of these methods rely on direct measurements acquired in situ. The targeted variables for estimating the snow drift and snow deposit extent are the wind characteristics (magnitude, orientation, and their spatial variation over short and long time intervals), wind-fetch length, snow deposition geometry (extent, shape, orientation), and rates of snow transport in the vertical direction. Investigations on drifting snow are typically made up to 5 m from the ground level. For example, the study conducted by Tabler (1994) is based on an extensive data set assembled from various studies carried out with diverse experimental methodologies, as seen in Figure 3.1.
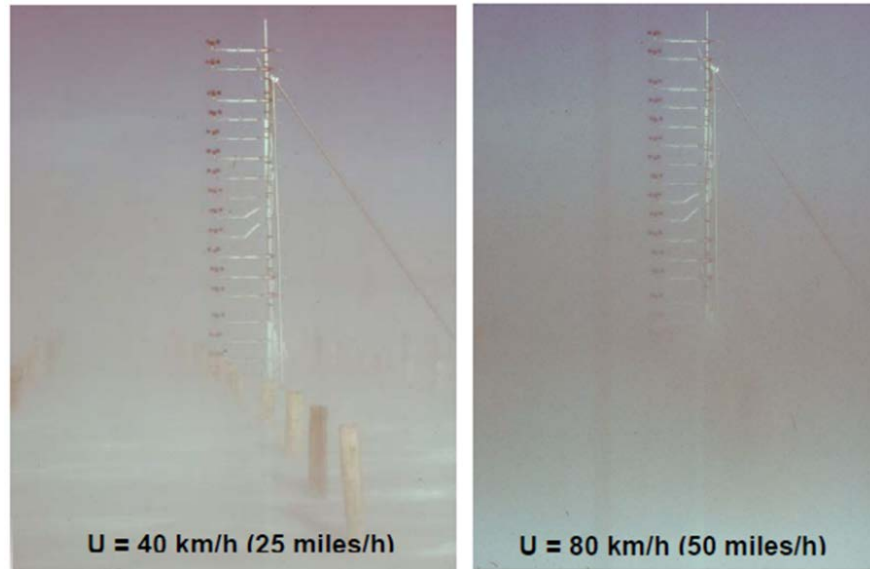
Tabler 1994, © 1994 Ronald D. Tabler

Figure 3.1. Direct measurement for wind velocity vertical profile using an array of anemometers (30 cm apart)

Most of the measurements are acquired with ground-based intrusive instruments, including snow traps (Budd 1966) and anemometer arrays (Tabler 1986), with complementary information provided by aerial photography.

Major pitfalls of measurements performed in particulate flows with an intrusive instrument regardless of the working fluid (i.e., water or air) result from the probe-particle interactions. Moreover, direct measurements of snowfalling, blowing, and drifting with intrusive approaches require long-term exposure to winter conditions, which sometimes limits the extent and accuracy of the experimental data. From this perspective, the use of non-intrusive methods such as those proposed in this study may result in improved accuracy and efficiency of measurement results. Measurement of snow particle transport with image-based methods is one of the best candidates

for this purpose. Not only can image-based techniques be controlled remotely, thus avoiding extended exposure to outdoor conditions, but the techniques' lack of interference with the natural movement of particles increases the accuracy of the results and provides simultaneous information regarding size, density, and velocity-derived quantities over a range of scales, up to the size of the imaged area. In this study, measurements of snowfall and drift are acquired using image-based methods in a natural environment subjected to various weather conditions. These methods are discussed next.

3.2 Image-Based Techniques

3.2.1 Image Velocimetry

Image-based methods for tracking particles stem from the visualization techniques that have been continually developed over time. The original purpose of these types of methods was to visualize flow patterns in free-surface flows. Later the technique was modified to quantify velocities of individual particles or groups of particles carried by the flow. Particle image velocimetry (PIV) and PTV are the most representative techniques from this family of methods (Adrian 2005). The PTV technique tracks individual particles, and PIV is used to track groups of particles moving within the flow from which the velocity vectors are estimated. The measurement principle of image-based techniques is based on the simple speed-distance-time equation, as follows:

$$Speed = \frac{Distance}{Time} \tag{3.1}$$

The estimation of the distance traveled in time by the particles is obtained by tracking individual particles or groups of particles with statistical inference tools (i.e., spatial autocorrelation or cross-correlation) applied to successive images taken at short time intervals. The end result of image velocimetry–based measurements is two-component velocity vectors estimated at discrete points across a two-dimensional (2D) slice of the flow field. The image velocimetry process includes four major elements: seeding, illumination, recording, and image processing. A generic schematic of the image-based velocimetry setup is provided in Figure 3.2.
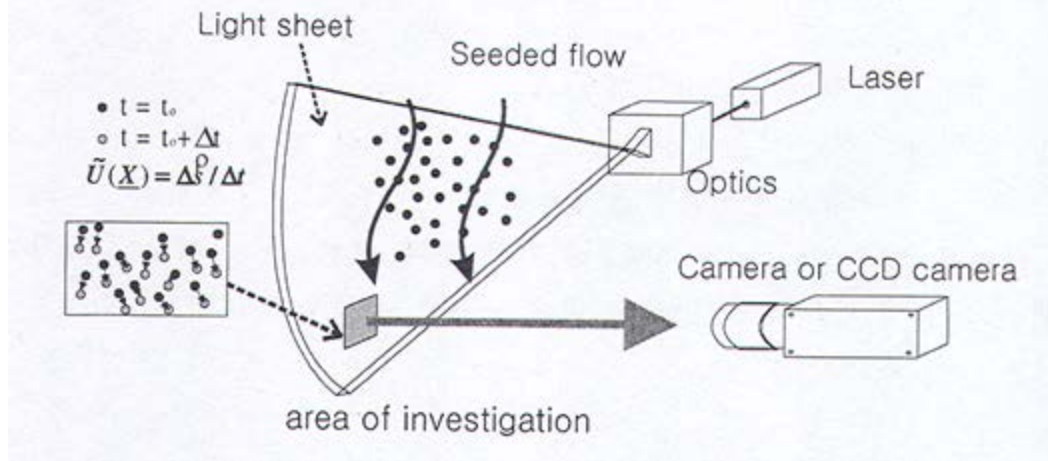
Figure 3.2. General configuration of a PIV system

Before starting the measurements, the working fluid in the experimental facility is "seeded" with small reflective particles that are assumed to accurately follow the structures in the flow. Next, the flow area to be investigated is illuminated with a thin sheet of light. Images are subsequently recorded from an angle perpendicular to the light sheet plane using specialized or conventional (off-the-shelf) cameras. There are several combinations of camera and illumination sequencing used to obtain sharp particle images and small displacement of the particle from one image to another (Westerweel et al. 2013).

The concentration of particles in the recorded images determines the type of algorithm used to estimate the velocity field. For low seeding concentrations, PTV processing algorithms are used to detect individual particles, estimate their displacement in time, and determine their speed with equation 3.1. These velocities can then be used to quantify the dynamics of the underlying flow or variables associated with particulate transport in the carrying flow (particle concentration, fluxes). For high particle concentrations, the tracking of the movement of individual particles becomes difficult. By contrast, PIV algorithms quantify the flow movement by tracking patterns formed by groups of particles suspended in the flow. The use of PIV allows a detailed characterization of turbulence structures in the flow. A short discussion of the four main steps used in image velocimetry techniques is provided below.

The concentration of particles in the recorded images determines the type of algorithm used for velocity estimation. For low seeding concentrations, PTV processing algorithms are used to detect individual particles, estimate their displacement in time, and determine their velocity with equation (3.1). The velocities obtained in this manner can be used to quantify the dynamics of the underlying flow or variables associated with the particulate transport in the flow (particle concentration, fluxes). For high particle concentrations, the tracking of the movement of individual particles becomes difficult. In contrast, PIV algorithms quantify the flow movement by tracking patterns formed by groups of particles suspended in the flow. The use of PIV is associated with the detailed characterization of the turbulence structures in various flows. A short discussion of each of the image velocimetry step is provided below.

3.2.1.1 Seeding

Although image velocimetry is categorized as a non-intrusive technique, the flow subjected to measurements has to be visualized by the addition of small quantities of flow tracers, a.k.a. seeding particles. Ideally, the particles must be neutrally buoyant so that they can follow the direction of the flow and travel with the small turbulent eddies. From this perspective, the particles should be light and small. At the same time, particles should be sufficiently bright for the recording device to be able to get accurate images of the particles within the illuminated flow field. Tracer particles for use with water flows are most often nearly neutrally buoyant glass or plastic microspheres. Metallic powders or natural particles (pollen) may also be used (e.g. Raffel et al. 2007) as seeding particles.

3.2.1.2 Illumination

Flow field illumination is typically accomplished with a combination of spherical and cylindrical lenses that produce a thin laser sheet, as illustrated in Figure 3.3.
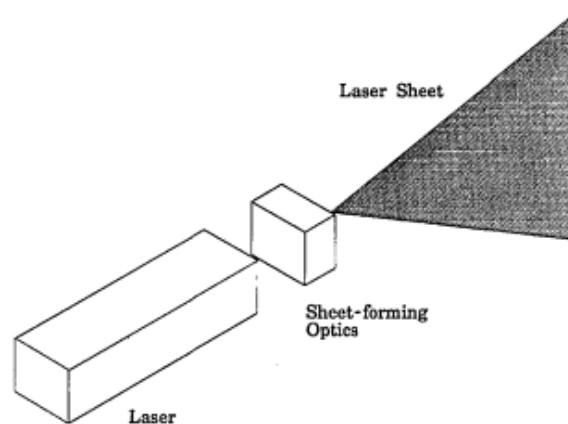
Lourenco et al. 1994, © 1994 Optical Society of America

Figure 3.3. Illumination

The actual illumination consists of short but intense light pulses fired into the flow at a high rate (Westerweel et al. 2013). Capturing these pulses requires a high-speed camera with high rates of recording.

3.2.1.3 Image Recording

The most often used contemporary image velocimetry recording device is the coupled charged device (Raffel et al. 2007). Recordings can be made in several ways: single frame with single, double, or multi-exposure; double frame with single exposure; and multi-frame with single or double exposure, as shown in Figure 3.4.
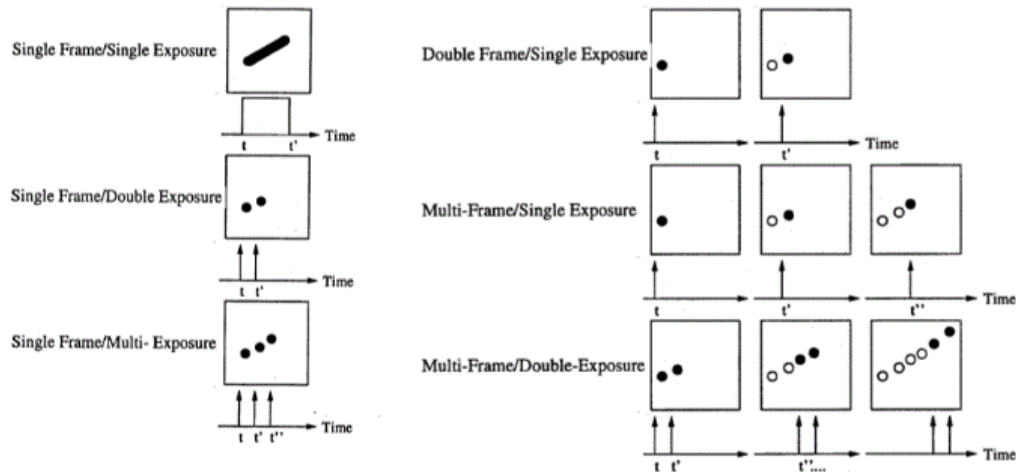
Figure 3.4. Single/Double frame exposure

To ensure that both the maximum and minimum velocities are captured, the operator has to anticipate the flow features present in the measurement area, define the measurement objectives, and appropriately design and operate the illumination-recording sequencing. With appropriate camera settings, images are successively acquired at time intervals commensurate with the goals of the measurement. For PIV measurements, this sequencing is stricter because the velocity evaluation is based on the assumption that patterns formed by the particles remain the same in image pairs (i.e., there is little or no relative change in the positions of the particles within the identified pattern).

3.2.1.4 Image Processing

Following their acquisition, the images are processed using statistical tools to determine the particle velocity. While PTV and PIV have many commonalities in terms of configuration, setup, and operations, there are considerable differences in their image processing algorithms. Because both techniques are used in the present study, the basic elements of the two processing algorithms are briefly presented below.

3.2.1.5 PTV

Figure 3.5 describes the standard PTV velocity measurement methodology (Admiraal 2017).
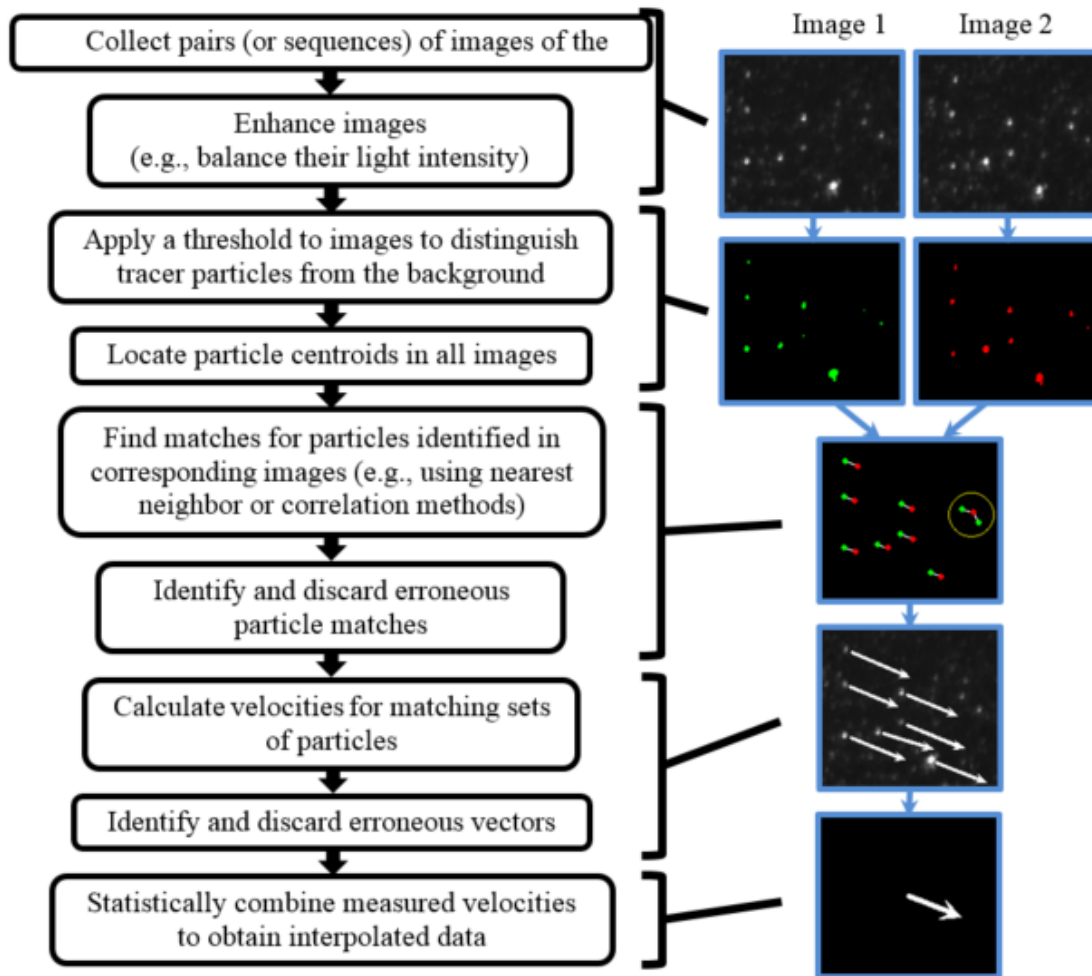
Figure 3.5. Flow chart illustrating the PTV methodology

To the right of the flow chart, the main steps of the methodology are demonstrated using subsections extracted from a pair of PTV images. The PTV process begins with the collection of a pair of particle images. The quality of the seeding and of the illumination-recording sequencing are critical for the accuracy of the PTV technique because the images have to contain more than one pixel in order for the particles to be located. Furthermore, large particle-image diameters should be avoided to optimize the fidelity of the velocity measurements in locations with strong temporal or spatial velocity gradients. After the PTV images are collected, some initial processing may be required to make sequences of images more uniform (brightness adjustments, background filtering, setting thresholds for particle identification, etc.).

Once individual tracer particles are found, the centroids of the tracer particle-images are calculated based on the contiguous pixels that form the tracer. After particles and their centroids are identified in consecutive images, an attempt is made to match pairs of particles in adjacent images that eventually will be used to estimate particle displacement in time. The estimation of

the potential displacement of each particle is made with various statistical algorithms (e.g., nearest neighbor, cross-correlation) applied to identical-sized particle candidates (Lloyd et al. 1995). After estimating the velocity for each particle (using equation 3.1), various filtering techniques are applied to the velocity estimate to remove the effect of possible errors. The velocity vectors estimated with PTV are randomly located throughout the flow field based on the positions of the tracer particles when the images were collected. It is usually desirable to know the velocity at selected points in the flow, so the PTV vector data must be combined to form weighted-average vectors at the selected points. Such vectors may be time averages of data collected from many PTV realizations or instantaneous averages of all of the tracers within a known radius of the point of interest (Admiraal 2017). Admiraal (2017) also mentions a large-scale PTV. The main difference between a large-scale and classic PTV is that in the former the image area is much larger than the one used in the latter (typically close to 20 x 20 cm).

3.2.1.6 PIV

Prior to applying the image processing leading to the velocity vector field, the recorded images are binned into small interrogation areas (IA), a.k.a interrogation spots or interrogation windows. For each individual IA, statistical approaches are applied to larger-size search areas (SA) centered on the IAs to determine the possible direction and magnitude of the possible IA displacement. During the evolution of PIV, several image processing algorithms were developed, driven by the technology available at the respective times. The first PIV systems used single-frame/multiple-exposure recordings that require autocorrelation-based algorithms for evaluation of the velocities (Adrian 1991). Subsequently, with the increase in camera frame rates, double-frame/single-exposure recordings emerged (Raffel et al. 2007), leading to the development of cross-correlation methods for evaluating flow velocities (Raffel et al. 2007).

Currently, the cross-correlation technique is the most common PIV interrogation technique. Several reasons explain why the cross-correlation method is increasingly applied for image processing. Not only can this technique resolve both the direction and magnitude of the velocity, but the processing of cross-correlation algorithms is more robust and easier to perform than auto-correlation, which needs to use other software to determine shifting of exposure. Given its extensive use and the fact that the large-scale particle image velocimetry technique presented below is based on the same algorithm, only the cross-correlation velocity estimation algorithm is presented here.

The cross-correlation approach used in the present study is described in Muste et al. (2008). In essence, a pattern matching technique is applied to the image intensity distribution in a series of images, as illustrated in Figure 3.6.
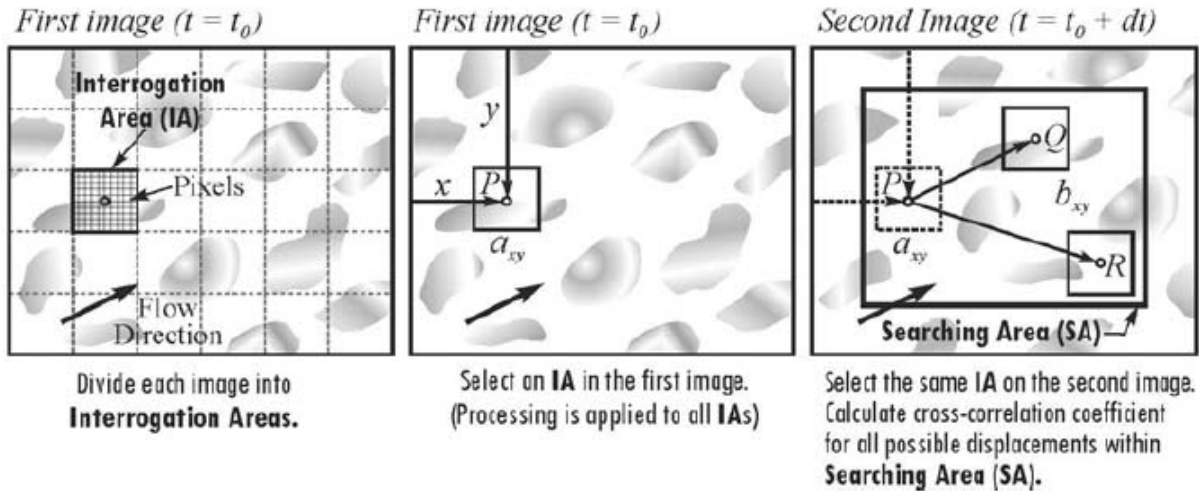
First image (t = t₀) — Interrogation Area (IA), Pixels, Flow Direction. Divide each image into **Interrogation Areas.**

First image (t = t₀) — Select an **IA** in the first image. (Processing is applied to all **IAs**)

Second Image (t = t₀ + dt) — Searching Area (SA). Select the same **IA** on the second image. Calculate cross-correlation coefficient for all possible displacements within **Searching Area (SA).**

Figure 3.6. General procedure for PIV measurement

The similarity index for patterns enclosed in a small interrogation area fixed in the first image is calculated for the same size window within a larger search area selected in the second image. The window pair with the maximum value for the similarity index is assumed to be the pattern's most probable displacement between two consecutive images. Once the distance between the centers of the respective small windows is obtained, velocity can be calculated by dividing it by the time difference (Δt) between consecutive images. This searching process is applied successively to all IAs in the image. The result of image processing is a velocity flow field covering the entire processed area with a density of velocity vectors that is decided by the user.

3.2.2 Large-Scale Particle Image Velocimetry

An extension of the traditional PIV was proposed for estimating velocity over large domains by Fujita et al. (1998). This innovation, labeled LSPIV, was first implemented for non-intrusive velocity measurement at the free surface of open-channel flows. LSPIV entails all of the components of conventional PIV (i.e., seeding, illumination, recording, and image processing). Given the large size of the imaged area, often recorded from a tilted angle, an additional step is needed before processing the images for estimating the velocities (Fujita et al. 1998). The differences between conventional PIV and LSPIV are synthesized in Table 3.1.

Table 3.1. Similarities and differences between conventional PIV and LSPIV

Component	Conventional PIV	Large-scale PIV (LSPIV)	LSPIV Additional Procedures/Features
Illumination	- small image areas (up to 0.20 m²)	- large areas (up to 100 m2)	- elimination of light reflections on the flow free surface and uniform distribution of the light intensity over the imaged area
Seeding Particles / Material	- strong illumination sources (CW or pulsed lasers) - micron-size, neutrally buoyant, uniformly dispersed in the flow	- conventional illumination: white natural or artificial light - cm-size, lighter than water density	- seeding material color needs to contrast background color (Muste et al. 1999)
Recording	- high-resolution or high-speed cameras - recording of a reference grid for scaling	- video-based cameras (low resolution, low speed) - recording of images to include marker points (known coordinates) needed	- special image processing algorithms required - geodetic survey of the marker points for image-to-real coordinate transformation
Pre-processing	- not needed	- removal of image distortion due to lens aberrations and perspective effects	- image reconstruction using geometrical mapping (Fujita and Komura 1994)
Processing	- reliance on individual particle images - 2D autocorrelation or cross-correlation of image pairs, usually with Fast-Fourier Transform (FFT)	- flow tracing made on local image patterns formed by groups of particles - 2D cross-correlation applied to image pairs in real space - de-coupling of the interrogation area from its fixed location in the first image of the pair to any arbitrary location in the second image of the pair	- use algorithms designed to process for low resolution images (Fujita et al. 1998) - flexibility in choosing the interrogation area shape and size - eliminates velocity bias and improves processing of vortical flows (Fincham and Spedding 1997)

Source: Muste et al. 2004

As shown in Table 3.1, LSPIV entails an extra processing step: image ortho-rectification. To extract accurate flow data from images recorded at oblique angles, they have to be rectified by an

appropriate image transformation scheme (Muste et al. 2004). This transformation requires a survey of at least six ground reference points (GRPs) that are included in the flow video frames at the time of image acquisition, as illustrated in Figure 3.7(a).

(a)

Fujita et al. 1998

(b)
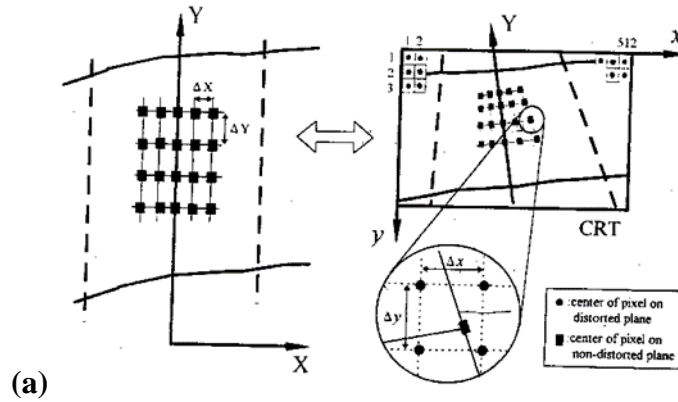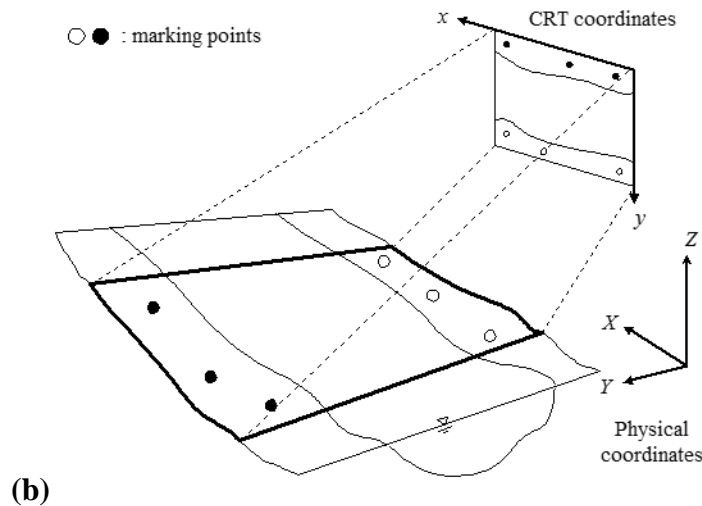
Figure 3.7. Image ortho-rectification: (a) imaging of the GRPs and (b) mapping of the GRPs from physical coordinates to camera coordinates

The control points are surveyed in the field using specialized equipment. The GRPs' selection is often dictated by what is accessible in the field (e.g., trees, power line poles, building corners) rather than what is desirable. These points are subsequently used in conjunction with a conventional photogrammetric relationship that maps the GRP coordinates in the physical space (X, Y, and Z) with their image coordinates (x and y), as shown in Figure 3.7(b).

Similar to PIV, LSPIV requires "seeding" in order to visualize the water body movement. The step-by-step procedure to determine LSPIV velocities is schematically shown in Figure 3.8.
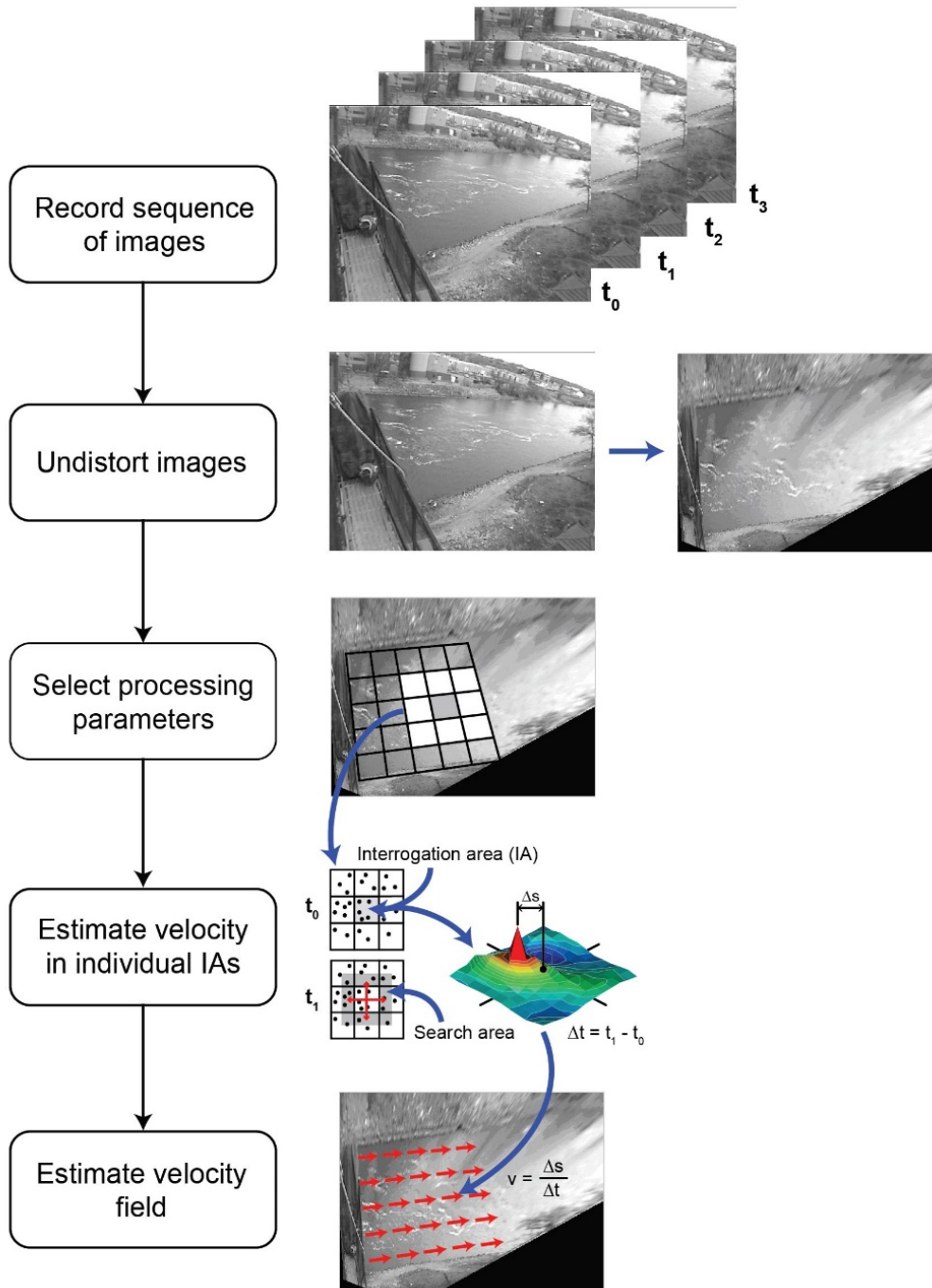
After Muste et al. 2014

Figure 3.8. LSPIV procedure for estimation of velocities in an open-channel flow

Seeding in the LSPIV context is defined as groups of particles floating at the free surface that collectively create image patterns that are distinguishable in the recorded images. Attaining uniform and adequate seeding over large areas is difficult in both controlled (laboratory) and

natural environments. Consequently, most of the seeding of the free surface in natural conditions is non-uniform and is rarely adequate.

To counteract the limitations associated with seeding in natural-scale environments, an image processing algorithm is adopted in the present study. This algorithm can estimate velocities from low-resolution images, such as those captured by standard video cameras from a long distance. The algorithm is similar to the correlation imaging velocimetry of Fincham and Spedding (1997), which considers each pixel in the interrogation area to be equally weighted in the interrogation process such that the background image is just as important as the pattern images.

The LSPIV algorithms for estimating velocities are the same as those used in conventional high-density-image PIV (Adrian 1991); see also Figure 3.8. The LSPIV measurement outcomes are the instantaneous vector fields. Each IA encompassed in the original free surface image has a vector attached to it. The obtained LSPIV vector field makes it possible to conduct Lagrangian and Eulerian analysis for determining spatial and temporal flow features, such as the mean velocity field, streamlines, and vorticity, as well as other velocity-derived quantities.

3.2.3. *Photogrammetry*

The main purpose of a photogrammetric survey is to use photographs to quantify the terrestrial space in three dimensions and also to replicate its texture as a continuum. Kunapo (2005) defines photogrammetry as the art and science of constructing reliable 3D landscapes from 2D photographs. While in photography a three-dimensional object is captured in two dimensions, in photogrammetry the process is reversed; a two-dimensional image is processed to create a three-dimensional object to be measured. This is accomplished by using two or more overlapping two-dimensional images so that it is possible to triangulate on the object points, as illustrated in Figure 3.9.
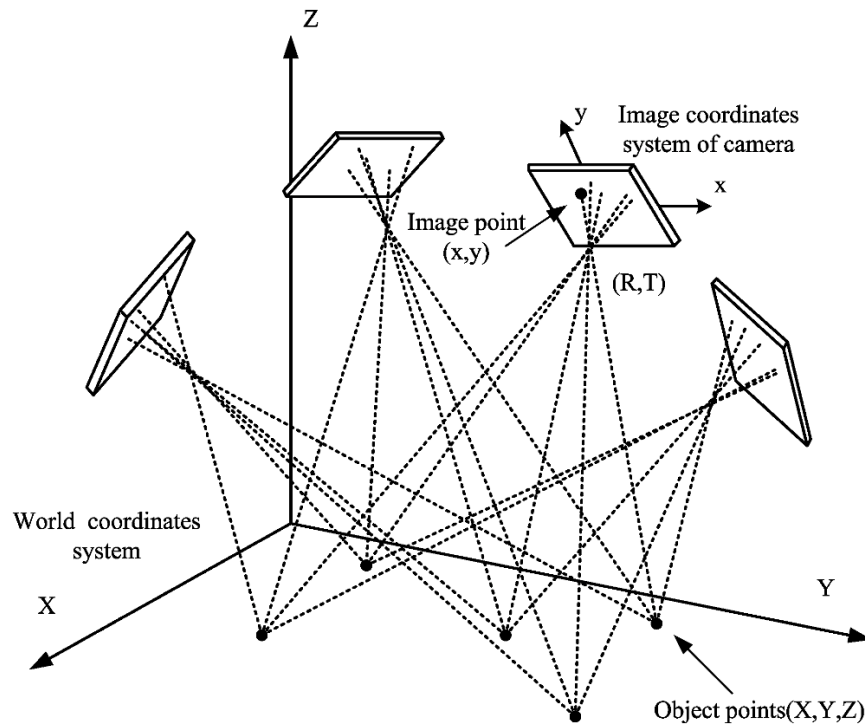
Figure 3.9. Principles of photogrammetry for creating a three-dimensional model

Multiple cameras are positioned at different angles and aimed at the object in order to recreate the object. The combination of two or more photos of the same object is also called stereoscopy. This method used to determine the height of the object.

Photogrammetry is comprised of two main operational steps: acquisition of photographs and metrology. There are two types of image acquisition used in photogrammetry: traditional (aerial) and non-traditional (close range). The classification depends on the location of the camera during the image recording. In aerial photogrammetry, the camera is mounted underneath an aircraft and images are acquired with the camera oriented vertically downward. In non-traditional, close-range photogrammetry (CRP), the camera is positioned closer to the object and is typically set on a steady pole or tripod (Matthews 2008). CRP typically involves reconstructing the actual terrain topography using a pair of photos of the same area (or object) taken from slightly different locations. However, the more overlapping images that are taken from different angles, the better the resolution of the 3D reconstruction of the object that can be generated (Kraus 1993, Wolf and Dewitt 2000, Cooper and Robson 1996).

Regardless of the type of image acquisition, high-quality photogrammetric outputs can be obtained only with high-quality photographs. The three main elements involved in capturing high-quality images involve camera settings: the focus, exposure time, and field of view. Cameras have to be adjusted to focus on the object/image plane in order to enhance the resolution of the texture used for photogrammetric reconstruction. The exposure time has to be long enough to allow multiple features of the recorded background surfaces to be distinguished.

The camera field of view determines the range of visibility of the images. Areas of the imaged surfaces that are outside the field of view appear blurred in the recordings and cannot be efficiently used to reconstruct the 3D image.

The second component of photogrammetry is metrology (i.e., the reconstruction of the three-dimensional space from combining two-dimensional images). In this step, a triangulation method is applied to a set of points that are recognized in the multiple images of the overlapping areas of the photogrammetric survey. To scale the 3D location of each object point in the images, it is necessary to conduct a survey of a few reference points at the measurement site (Basnet et al. 2016). These ground reference points are specified by the operators and can be marked using paint, tape, or stakes. The GRPs' actual coordinates need to be associated with the image coordinates, and typically each set of images needs at least three GRPs, as illustrated in Figure 3.9. With the lines and points overlapping, pixels representing the same point in different images can be recognized and the triangulation principle can determine the accurate location/depth of the object. These overlapping points within the area covered by the multiple photographs are generated by sophisticated photogrammetric software (i.e., Agisoft) and identified as tie points. The more tie points that are generated, the higher the probability that the same location of the surface in the images can be recognized. Tie points are used along with the physical coordinates of GRPs to scale and evaluate the geometry quantitatively (Basnet et al. 2016). Agisoft software is then used to generate the cloud of tie points (typically thousands) with the known accurate coordinates as the final output data, which is plotted in the Agisoft software for the quantitative visualization of the volume. Several additional steps are involved in the reconstruction of the final three-dimensional model: aligning the photos to auto-detect the tie points, building a dense cloud to identify the number of tie points, building a mesh in order to connect the points to generate polygonal surfaces, and building texture to define the appearance and color for each polygon.

The final output of CRP is an easily understandable 3D representation of the landscape, not a typical topographic visualization of the terrain (i.e., not similar to a map with iso-contours). Photogrammetric surveys are increasingly used due to some distinct advantages over other types of surveys: cost efficiency, because they only require a camera and software; reduction of the safety risk compared to that associated with performing actual field survey measurements; and relative ease of obtaining data remotely without the need to access the site.

3.3 Instrumentation and Preliminary Tests

3.3.1   Summary of Instrumentation and Software used in this Study

Two different image techniques, PTV and PIV, were applied in this study to measure the main variables of interest. PTV was used to quantify the snowfall and PIV was used to determine the horizontal transport of snow particles in the form of snow drift. A summary of the PTV and PIV features employed in the present study is presented in Table 3.2.

Table 3.2. Summary of different image techniques used for tracking particle velocity

Image Technique	Role	Image Velocimetry Components				Software
		Seeding	Illumination	Recording	Processing	
PTV	Measurement of snowfall (vertical)	Snowflakes	Natural / Artificial light	Sony 4K video camera	Cross-correlation	EDPIV
PIV (as used in LSPIV)	Measurement of snow drift (horizontal)	Snowform migrating on the snow deposits	Natural / Artificial light	Sony 4K video camera	Cross-correlation	FUDAA

As shown in Table 3.2, PIV and LSPIV recordings were made using the same camera. Acquiring photographs from which the velocity of the particles (snowflakes) can be determined was challenging for several reasons, including the need for sufficient lighting (in both day and night conditions) and the need to use a high-resolution camera that has both adjustable optics to focus the camera field of view and high-speed capabilities to capture the high velocity of snowflakes carried by the wind.

3.3.1.1 Testing Camera Settings

Prior to establishing the measurement protocols for PIV and LSPIV measurements, an evaluation of the camera settings was undertaken. The PTV recordings were made with a camera adjusted manually for focus, shutter speed, and frame rate. The main reason for using manual focus rather than autofocus with default values was to accurately image individual snowflakes. This was required because sizing and concentration measurements are also needed for the measurement of snowfall. If the camera were used with autofocus, it would not be able to focus on the moving particles because the autofocus adjusts automatically for various planes according to the individual particle that dominates the image plane. The adjustment of the shutter speed of the camera is mandatory to get the image of the particle with high accuracy. Shutter speed controls the time of exposure of the image sensor to the imaged object. That is, if the shutter speed is high, less light goes into the camera through the aperture. If the shutter speed is low, the particle images are captured in motion, which leads to particle images being captured as short segments rather than individual snowflakes. The length of the particle-driven streaks depends on the camera shutter speed setting and the wind velocity. Preliminary measurements were made to check the proper shutter speed for the given wind conditions (see Figure 3.10).

Shutter Speed: 1/60   **Shutter Speed: 1/180**

Shutter Speed: 1/250   **Shutter Speed: 1/500**

Shutter Speed: 1/1000
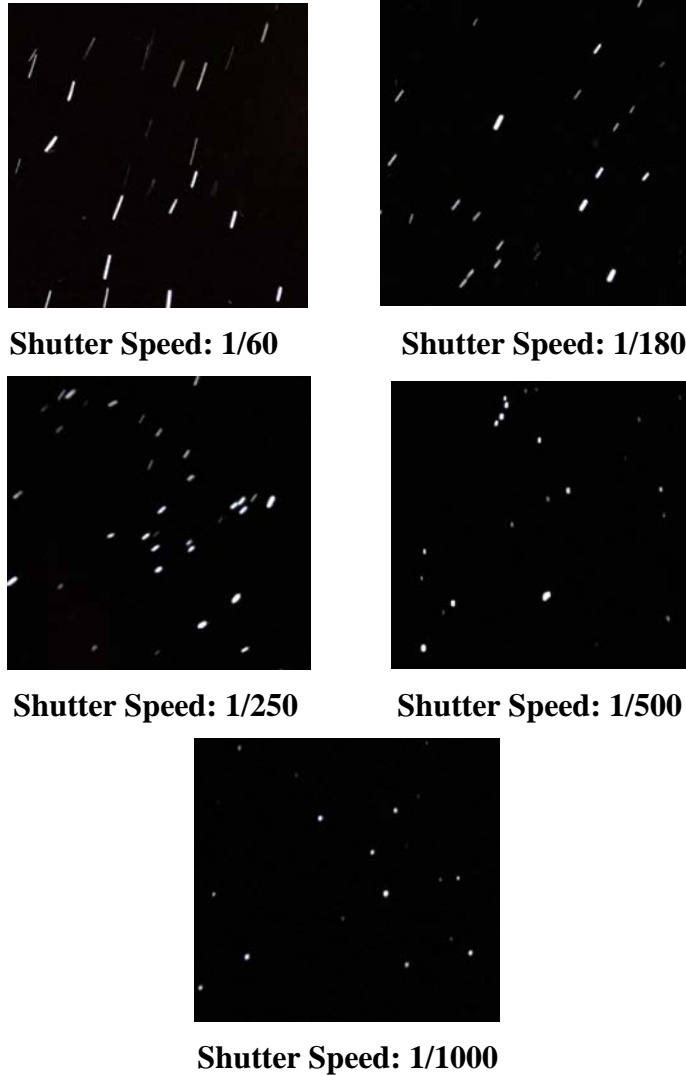
Figure 3.10. Sensitivity of shutter speed

The reduction of the shutter speed inherently leads to less sensor exposure and the possibility of smaller particles not being imaged at all. A tradeoff between illumination conditions, snowflake particle size, and wind velocity has to be made to get an optimum shutter speed for a specific situation. For safety, the recording of each test was done with a minimum of three shutter speeds so that the best combination could be selected during post-processing.

3.3.1.2.Photogrammetry

The images for the photogrammetric survey were acquired with an unmanned aerial vehicle (UAV): DJI Inspire 1 model with the Zenmuse X3 Gimbal camera attached (see Figure 3.11).

Figure 3.11. DJI Inspire 1 unmanned aerial vehicle

The DJI Inspire 1 model has the ability to take 4K resolution videos or 12.4 megapixel photos and store them on a micro SD card. The camera focal length is 20 mm. The drone can operate with a maximum speed of 49 mph at a temperature range of -10 to 40°C; the average flight time per battery is 18 minutes (http://www.dji.com/inspire-1/info). The images taken from the UAV are then input into the Agisoft software. The Agisoft software can generate a cloud of points with known coordinates surveyed by real-time kinematics (RTK). It can then extract the 3D terrain data from these images. Table 3.3 summarizes the individual components used for carrying out the photogrammetric survey.

Table 3.3. Summary of the components associated with the photogrammetric surveys

Image Technique	Role	Camera	Survey	Software
Photogrammetry	Reconstruct terrain/snow deposits	Zenmuse X3 Gimbal camera	Aerial (UAV)	Agisoft

3.3.1.3 Real-Time Kinematics (RTK)

Satellite navigation is a surveying technique used for geo-referencing the locations of the GRPs needed in the photogrammetric surveys in this study. RTK is a GPS-based positioning system capable of recording the real-time horizontal and vertical elevation of [x,y,z] coordinates. During the measurement, RTK is consecutively placed on the top of each reference point to get the final reading. The three main devices constituting the RTK instruments—receiver, hand-held data collector, and phone used for wireless communication—are shown in Figure 3.12(a).

Figure 3.12. Real-time kinematics: (a) components, (b) testing location, (c) mapping result showing bathymetry

The instrumentation uses the wavelength of the signal to connect to the satellite to obtain accurate coordinates. The RTK accuracy has continued to improve over time to such a degree that today the RTK accuracy for locating a survey point is sub-centimeter in the horizontal plane and on the order of few centimeters in the vertical plane. Results of preliminary runs conducted with the RTK to become familiar with its usage and refine the survey protocols are shown in Figures 3.12(b) and 3.12(c).

3.3.1.4 Real-Time Communication Web Camera

The imaging instruments used for monitoring the snow drift experiment was a Moultrie P-180i video camera, as shown in Figure 3.13(a).

Figure 3.13. Imaging instruments: (a) Moultrie P-180i camera, (b) Moultrie Mobile Field Modem MV1, (c) site with the Moultrie products installed, (d) user interface of the real-time monitoring system, (e) sample image taken from Moultrie camera

The monitoring scope was two-fold: to observe the dynamics of snow accumulation at the fence site and to check the integrity of the equipment deployed in the field. The camera is equipped with the ability to take 180° panoramic view images at full 4K resolution. The camera was set to record images every hour under the time-lapse option and to store the images on the external memory card. The camera was attached to a communication unit (modem), shown in Figure 3.13(b). This was needed to transmit the images recorded with the camera to the Moultrie Mobile server. The camera, modem, and external battery to supply the power were bundled inside a weather-proof case for convenience and safety purposes, as shown in Figure 3.13(c). In this configuration, the camera system is a standalone, self-powered, real-time data transmission device. The client-user interface and a sample image taken from the Moultrie camera are provided in Figures 3.13(d) and 3.13(e), respectively.

An additional webcam was installed at the same experimental site, as shown in Figure 3.14(a).

(a)   (b)
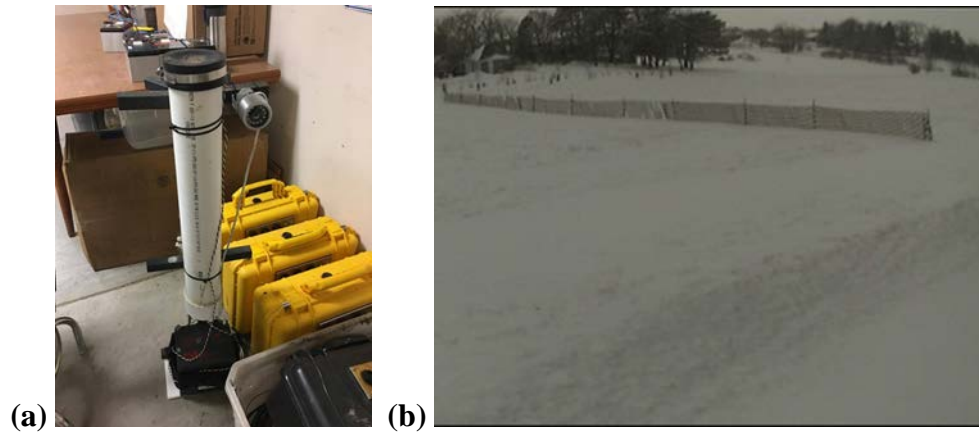
Figure 3.14. Webcam components: (a) IFC webcam and (b) sample image taken from IFC webcam

This prototype webcam with real-time communication capabilities was built by the Iowa Flood Center (IFC) and deployed as backup in case of failure of the Moultrie camera and possibly to gather more information. The camera was fitted with an external battery to supply power and was programmed to sample images at a rate of one image per hour and transmit the images to the server. A sample image taken with the IFC webcam is provided in Figure 3.14(b). The overall setup of the Moultrie and IFC camera assembly deployed at the snow drift experimental site is shown in Figure 3.15.

(a)   (b)
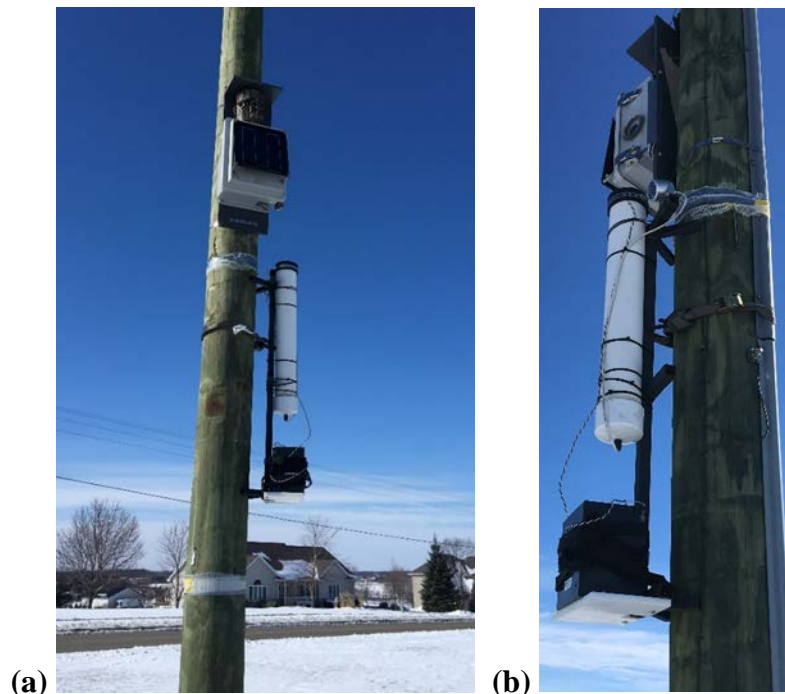
Figure 3.15. (a) Front and (b) side views of the Moultrie and IFC web camera assembly

The Moultrie Mobile and IFC webcams were not used for quantitative mapping of the snow deposition; rather, they were used to observe the site, plan site visits, and capture the dynamics of the snow deposits during and between storm events.

Three anemometers for measurement of the local wind velocity were installed at various experimental sites and were tested: a Vaisala anemometer, a Young anemometer, and a Davis Vantage Pro2.

The Vaisala anemometer is a custom-made instrument assembled by IIHR – Hydroscience & Engineering in 2012. It is a standalone unit that contains its own house-made cell modem in order to transmit the signal and connect to an IIHR server and a 12V external battery attached to the solar panel, as displayed in Figure 3.16(a).

(a)   (b)
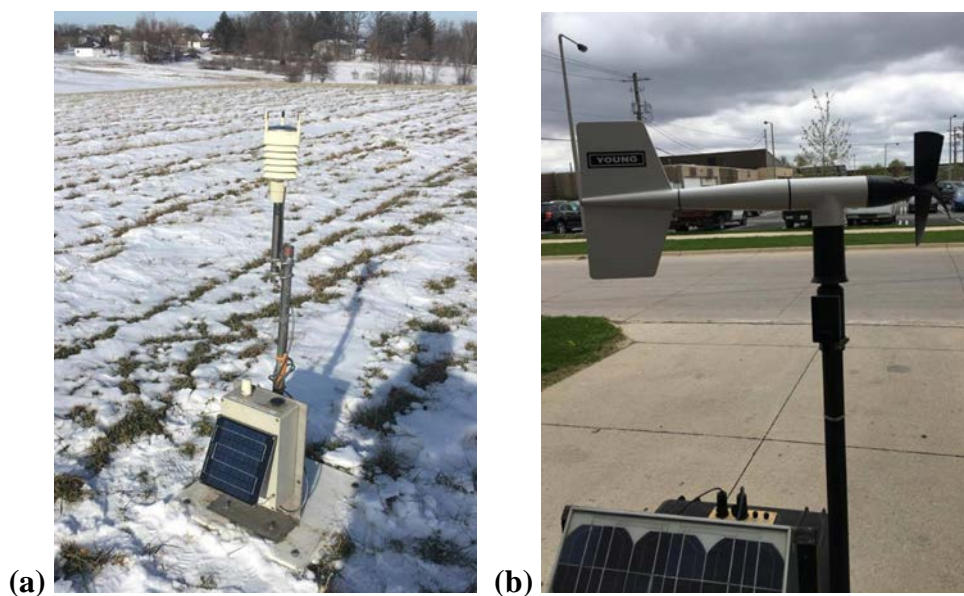
Figure 3.16. Anemometers: (a) Vaisala anemometer and (b) Young anemometer

The Vaisala anemometer measures wind velocity by using the speed of sound. The wind sensor has three equally spaced ultrasonic transducers. To determine the wind speed and wind direction, the anemometer measures the time the ultrasound takes to travel from each transducer to the other two.

The Young anemometer wind monitor model 05103, shown in Figure 3.16(b), is a commercial standalone anemometer connected to a Campbell Scientific CR10X datalogger. The anemometer can be adjusted for sampling time, duration, and the type of output data. The recorded wind data is stored internally on a memory unit.

Both the Vaisala and Young anemometers were programmed to sample every 15 seconds and to transmit the wind data every hour to the database. The measurement output for the two anemometers consists of wind magnitude and direction.

The Davis Vantage Pro2 anemometer is a meteorology station containing the Vantage Pro2 console, as shown in Figure 3.17.

Figure 3.17. Wireless Vantage Pro2

The console monitors several weather parameters: wind intensity, wind direction, temperature, humidity, barometric pressure, and daily and monthly precipitation data. The data are stored internally in the station, but the anemometer is very limited in terms of the adjustments that can be made to the data sampling parameters.

3.3.2   EDPIV PTV Software

The PTV measurements for this study were processed with a customized EDPIV software (http://lcgui.net). EDPIV stands for "evaluation software for digital particle image velocimetry" and was developed at IIHR – Hydroscience & Engineering. The software contains a wealth of PIV and PTV processing algorithms that can be engaged in complex measurement conditions to overcome issues associated with limitations in one or more image velocimetry components (e.g., illumination or flow seeding quality). The software accepts only black and white images in 8-bit Windows bitmap format that are obtained with additional software (Adobe Photoshop). Beyond containing robust PIV and PTV spatial analysis algorithms, the software includes several image conditioning steps such as image conversion and the removal of background disturbances and background noise.

3.3.2.1 Setting Image Processing Parameters

With a given set of recorded images, a trial-and-error approach is needed before processing the snow experiment data. It is essential to select the appropriate interrogation and searching areas when doing the post-processing in PIV so that velocity is accurately estimated. This limits the maximum size of the interrogation and searching areas. However, the expected particle movement from the images has to be determined before applying the size of the searching area in

42

order to optimize the velocity vectors. When the statistical algorithm is implemented, some error in the predicted value of the velocity vector will result if the particle can move out of the searching area. Setting the searching area to be larger than the expected particle displacement also reduces the accuracy of the algorithm. Typically, another filter is then applied to set up the velocity vector correlation. Therefore, by estimating the average displacement of the particles between images to specify the correct searching area size and by applying an appropriate correlation factor, the accuracy of the instantaneous velocity vector field predicted by the algorithm can be dramatically improved.

The main steps in using the EDPIV for our snow experiment are summarized in Figure 3.18.
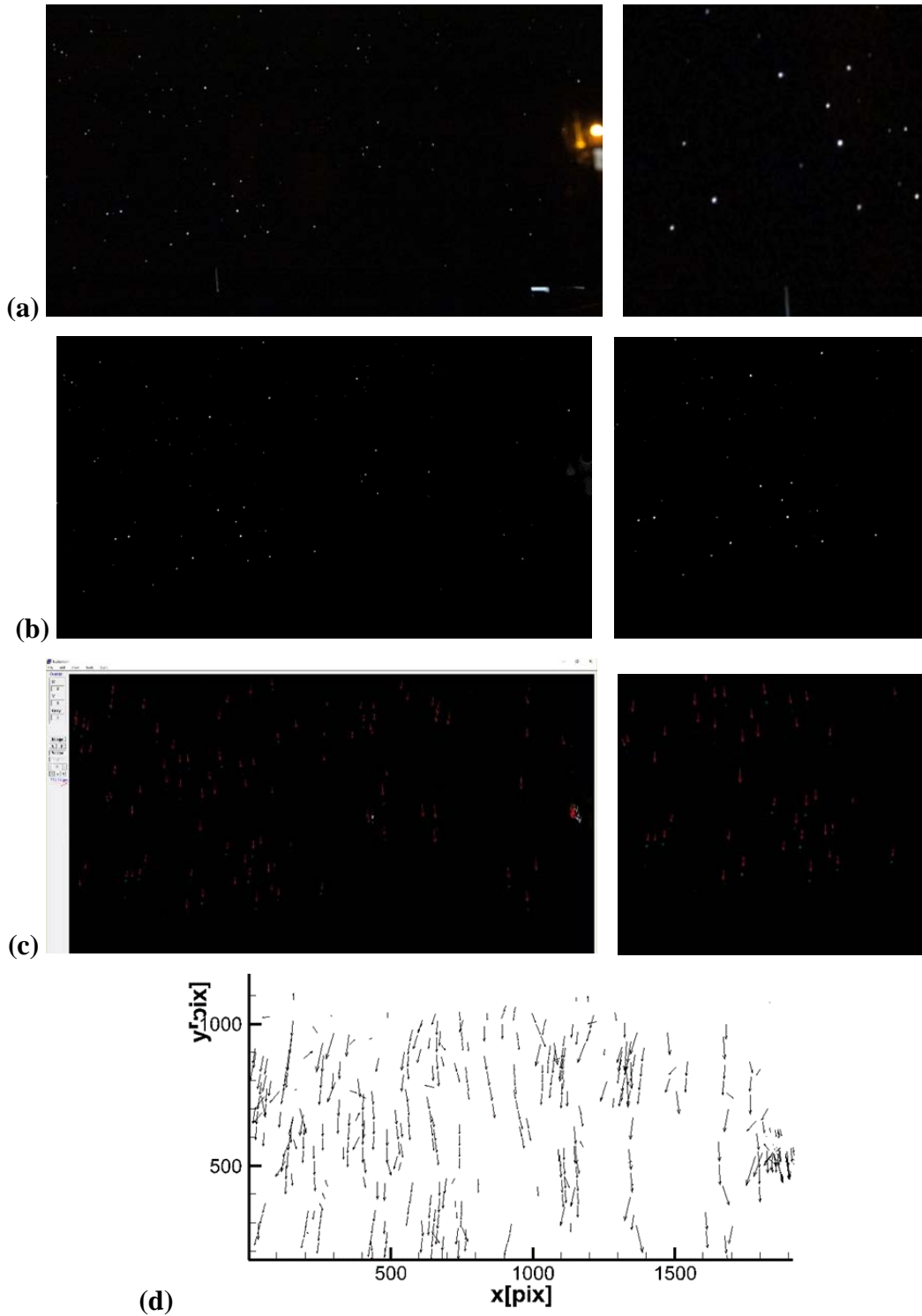
Figure 3.18. Selected screenshots of the EDPIV software applied to snowfall measurements: (a) sample raw (color) image from a snow fall event, (b) sample image after removing background noise and applying size filtering, (c) instantaneous velocity field plotted within the EDPIV software interface, (d) Tecplot file of the averaged velocity field for 200 processed images

3.3.3 FUDAA-LSPIV Software

An alternative image-based method used for the quantification of snow transport dynamics is LSPIV. The LSPIV experimental data were processed with open-source, customized software called FUDAA-LSPIV (https://forge.irstea.fr/projects/fudaa-lspiv). FUDAA-LSPIV was developed by Electricite de France Company (EDF) and IRSTEA (National Research Institute for Environment and Agriculture). The software contains user-friendly graphical interfaces for processing LSPIV data and calculating the final velocity vector field. This software uses a 256 gray-level format and VirtualDub software to convert the videos into images of a specific format. The FUDAA-LSPIV software features a Java interface atop a Fortran executable that allows the user to ortho-rectify the images, calculate the surface velocities of tracer movement from the statistical analysis, apply filters to time-average velocities, and visualize the velocity vector field.

The LSPIV software was tested to track the snowfall movement. The experimental setup for the preliminary tests was set to use a background (canvas) that contrasted with the snow particles and that used artificial light to enhance particle visibility. The orientation of the canvas background was determined using a handheld anemometer to ensure that the background was aligned with the dominant wind direction. Eight points were also marked/painted for reference. Figure 3.19(a) shows the experimental setup for the preliminary runs, and Figure 3.19(b) shows the images taken during the snow event.
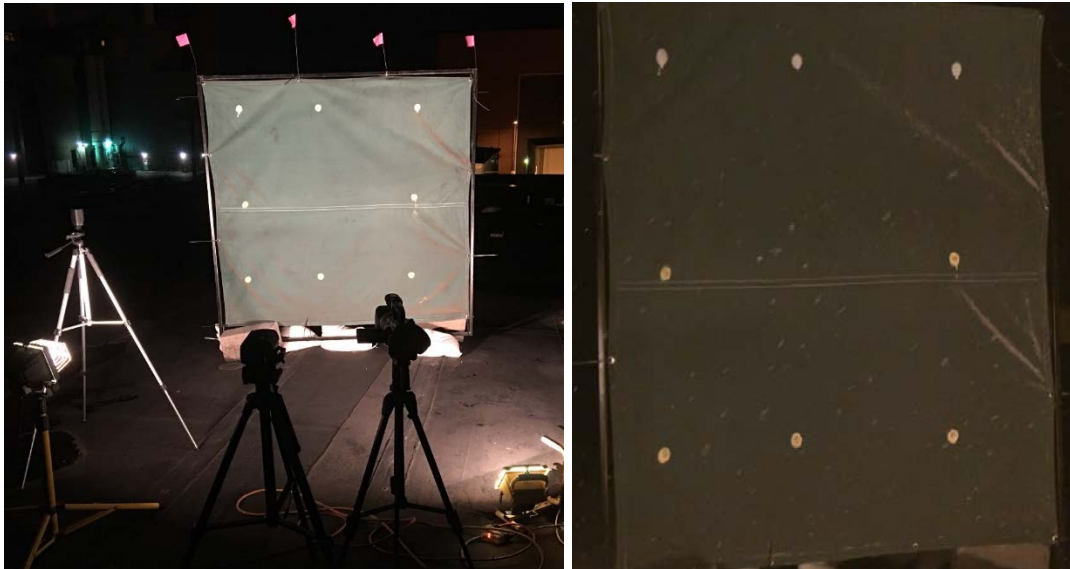
Figure 3.19. Preliminary LSPIV testing: (a) experimental setup and (b) image taken during November 20, 2015 event

The final velocity vectors shown in blue in Figure 3.20 were obtained using the FUDAA-LSPIV software.
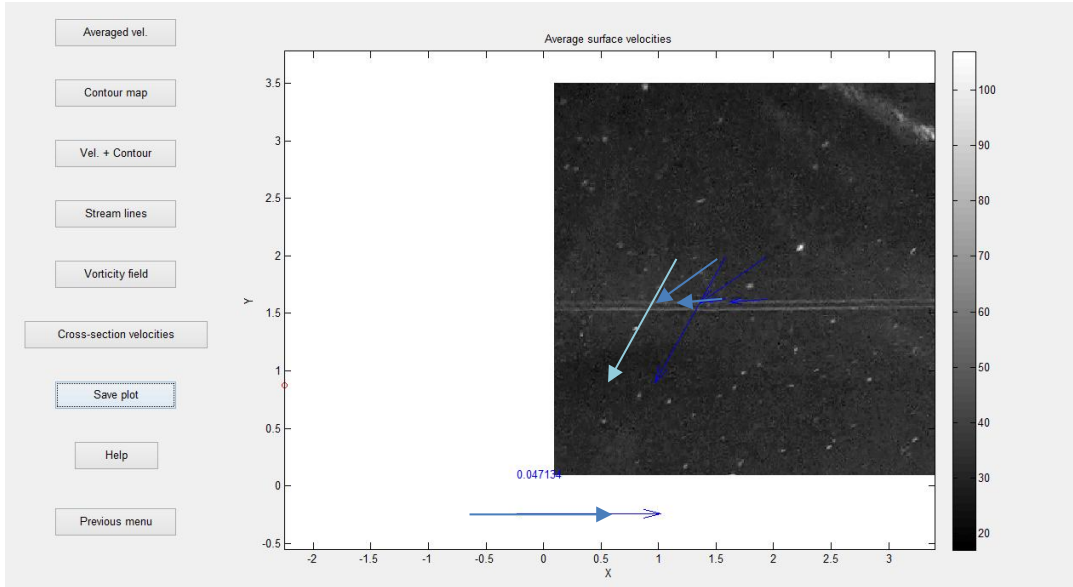
Figure 3.20. Final results computing by FUDAA-LSPIV software for preliminary tests

The technique was originally intended for the quantification of snow drift, but during the preliminary measurements it was concluded that the technique is not adequate for quantifying snowfall. Later in the study, however, field observations led to the conclusion that this technique is suitable for measuring snow drift; therefore, it was kept as one of the study tools. FUDAA-LSPIV does not produce good results for tracking vertical snowfall velocities; therefore, the FUDAA-LSPIV software was used for quantifying horizontal snow drift in this study.

3.3.4 Photogrammetric Survey

Photogrammetry surveying was used in this study to measure the deposition of the snow. Traditional aerial photogrammetry was applied. Multiple images were taken at various angles using the UAV DJI Inspire 1. The camera was attached underneath and was pointing straight down toward the region to be imaged. Figure 3.21 summarizes the measurement protocol.
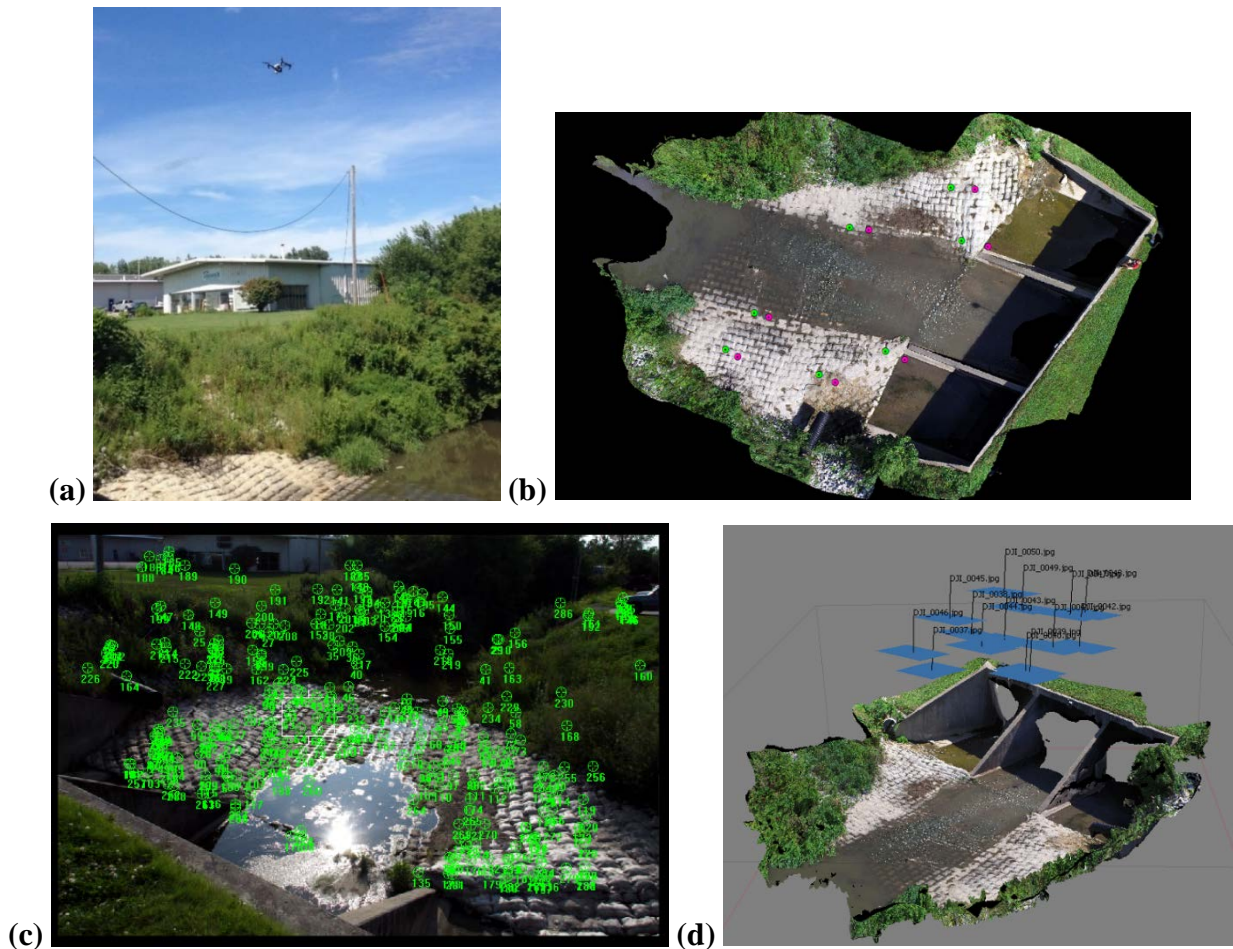
Figure 3.21. Measurement protocol used for UAV photogrammetry survey at a culvert site: (a) UAV mapping the three-box culvert, (b) covered area for photogrammetry survey, (c) clouds of tie points generated by software, (d) 3D reconstruction of culvert using photogrammetry method

Figure 3.21(a) shows the DJI Inspire 1 drone taking images over a three-box culvert with the image framing covering an area of 1500 m^2. Fourteen ground reference points were marked by temporary paint and then surveyed using RTK, as indicated in Figure 3.21(b) by green and red dots, for post-processing. Although the Agisoft software generated tie points, it did not visualize the tie points used. Figure 3.21(c) shows an example cloud of tie points created by the previous experiment's software (ERDAS) for the reconstruction process. The final output from Agisoft is displayed in Figure 3.21(d). This example shows the high resolution of this approach, which is able to accurately recreate a 3D model of the culvert using data from the photogrammetric survey. However, because the culvert contains a broad spectrum of colors and texture gradients, careful attention is required when applying the photogrammetric survey technique to determine the shape of the snow deposit at a (snow fence) site.

CHAPTER 4: PROTOCOLS FOR METHODOLOGY VALIDATION

Three experimental sites were chosen to validate the methodologies used to quantify the snowfall and snow drift velocities. Both snowfall and snowdrift sites were intentionally selected close to Iowa City, Iowa, to allow deployment of the instrumentation as soon as a storm event occurred.

The snowfall experiment was assembled on the rooftop of the IIHR – Hydroscience & Engineering building, which is indicated by a red dot in Figure 4.1. The experiment was conducted using the PTV technique described in Chapter 3.

The goal of the snow drift experiment was to visualize and quantify the horizontal movement of snowflakes near the ground. The LSPIV technique was used for this analysis. The snow drift measurement site is located along a railroad. Its position is indicated by the green dot in Figure 4.1.
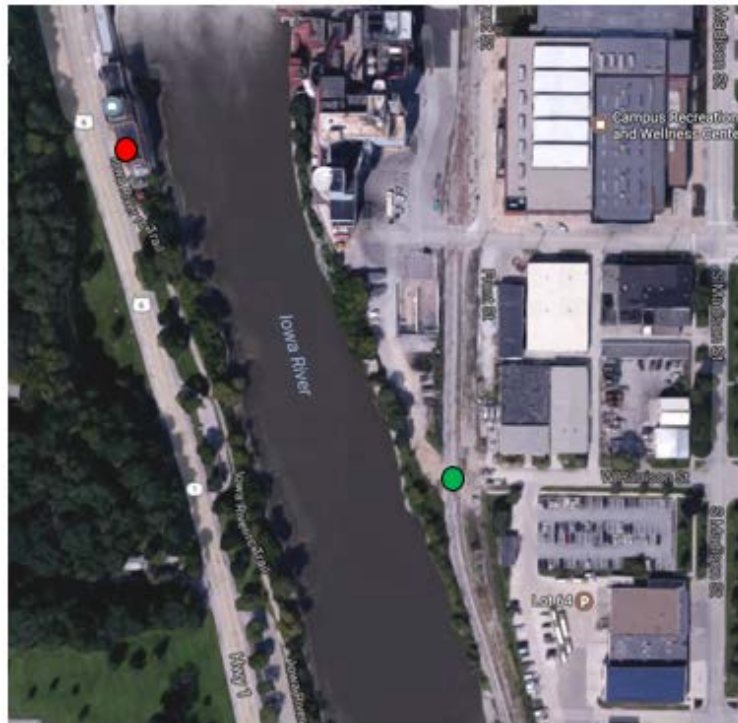
Figure 4.1. Locations of the snowfall and snowdrift experimental sites

There is a free fetch for the wind to pick up at the measurement site. The site is situated in a relatively flat area, where the wind is practically undisturbed by the presence of buildings.

Lastly, the in situ snow drifting site located in Shueyville, Iowa was suggested by the Johnson County Secondary Roads Maintenance Superintendent to evaluate the SRC and to map the volume of snow deposited at the fence during the winter season.

4.1 Snowfall Measurements (2015–2016 Winter Season)

4.1.1 Experimental Arrangement

The snowfall experiment was conducted on the rooftop of the IIHR – Hydroscience & Engineering building, which is located in Iowa City, Iowa, on the bank of the Iowa River. The building is fairly isolated from the other buildings on the university campus, precluding the interference of flow disturbances (e.g., wakes) induced by the presence of other buildings. The vertical distance from the sidewalk to the rooftop, where the snowfall experiment was conducted, is 14.33 m, as shown in Figure 4.2.

Figure 4.2. IIHR – Hydroscience & Engineering building where the snowfall experiment was conducted

The experimental setup of the snowfall experiment is shown in Figure 4.3.
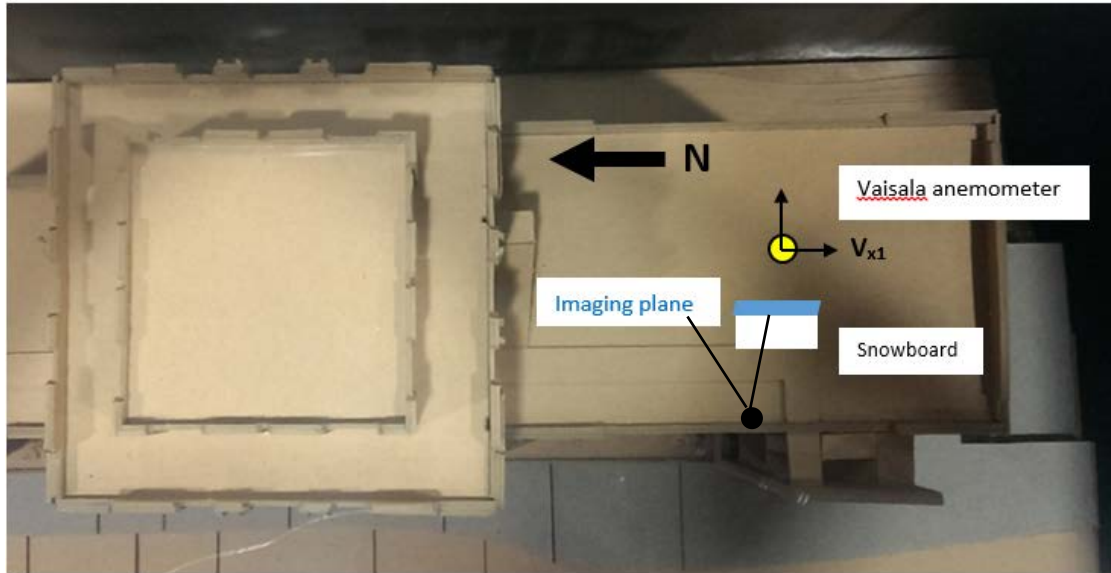
Figure 4.3. Experimental setup used for the snowfall experiment

In this study, a snowboard (white board), as recommended by meteorological standards, was used to measure the snow depth. A Vaisala anemometer (the yellow dot in Figure 4.3) was used to measure the local wind velocity at the site. A Sony 4K video camera (FDR-AX100) (the black dot in the same figure), which was attached to the handrail of the ladder, was used to record the snowflakes' movement continuously during the snowfall event.

The standard procedure used by the Community Collaborative Rain, Hail, and Snow Network (CoCoRaHS) recommends that a snow measuring board created from a 16 in. by 16 in. piece of ½ in. or ¾ in. plywood be employed. Although the board installed on the rooftop of the IIHR – Hydroscience & Engineering building was a 3 ft by 5 ft piece of plywood with a ½ in. depth that allowed the measurement of the "in-depth" snow, as shown in Figure 4.4, the differences in the dimensions of the plywood were inconsequential to the results.

Figure 4.4. Snow measurement board used to measure snow accumulation as part of the rooftop experiment

The camera's field of view consisted of a rectangular plane with dimensions of 0.73 m by 0.43 m (W×H), as presented in Figure 4.5.

Figure 4.5. Vertical plane in which the movement of the snowflakes was visualized

The imaging plane was orientated parallel to the local dominant wind direction and perpendicular to the camera. A ruler was attached to the experimental setup to estimate the relative scale of the image. Given the close distance between the camera and the imaged field and the normal-to-image angle, it was unnecessary to correct for image distortions when the PTV processing algorithm was applied to the recorded images. This approach is called the large PTV technique because the image is large, irrespective of whether the images are distorted or not. The method is described in detail by Admiraal (2017).

A Vaisala anemometer was chosen because it measures wind magnitude and wind direction in two dimensions, labeled here as V_{X1} and $V_{Y1,}$ respectively. The x-direction of the rectangular plane shown in Figure 4.5 is co-directional with the Vaisala anemometer's V_{X1} direction (see Figure 4.3). A comparison of wind velocity estimates given by three different types of anemometers are presented in Chapter 4.1.3 as part of assessing the Vaisala anemometer's accuracy in measuring wind velocity.

Using the recorded videos of the snow events in conjunction with the image velocimetry EDPIV software, the individual snowflake velocity vectors can be obtained. The EDPIV processing procedure described in Chapter 3.3.2 provides snow particle velocities in the V_X and V_{Y1} directions. The V_X velocities obtained using EDPIV were compared to the wind data output from the Vaisala anemometer, V_{X1}, to determine the relationship between these two velocity vectors. The main assumption is that the snowflakes behave as "good" air-flow tracers because they are relatively light and small.

Once the snowfall experiment site was chosen, several issues regarding optimization of the recording process had to be addressed. In order to track particles with the image-based technique, the background color of the image has to contrast with the snow particles' color for accurate particle identification and for specification estimation for sizing purposes. The University of Iowa's power plant located across from the IIHR – Hydroscience & Engineering building has red brick walls. By facing the camera toward the power plant, the needed background was created. Using this experimental setup, it was easier to identify the snow particles and to track them during daytime measurements. Given that during the 2015–2016 winter season the majority of the snowfall events occurred during the night, a Rigidhorse 42 in. 240 W straight Philips LED light was deployed, as shown in Figure 4.6, and placed in front of the snow measurement board in order to create a light sheet shining upwards, as shown in Figure 4.7.
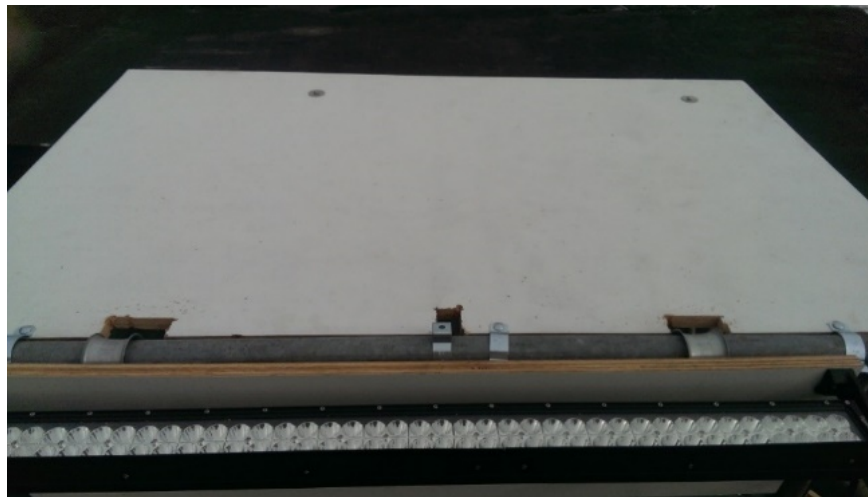
Figure 4.6. Rigidhorse Philips LED light used for nighttime illumination

Figure 4.7. Rigidhorse Philips LED light used to conduct nighttime snowfall experiments

The light sheet created by this source was effective in illuminating the particles during nighttime, as shown in Figure 4.8.

Figure 4.8. Sample of enhanced image of snowflakes obtained using the EDPIV software

The raw images were adequate to be processed by the EDPIV software after more preprocessing steps were applied to the raw images.

4.1.2   Measurement Protocols

Several protocols for efficiently capturing the particle movement during the snowfall experiments were tested and then deployed. The first step was to monitor and document the weather conditions using data provided by local meteorological stations (https://weather.com). This step was needed to identify possible events and trigger preparation of the experiment whose purpose was to measure snowfall during a snow event. Once a high chance of snow precipitation was forecast, the various devices needed to perform the experiment (video camera, lighting, power for instruments) were deployed at the site. During each snow event, a camera was attached to a tripod, which was connected to the handrail on the top of the IIHR – Hydroscience & Engineering building. Once the camera was in place, several parameters had to be adjusted: zoom level to aim at the area of interest, manual shutter speed to optimize the image quality, and manual focus for the camera lens to focus on the image plane. For each storm event, multiple recording segments ranging from 30 to 60 seconds were captured to provide a mean description of the snowfalling movement. In most cases, recordings were taken in three segments. These data were then used to obtain an averaged value of the total snowfall velocity for each event. After the recording process was finished, the next step was to estimate the snow depth using the snowboard device and the snowflake size using the black cardboard and information on the snow type, as seen in Figure 4.9.

Figure 4.9. Snowflakes on cardboard, used to infer snowflake characteristics

This was needed because the snowflake shape and density are a function of the surrounding pressure, temperature, and precipitation type (Garrett et al. 2012, McClung and Schaerer 1993).

4.1.3 Wind Data Acquisition

Three anemometers were tested during the 2015–2016 winter season: the Vaisala anemometer, the Young anemometer, and the Davis Vantage Pro2 device. The locations of the three anemometers are shown in Figure 4.10.
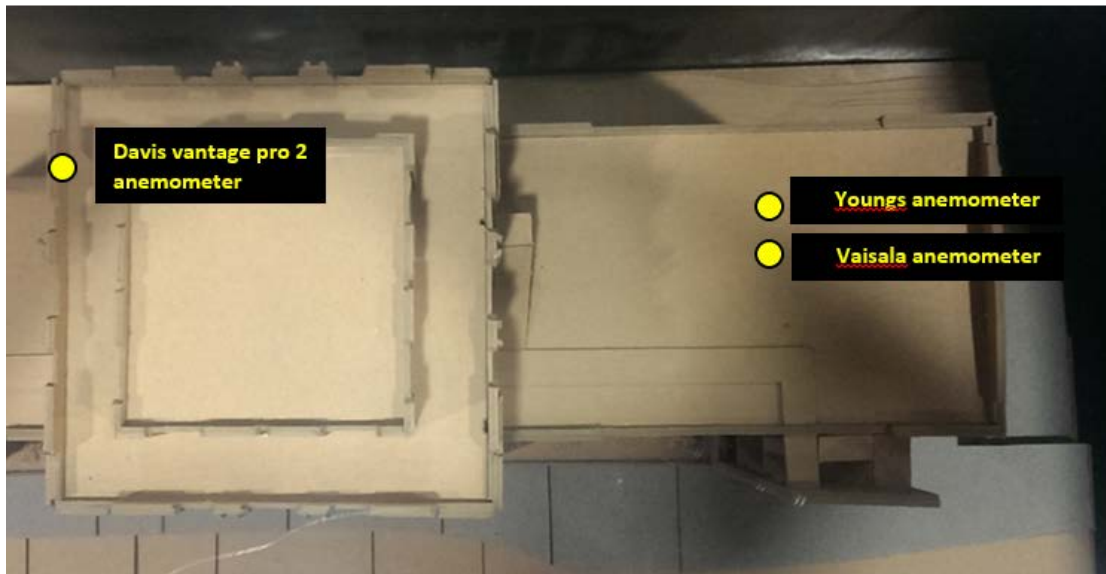
Figure 4.10. Locations of the three anemometers used to measure wind velocity during the snowfall experiments

The purpose of this comparison was to identify the optimum wind measurement instrument for the experiments. An essential feature of the instruments used to measure the wind velocity was that they be able to record the data continuously and store them for subsequent retrieval.

During the deployment, each of the three anemometers was aligned with the true north direction and marked with an arrow printed underneath each sensor. This was needed to ensure that the measurement instruments obtained measurements in the same coordinate system. The outputs of the Vaisala and Davis Vantage Pro2 anemometers contain various weather parameters, including the following: wind mean direction (D_m), wind maximum direction (Dx), wind mean speed (Sm), wind maximum speed (Sx), ambient temperature (Ta), relative humidity (Ua), barometric pressure (Pa), rain accumulation (Rc), rain duration (Rd), rain intensity (Ri), and rain peak (Rp). The Young anemometer was programmed to output only wind mean speed and mean direction. The essential variables that needed to be measured for the present experiments were the wind mean direction in degrees and wind mean speed in meters per second.

The Vaisala and Young anemometers were deployed on the rooftop and placed side by side to test the variation and similarity of the wind data, as shown in Figure 4.11.

Figure 4.11. Setting of the Vaisala and Young anemometers on the roof of IIHR – Hydroscience & Engineering building

Both instruments were programmed to have a sampling time of 15 seconds over a recording period of 10 minutes for a total of 40 outputs. Because the Davis Vantage Pro2 anemometer could not be programmed to sample every 15 seconds, the data had to be catalogued every 15 seconds in real time and then compared with data from the Vaisala and Young anemometers for shorter time spans.

Two experiments were conducted to compare the measurements of the three anemometers. The experiments were conducted on February 19 and 22, 2016. The wind intensity and direction during these two experiments are plotted in Figure 4.12(a) and 4.12(b), respectively.
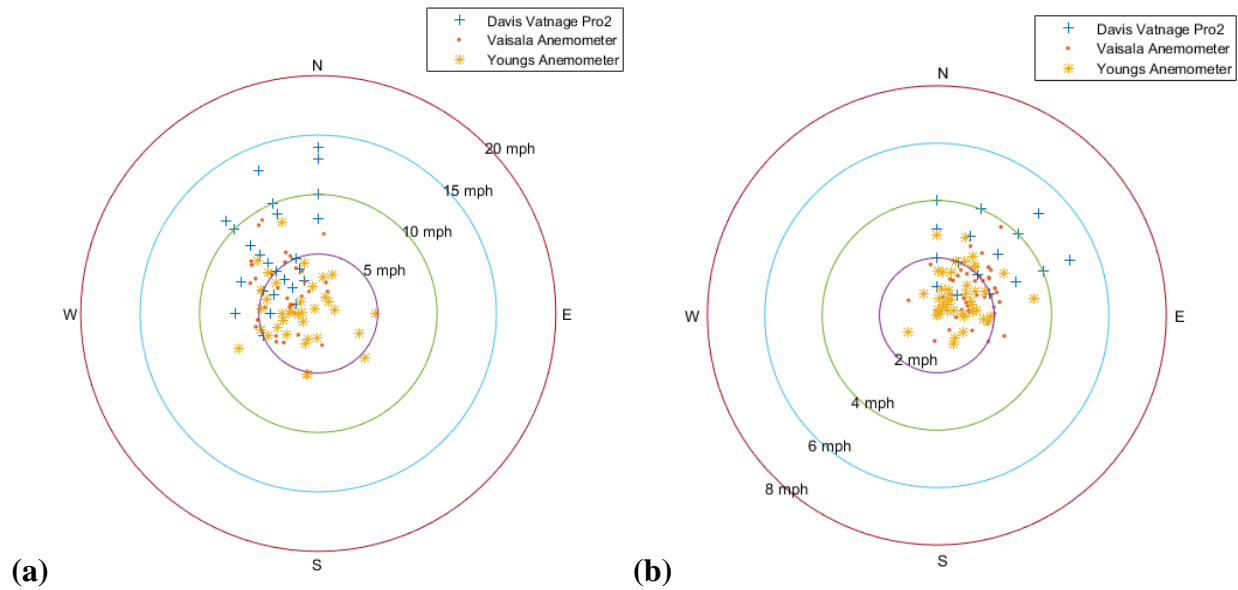
Figure 4.12. Comparison of data recorded by the three anemometers on (a) February 19, 2016 and (b) February 22, 2016

Wind intensities measured by the Davis Vantage Pro2 anemometer were always biased high compared to the measured values given by the other two anemometers. This can be attributed to the fact that the Davis Vantage Pro2 anemometer was installed at the highest elevation at a location where no obstruction could affect the measured data. However, due to the design of the IIHR – Hydroscience & Engineering building, both the Vaisala and Young anemometers' data could have been interrupted if the wind field was affected by the presence of some obstruction near the anemometers. The comparison of the measured data showed that the Vaisala and Young anemometers captured the wind variables relatively well during the snowfall event. The average differences in the wind intensity and direction between measurements conducted with these two anemometers are not statistically significant.

Another concern for the experimental arrangement was to ensure that the position of the test section was not subjected to artificial effects induced by the building geometry. Specifically, the test section was located on the lower roof of the building where the presence of the central, more elevated, part of the building could induce the development of a wake region with large-scale turbulence and changes in the mean wind direction. Sensitivity tests were conducted on February 27, 2016. During these tests, the Vaisala anemometer remained in the middle of the rooftop site, while the Young anemometer was placed at five different locations to measure the wind variables under various wind directions. Figure 4.13 shows the location of the Vaisala anemometer and the five locations where the Young anemometer was placed.
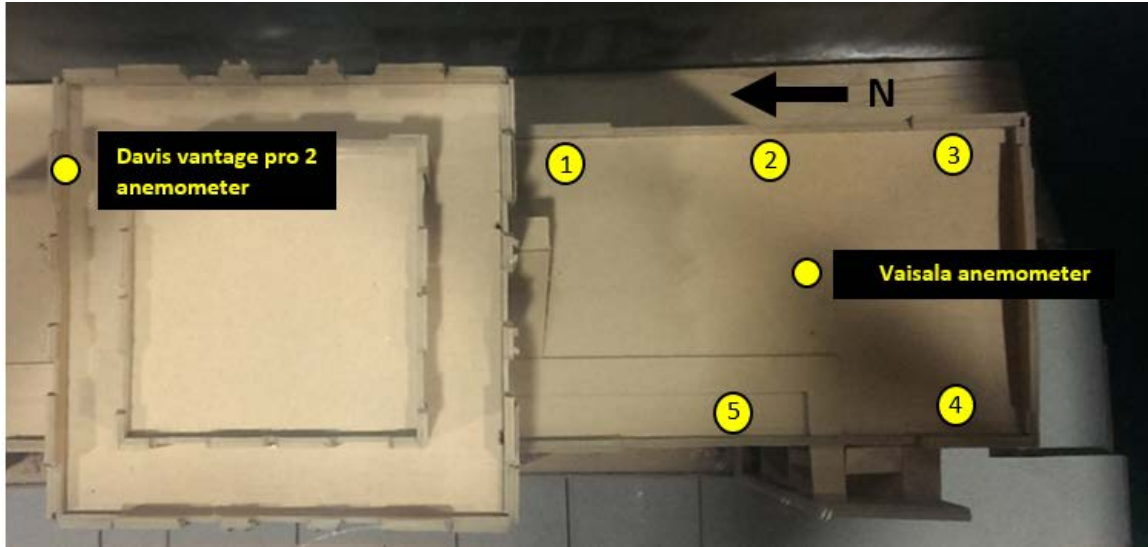
Figure 4.13. Locations of the Davis Vantage Pro 2 and Vaisala anemometers and the five locations where the Young anemometer was placed on the roof of the IIHR – Hydroscience & Engineering building

The results of placing the Young anemometer at five different locations are shown in Figure 4.14.
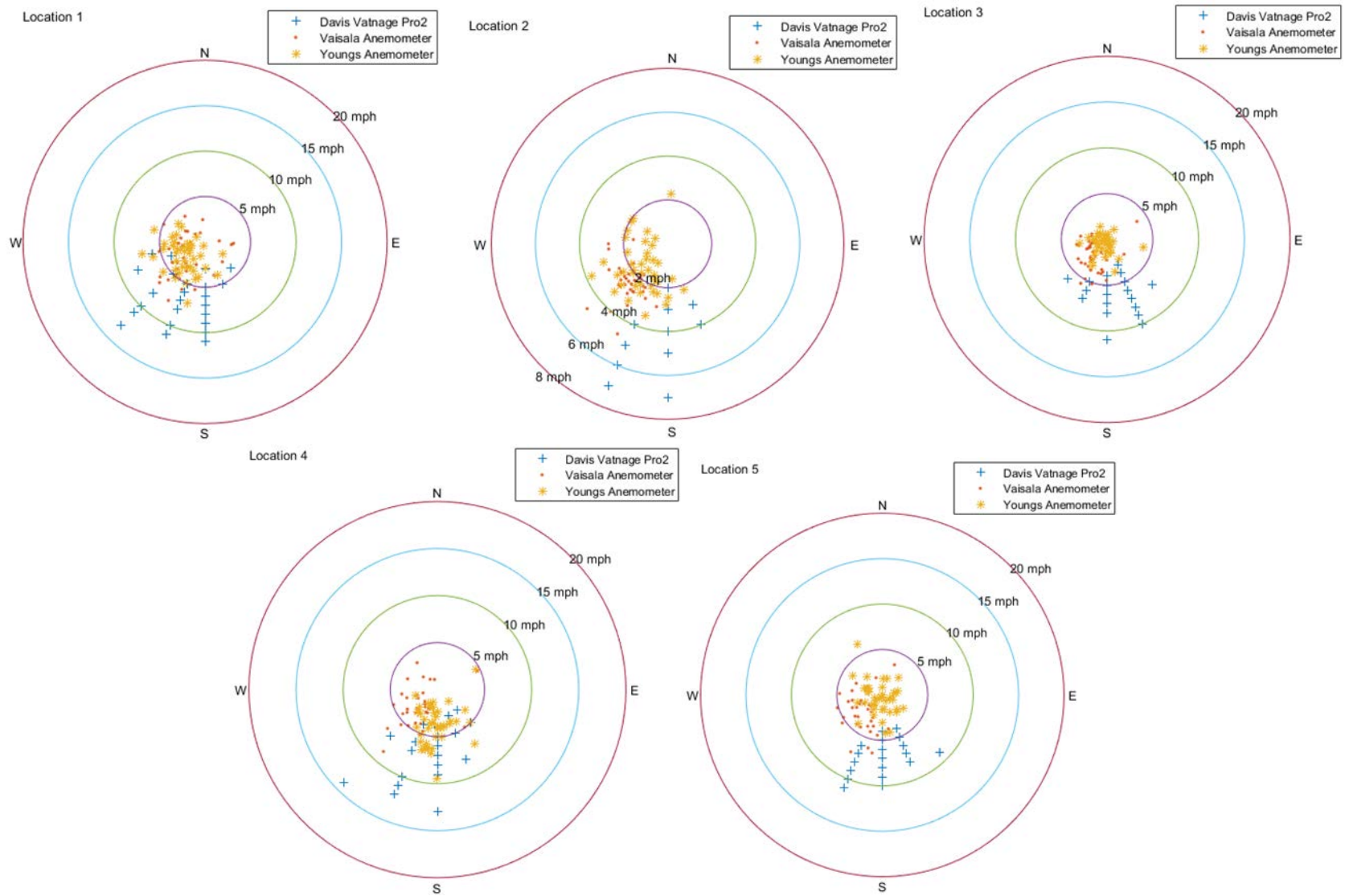
Figure 4.14. Comparison of wind specifications acquired using the three anemometers, with results shown for measurements conducted with different locations of the Young anemometer

The wind recordings are different for each of the five locations. However, most of the time good agreement between the Vaisala and Young anemometer readings was observed.

Following these tests in which three anemometers were used to measure wind variables, the Vaisala anemometer was chosen as the reference device to measure wind velocity and orientation. This decision was made because the Vaisala anemometer had the capability of storing large amounts of measured data on the server. By comparison, the Young anemometer requires the manual retrieval of the data with a computer or a laptop.

4.2 Snow Drift Estimation

4.2.1   Experimental Arrangement

The measurement of the snow drift required much more experimental testing prior to establishing a working measurement protocol. These measurements brought critical challenges for the image-based methods from several perspectives: lack of a sufficiently contrastive background for the snowflakes moving close to the bed and highly random snowflake behavior as the flakes approached the fixed snow layer and as they rolled along the snow bed. Moreover, the area of interest for determining the snow drift is located near the bed (for low winds, the process is confined to within a 2 ft height from the fixed snow layer). This left few choices for setting the camera in a position that would allow recording from an angle normal to the image plane. To accomplish the desired results, four different approaches, labeled herein as experimental arrangements (EA) 1 to 4, were implemented during the snow events that occurred during the 2016–2017 winter season. These arrangements are presented below with their strengths and weaknesses.

The EA 1 approach used a mobile station that contained an LED light and a 12V external battery placed about chest height. The illuminated area was aligned with the dominant wind direction. The main goal of the arrangement was to capture the snow drift movement at less than a person's height (Weather Online) to trace the snow drifting movement. A video camera with manual focus was used to focus on the image plane, as shown in Figure 4.15(a). The sample image obtained using this approach is shown in Figure 4.15(b).
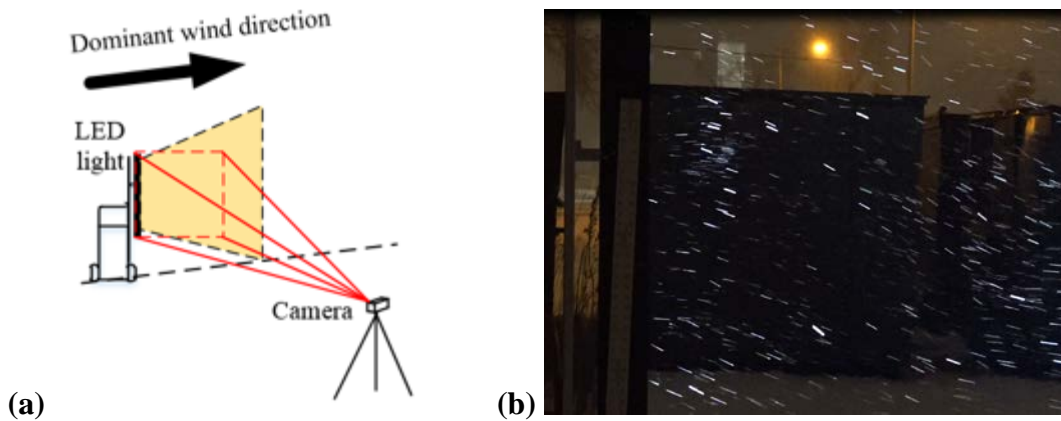
Figure 4.15. Experimental arrangement EA1: (a) experimental setup and (b) sample image

The EA2 setup was similar to that of EA 1, but the LED light was positioned lower. This allowed focusing on the near-bed movement. The EA2 setup is shown in Figure 4.16(a), and a sample image obtained at the site is shown in Figure 4.16(b).
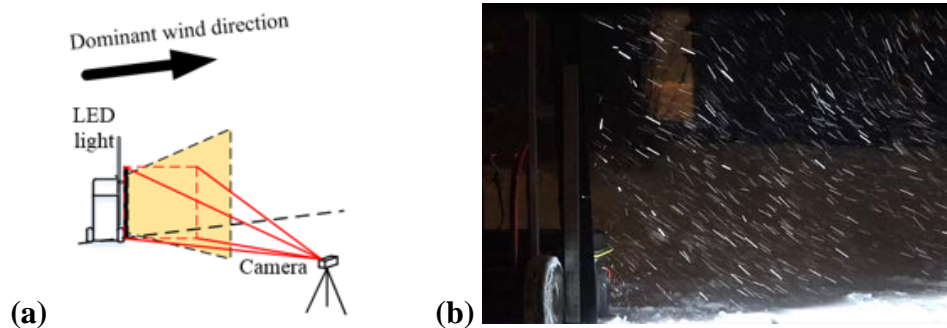
Figure 4.16. Experimental arrangement EA2: (a) experimental setup and (b) sample image

In the EA 3 setup, the LED light was placed horizontally with respect to the bed so that the light shone up. This allowed the entire vertical profile of the snow movement to be visualized, as shown in Figure 4.17.
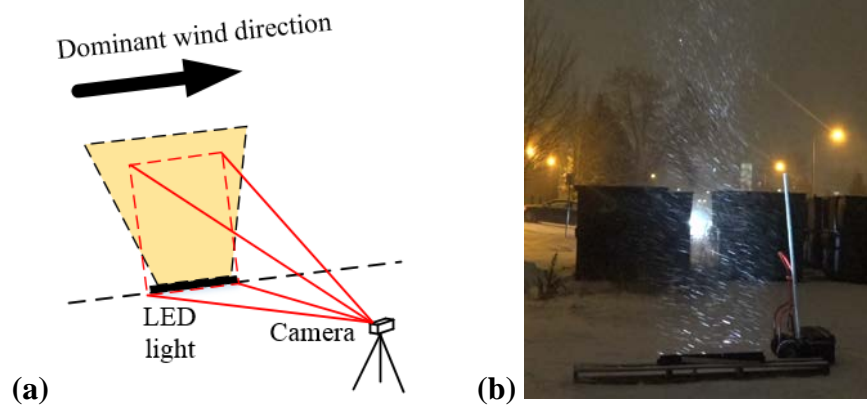
Figure 4.17. Experimental arrangement EA3: (a) experimental setup and (b) sample image

The setup of the EA4 experiment was similar to that of EA2, but setup for EA4 retained the ability to visualize the horizontal boundary layer, as shown in Figure 4.18.
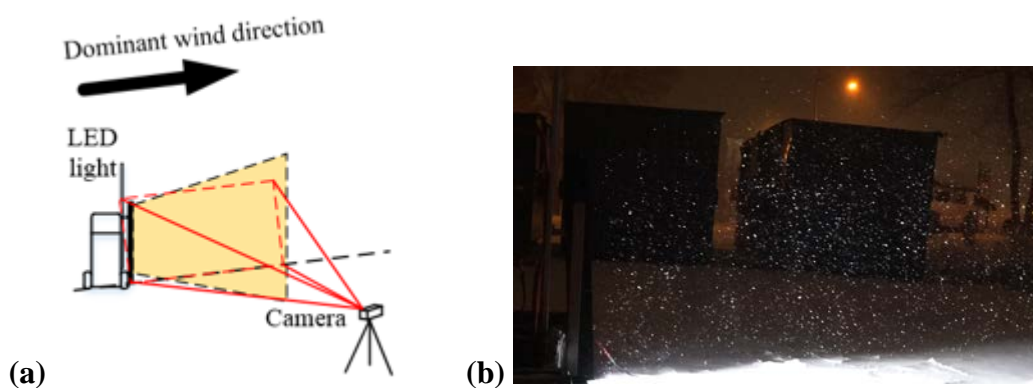
Figure 4.18. Experimental arrangement EA4: (a) experimental setup and (b) sample image

A concern about the setup of the snow drifting experiment was that the mobile station was on the same side as the dominant wind. Under this circumstance, the snow movement near the ground might be disturbed because the instrument could potentially block the snow transport. The aforementioned four setup configurations for the camera and light assembly with respect to the direction of the dominant wind near the ground were tested progressively and used to develop the new protocols for snow drift measurement.

Taking into consideration the lessons learned from the previously described tests, two new arrangements, EA5 and EA6, were proposed for performing future measurements that can accurately measure the snowfall and snow drift with a mobile station. EA5 was similar to EA4 but the station was placed against the dominant wind direction so that the snow drift area subjected to the measurements would not be disturbed by the instrument deployment (see Figure 4.19).
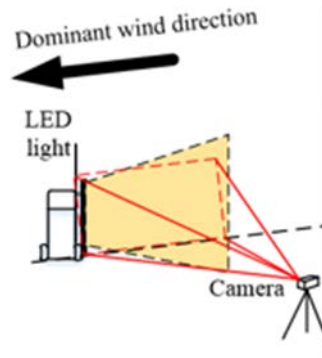
Figure 4.19. Experimental setup for EA5

To be able to perform more precise measurements near the bed, the LED light was placed horizontally and pointed down and focused on the bed. The goal was to track the snow sheet and the movement of the snow surface bedforms as a pattern instead of the movement of individual particles using particle image velocimetry techniques. This method was the best approach for quantifying snow drift because most of the snow transport contributing to the formation of the snow bedforms is associated with the movement of snow sheets that slowly advance over the stationary layer of snow deposited on the ground. Moreover, this method can be deployed even without the presence of active snowfall when only the drifting snow process is active, as shown in Figure 4.20.
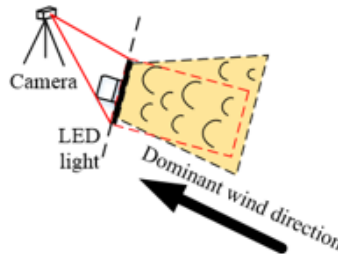
Figure 4.20. Experimental setup for EA6

Due to the insufficient number of major snow events during the 2016–2017 winter season, the performance of the EA6 experimental setup was tested in laboratory conditions. The snowflake and snow bedform movements were simulated by melamine plastic particles. These particles were identified through several preliminary tests aimed at replicating the snow drift movement over fixed snow deposits. This measurement arrangement and the ancillary experiment and processing protocols were first introduced as acoustic mapping velocimetry (AMV) by Muste et al. (2016). The implementation of the non-intrusive AMV technique for the snow transport case is readily applicable because sand transport in the boundary layer over a loose bed in an open-channel flow is similar to snow transport over a layer of deposited snow.

The new AMV implementation was tested using the experimental arrangement shown in Figure 4.20.
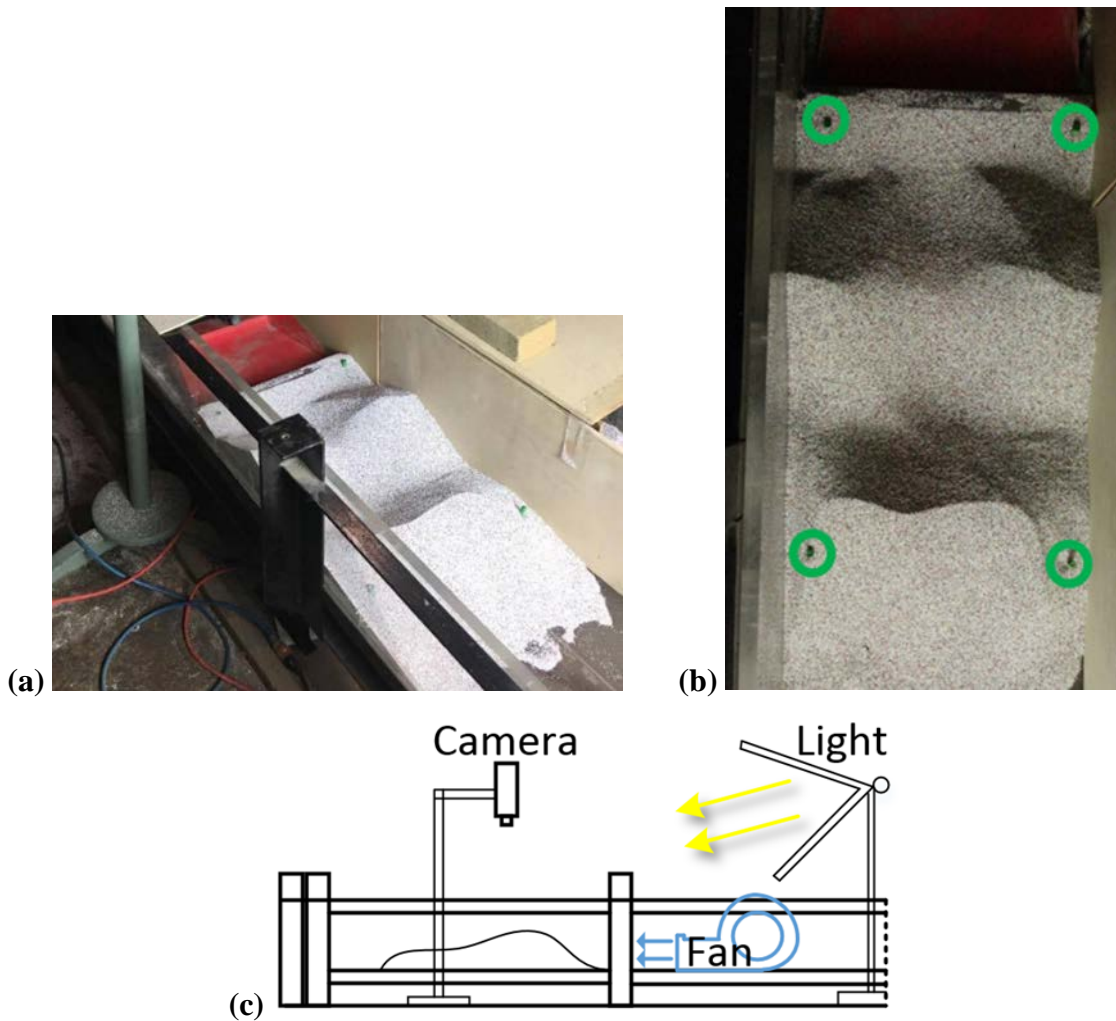
Figure 4.21. Experiment to simulate snow drift: (a) experimental flume, (b) test area as captured by the video camera, and (c) experimental setup

The experimental flume was 6 m long, 0.75 m wide, and 0.4 m deep, as shown in Figure 4.20(a). The testing area was 0.6 m long and 0.4 m wide, as shown in Figure 4.20(b). The entrance of the channel was connected to a Viper Racer, three-speed, transportable, 1/3 horsepower carpet fan to create a uniform wind intake. The wind conditions were controlled by setting three different speeds (approximately 10, 12, and 14 m/s) on the fan. Four ground reference points were created and painted in green. A trapping system extending over the whole width of the channel was designed to collect the particles moving as "bedload" associated with particle drifting. The Sony 4K camera was mounted on top of the flume, as shown in Figure 4.21(c).

The camera features a multi-angle positioning system that fulfills the needs of both LSPIV and photogrammetric analyses. The multiple angles are required to reconstruct the 3D model of the bedforms and snow dunes, as described in Chapter 4.2.2. Illumination was created by pointing the light at a low position toward the direction of flow to visualize the shadow from the dunes. This approach is readily usable for in situ night conditions and during daytime if a stronger light source is used for illumination to add the shadow effect. As demonstrated by Muste et al. (2016)

and in the next section, this experimental arrangement allows combining LSPIV and photogrammetry for tracking the dynamics of the snow bedforms and eventually estimating snow drifting fluxes.

4.2.2 Experimental Protocols

The protocol for measuring the snow drift focused on the moving layers migrating atop the fixed snow deposits rather than on the suspended snowflakes. The fraction of snowflakes in suspension is an integral part of the snow drift, but it represents a small fraction of the volume retained by the snow fence. This assumption is based on two considerations: (a) the concentration of snow in suspension decreases rapidly with the distance from the bed and (b) the mobility of the snow in suspension is considerably higher than that of the rolling bedforms approaching the snow fences. From a practical perspective, the latter process has the most negative influence on road visibility. Moreover, after snow starts being trapped by the snow fence, the suspended snow travels atop the trapped layer of snow and contributes little to the volume of snow trapped by the snow fence. From this perspective, the adoption of the AMV measurement protocol as developed by Muste et al. (2016) was expected to capture the main part of the snow transport relevant to snow fence design.

The AMV is, in essence, a combination of two techniques introduced in Chapter 3: image velocimetry and snow deposit mapping. The principle of the method used for snow deposit mapping performed using acoustic instruments is illustrated in Figure 4.22.
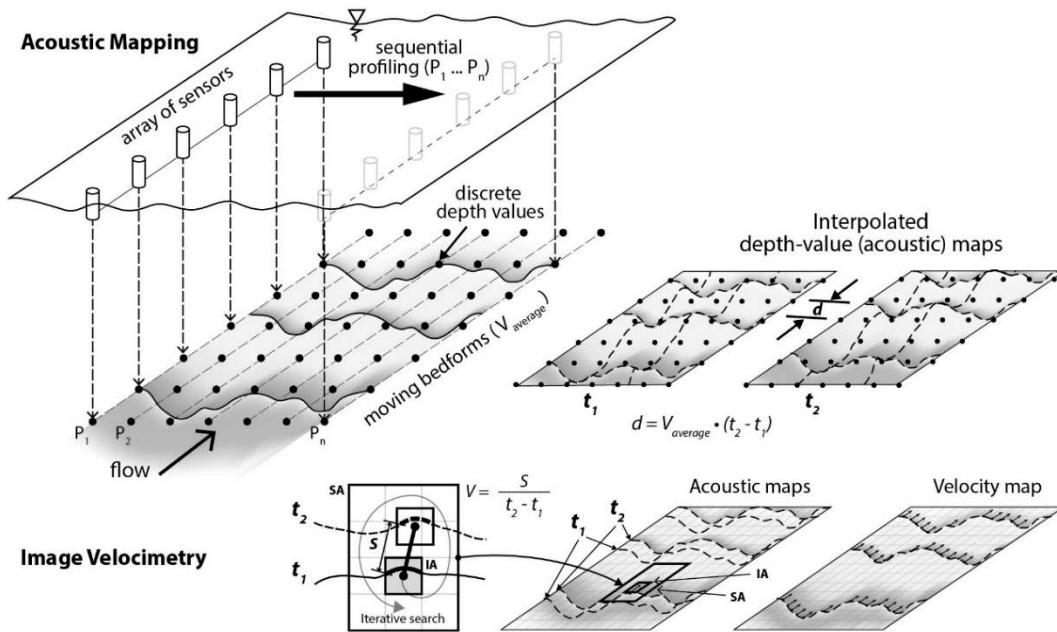
Adapted from Muste et al. 2015

Figure 4.22. Example of time sequenced bathymetry of a dune field obtained by acoustic mapping velocimetry

65

The raw bedform maps were obtained by scanning the channel bed with a linear arrangement of sensors while the flow in the channel was running. If bedform scanning is conducted with a sufficient density of data points, the discrete depth values acquired by each sensor can be interpolated to obtain a map of the channel bottom, as illustrated in Figure 4.22. Subsequently, acoustic maps are created as a continuous-depth data layer covering the target area of the channel bottom by interpolating the measured depths. This step is the basis for all sounding techniques and produces the conventional bathymetric maps. The acoustic maps provide a full 3D description of the geometry of the bed forms. In the second step, the acoustic maps are converted to "image equivalent" maps by resampling the raw information in pixel coordinates (Muste et al. 2015). Images obtained at different time steps are subsequently processed using an image velocimetry technique (Muste et al. 2008). Bedload rates are obtained by combining the outcomes of the acoustic mapping carried out in the first step along with the velocity fields obtained in the second step using analytical relationships for predicting sediment transport rates for the bedload (Vanoni 2006).

An attempt to take measurements with real snow was made at a site in northern Iowa after a snow storm occurred in the area. A wind blower and actual snow were used in the experiment, as shown in Figure 4.23.

Figure 4.23. Attempt to measure snow drift in situ: (a) test section, (b) snow blower used for entraining the snow, (c) aggregation of snowflakes due to compactness in the snow layer and high temperatures

Despite several tests conducted in the field, the snow did not move similarly to drifting because the compactness of the deposit and the high local temperatures had consolidated the snowflakes. The snow particles aggregated and subsequently moved as larger snow balls in the test area.

Several auxiliary variables needed to be measured in conjunction with the snow drift estimation in the laboratory test, such as wind speed, volume of deposit, and weight of the melamine plastic particles. Prior to the experiment, artificial dunes were created as the initial condition (time = 0 minutes). A total of six images were taken after the dunes formed for the purpose of photogrammetry mapping. One continuous recording was taken to process the velocity vector field using the LSPIV technique. In total, five cases (time = 1, 2, 3, 4, and 5 minutes) were completed and used and used to infer dune displacement for each case. The same procedure of taking six images at different angles (Figure 4.24) was applied after each individual case was completed to plot it and map the propagation of the dunes for all of the cases.

| Location 1 | Location 2 | Location 3 |
| Location 4 | Location 5 | Location 6 |
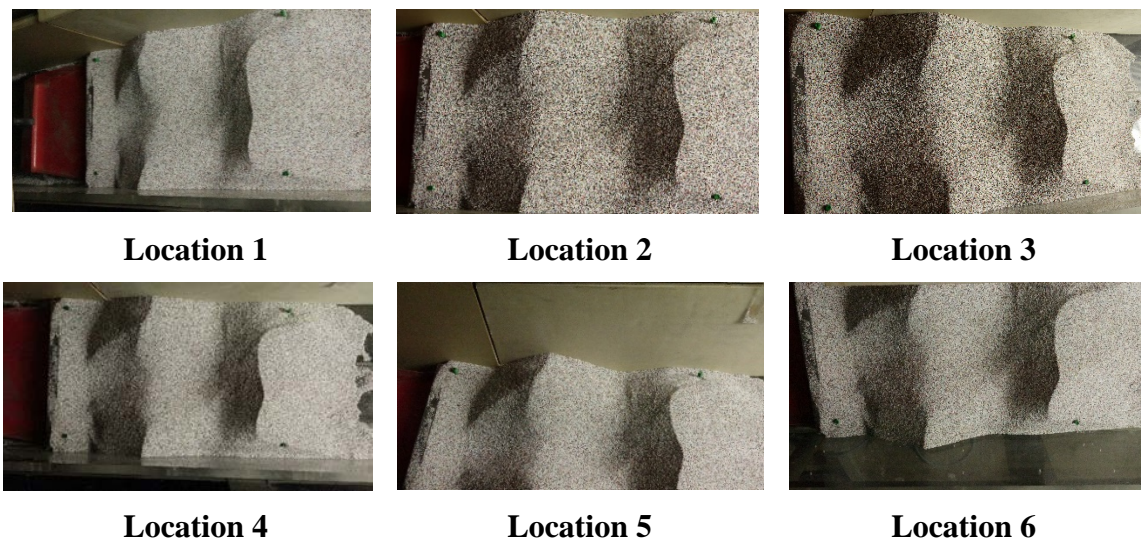
Figure 4.24. Temporal evolution of the dunes during one laboratory experiment, with six images processed per case

4.3 In Situ Snow Deposit Tracking at Snow Fences

4.3.1 Long-Term Observations of the Snow Fence Site

This experimental field site was located in Shueyville, Iowa. Two snow fences were located near the Shueyville United Methodist Church. The present investigation focuses on the snow fences situated on the west side and left side of the school driveway situated near the church. The site location was chosen after consulting with the Johnson County Secondary Roads Maintenance Superintendent. Following his recommendation, several visits to the site were completed during the 2015–2016 winter season. This specific location was found to match all of the needs for the present project research.

During the 2016–2017 winter season (from December 2016 to March 2017), measurements of the snowfall and snow drifts were conducted at this site. The measurements were conducted outside of the school perimeter on the left side of the school driveway, as indicated in Figure 4.25.

Figure 4.25. Experimental field site in Shueyville, Iowa, containing a snow fence, with the position of the cameras and instruments used to measure wind

Two real-time cameras and one anemometer were deployed at the site next to the electrical poles (see Figures 3.12 to 3.15). All three instruments were self-powered with solar panels and did not require any supervision or maintenance. Images of the fence taken during the winter of 2016–2017 are shown in Figure 4.26.

Figure 4.26. Snow fence on the west side of the Shueyville experimental site

The measured variables for the deployed instruments included time series of images and wind velocity characteristics, as discussed in Chapter 5.

4.3.2   Event-Based Observations of the Snow Fence Site

Another type of in situ snow drifting tracking experiment was performed to observe snow deposition following a storm event. The original intention was to use a drone-based photogrammetric survey, as described in Chapter 3. However, due to the new regulations proposed by the Federal Aviation Administration (FAA), the photogrammetry survey using a drone could not be conducted. Another type of photogrammetric survey was attempted using close-range photogrammetry, as described in Basnet et al. (2016).

Images from this survey (this was the only survey performed due to the lack of major storm events in the 2015–2016 and 2016–2017 winter seasons) are shown in Figure 4.27(a) through Figure 4.27(c).

(a)

(b)

(c)
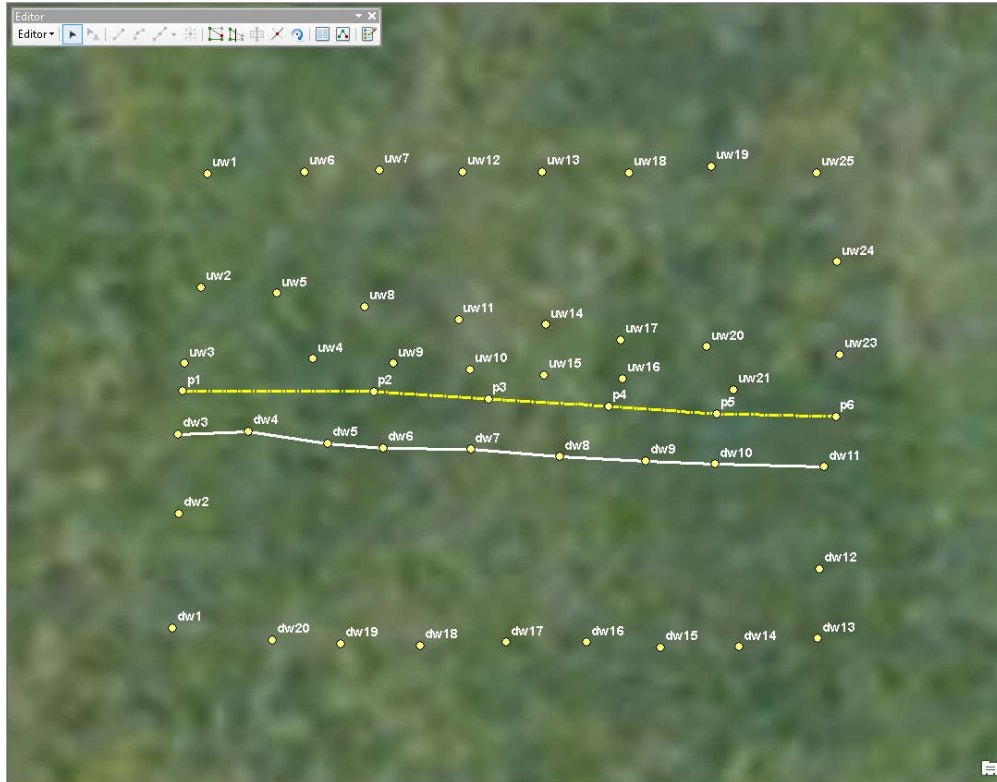
(d)
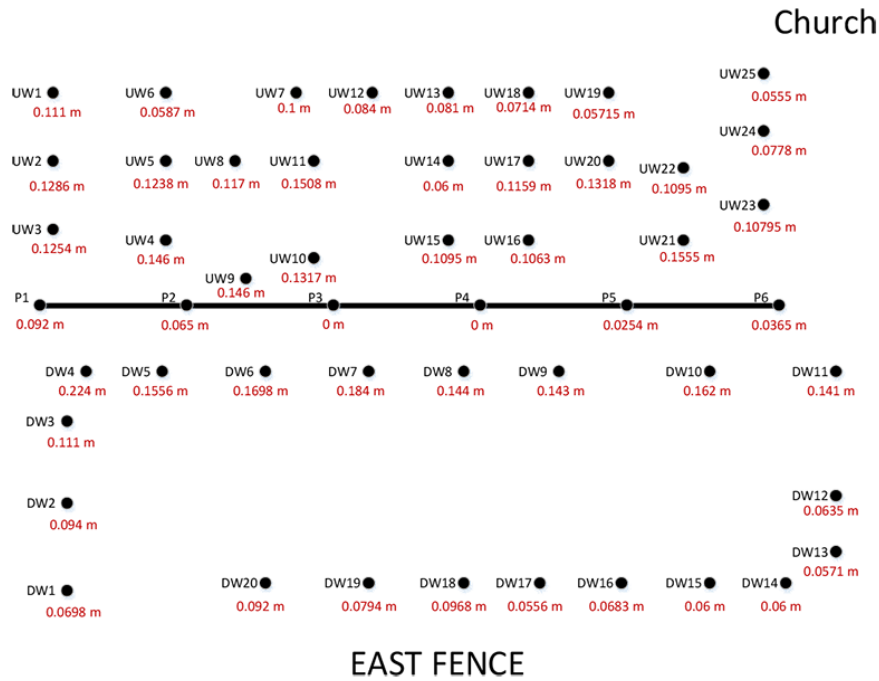
(e)

Figure 4.27. Event-based mapping: (a) the survey site following the March 14, 2017 snow storm, (b) downwind area of the fence with marker points, (c) upwind area of the fence with marker points, (d) and (e) results of the survey

The survey was conducted following the March 14, 2017 snow storm. Images were consecutively taken from several positions surrounding the area of interest. Prior to acquiring these images, a GRP survey, as required by the photogrammetry method, was conducted downwind and upwind of the fence, as shown in Figures 4.27(b) and 4.27(c). The GRPs were obtained by spray painting the snow in several places. The results of the survey are shown in Figures 4.27(d) and 4.27(e).

Two to four images were acquired from each position to allow the images to be stitched for 3D reconstruction. To avoid the difficulty of identifying the tie points required by photogrammetry on the snow deposits, artificial "seeding" was applied using dry leaves. Figure 4.28(a) shows the instruments (a power generator and a leaf blower) used for seeding. The results obtained after the seeding was applied are shown in Figures 4.28(b) (upwind area) and 4.28(c) (downwind area).

(a)

(b)

(c)

Figure 4.28. Seeding used for supporting the photogrammetric survey: (a) instruments used to conduct the seeding (power generator and leave blower), (b) view of the upwind area of the snow fence, (c) view of the downwind area of the snow fence

The results obtained using photographic mapping are provided in Figure 4.29. Due to the relatively small deposition heights observed during the snow event, the results are within the accuracy of the photogrammetric survey.
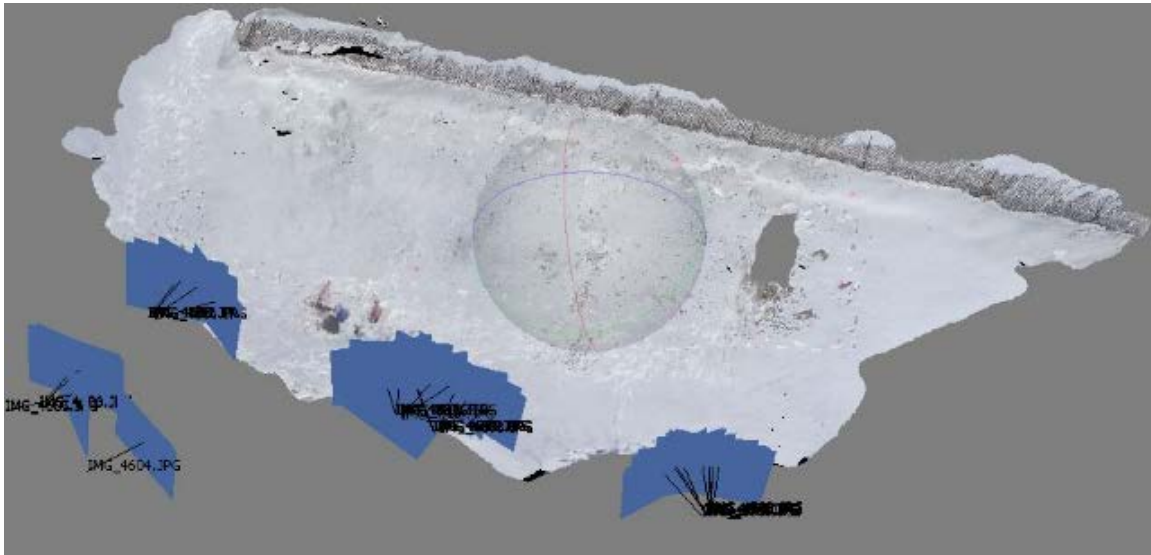
Figure 4.29. Photogrammetry results for snow deposit mapping

CHAPTER 5: EXPERIMENTAL RESULTS

The main goals of this research were to propose a set of protocols for local measurement of snowfall and snow drift at a site as well as for mapping snow deposits at snow fences. A large part of this research was devoted to selecting the appropriate instruments, proposing appropriate measurement and processing methods, and developing and optimizing the experimental arrangements and measurement protocols.

Following the finalization of each of the new measurement protocols, attempts were made to implement the research outcomes through proof-of-concept experiments. Unfortunately, the last two winter seasons were milder than usual, and there were few major storm events recorded in central Iowa during these two winter seasons. Given this situation, the measurement of snow drift was tested in the laboratory using synthetic snow, an experiment that was not included in the original research plan.

Reported in this chapter are the laboratory and field experimental results that were used to validate the proposed approaches to measure snowfall, snow drift, and snow deposit at snow fences.

5.1 Snowfall Measurements Using PTV

5.1.1 PTV Results for Storm Events

Following the initial experiments, whose main purpose was to propose a new methodology to measure snowfall, a series of snowfall events were documented using the developed PTV experimental protocol. The in situ measurements were collected with the instrumentation and protocols described in Chapters 3 and 4. A sample of the meteorological conditions during the monitoring of a snowfall event is provided in Figure 5.1.
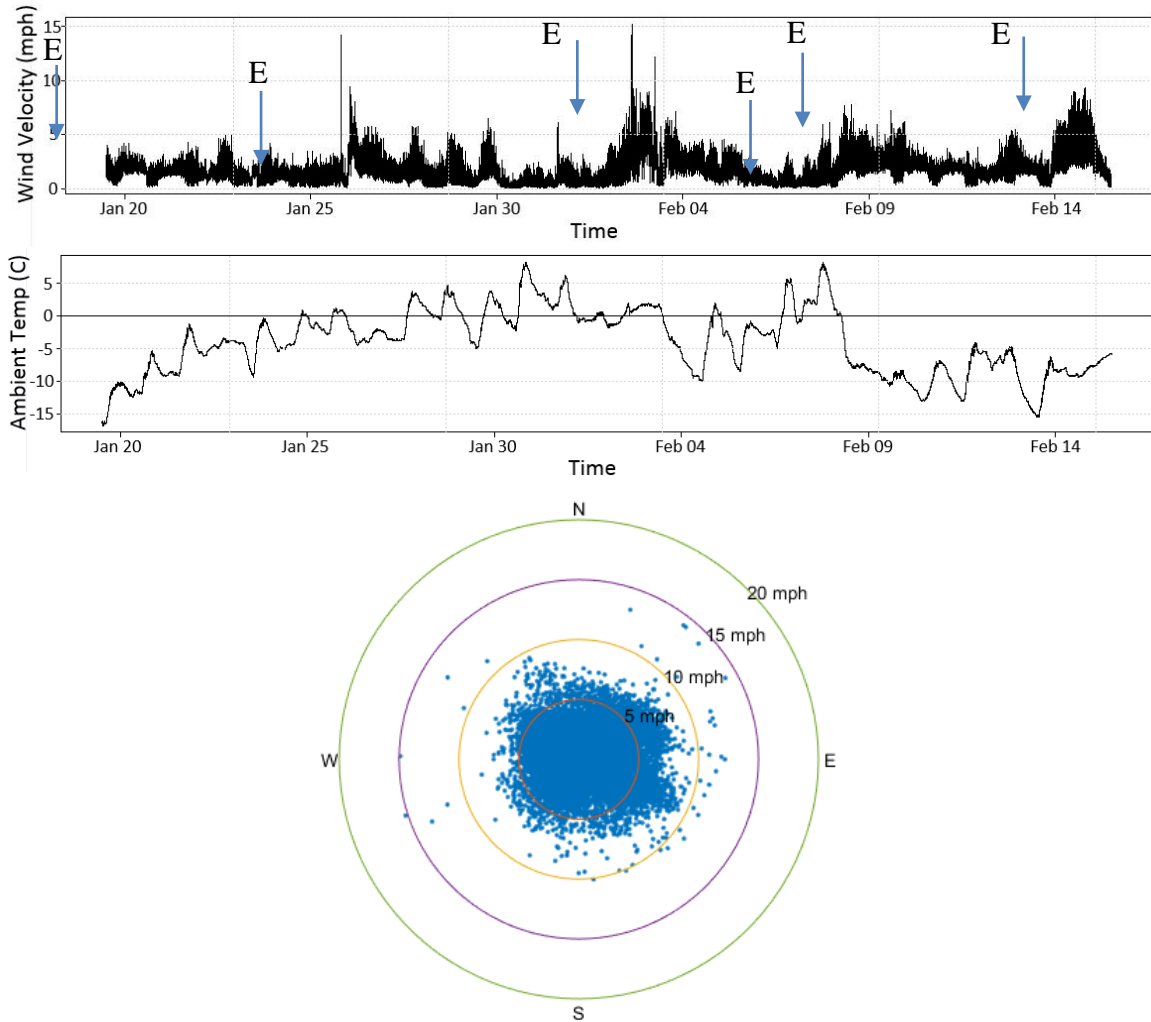
Figure 5.1. Sample of wind velocity, wind direction, and temperature time series recorded during a snowfall event during the 2015–2016 winter season

Overall, the wind intensity and temperature reported in the figure are typical for the snow storms that took place during the 2015–2016 winter season. The output files containing wind data are given in the following format: f (001, 1980-01-09, 21:35:23.1, 71, Dm, $D_x, S_m, S_x, T_a, U_a, P_a, R_c, R_d, R_i, R_p$), where 001 is the number of measurements in each transmit sampling time of 5 minutes, date = year-month-date, time = hh:mm:ss, and 71 is the Vaisala serial number. The definitions of the remaining variables are provided in section 4.1.3. For the 2015–2016 winter snowfall experiment, the dominant wind direction was between the northwest/southeast direction and the northeast/southwest direction. At most times, the wind velocity was below 10 mph.

Several videos of snowfall events were recorded during January and February 2016, resulting in a total of six different observed snow events. The individual snow events are listed in Table 5.1, with the corresponding date, event duration, number of recordings, and event description.

Table 5.1 Summary of snowfall events monitored during the 2015–2016 winter season

#	Event Date	Event Duration	# Recordings/ Event	Event Specifics
1	Jan 19, 2016	2 hrs	1	Moderate snow, nighttime
2	Jan 25, 2016	2.5 hrs	1	Light snow, nighttime
3	Feb 2, 2016	1 hr	1	Mix of snow with rain, daylight
4	Feb 7, 2016	0.5 hr	1	Light snow, nighttime
5	Feb 8, 2016	8 hrs	3	Moderate snow, daytime and nighttime
6	Feb 14, 2016	4.5 hrs	1	Moderate snow, nighttime

For Event 5, three recordings were done throughout the day, labeled S1, S2, and S3.

Each time of observation was matched with the wind data provided by the Vaisala anemometers, as stored on the server. After determining the desired time period, the mean wind direction (Dm) and mean wind speed (Sm) were calculated. In summary, the calculated wind direction and intensity for all six storm events are shown in Table 5.2.

Table 5.2 Summary of mean wind velocity and wind direction during the snowfall events

Event	Total averaged wind velocity (m/s)	Average wind direction measured with respect to the North (°)
1	1.991	97
2	1.670	272
3	3.576	84
4	0.610	274
5 – S1	3.800	318
5 – S2	2.600	346
5 – S3	1.000	316
6	3.620	115

The instruments used to perform the measurements are described in Chapter 3.3.1. The measurement protocols are provided in Chapter 4.1.1. Using EDPIV software applied to successive video recordings, the snowflakes' velocity vectors can be inferred. Following the processing procedure described in Chapter 3.2.3, the components of the velocity vector of the individual snowflakes can be estimated in the x and y directions (V_X and V_Y). The wind data output from the Vaisala anemometer also provides the V_{X1} and V_{Y1} wind velocity components. The measurements and calculations performed for Event 1 (January 19, 2016) are summarized in Figure 5.2.
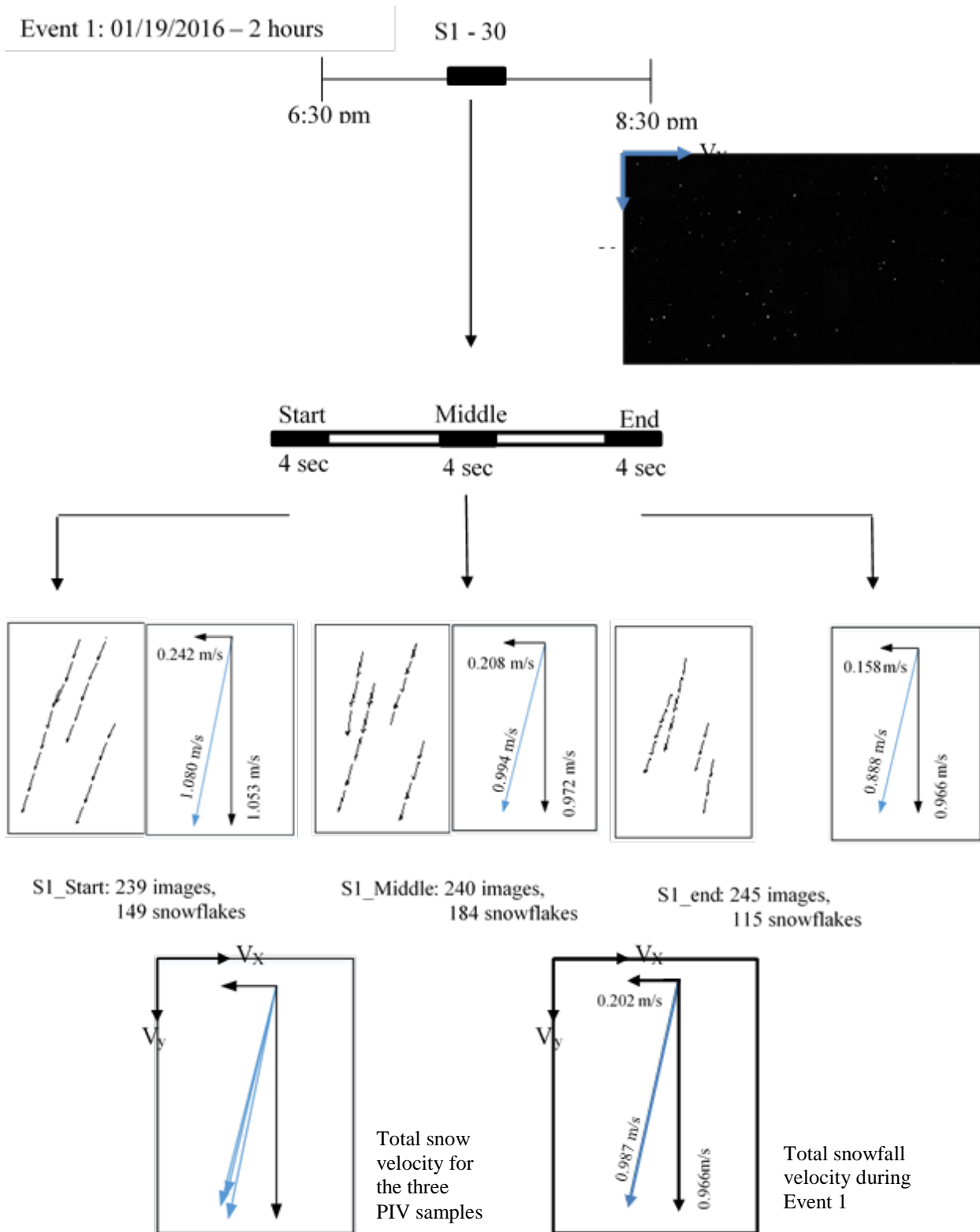
Figure 5.2. Processing stages leading to estimating the components of the velocity vector of the snowflakes during Event 1

The full analyzed results for Events 2 to 6 are presented in Appendix A. In each individual event, the video recordings ranged from 30 seconds to 1 minute. Within each recording, three bursts were calculated in the first 4 seconds, middle 4 seconds, and last 4 seconds of the recording segment. Once the x and y components of the velocity vectors for each burst were decomposed and analyzed, the average of these values was assumed to be the final velocity in the x and y directions for the event.

Another essential variable used to estimate the snow relocation coefficient is the flux of snow in the vertical and horizontal directions. The flux can be estimated if the particle velocity and concentration are determined, which is possible using a PTV-based measurement technique. Previous studies concluded that snowflakes can be assumed to be of spherical shape (Muramoto et al. 1995). Based on this assumption, the tracked particle size output (in pixels) from the EDPIV software can be used to determine the average particle diameter. The concentration of the particles (snowflakes) can subsequently be determined by dividing the sum of the areas occupied by the individual particles by the image area. The results obtained for Event 1 that characterize the type of snow and the snowfall dynamics are summarized in Table 5.3.

Table 5.3. Summary of wind velocity predictions during snow Event 1

	V_x (m/s)	V_y (m/s)	Total Velocity (m/s)	Avg. Particle Snowflake (pix)	Concentration (%)
E1_S1_Start	-0.242	1.053	1.080	25.73	0.144
E1_S1_Middle	-0.208	0.972	0.994	29.04	0.178
E1_S1_End	-0.158	0.874	0.888	22.28	0.131
E1_S1_Average	-0.202	0.966	0.987	25.68	0.151

As this specific example shows, a snowflake size of 25.68 pixels is equivalent to a diameter of 3.12 mm based on the relative pixel size. The inferred diameter of the snowflake is then used to calculate the snow flux. The horizontal velocity, V_{X1}, measured by the Vaisala anemometer was interpolated by decomposing the resultant vector, as shown in Table 5.4.

Table 5.4. Summary of observed wind conditions for Event 1

	V_{x1} (m/s)	V_{x2} (m/s)	Total Wind Velocity (m/s)
E1_Wind	-0.246	-1.976	1.991

Angle from north is 97°

5.1.2 Comparison of Vaisala Anemometer and PTV Predictions of Wind Velocity

Because these experiments focused on the horizontal movement of the snow particles, the predictions of the x-component of the mean snowflake velocity vector given by the PTV (V_X) and the Vaisala anemometer (V_{X1}) are compared in Table 5.5 for the six events.

Table 5.5. Summary of PTV predictions of snowflake-related variables and comparison with the Vaisala anemometer prediction of the horizontal velocity component

Event	V_X from PTV Measurement (m/s)	V_{XI} from Anemometer Measurement (m/s)	Total Wind Velocity (m/s)	Wind Angle from North (°)	Avg. Particle Snowflake Diameter (mm)	Concentration (%)
1	-0.202	-0.246	1.991	97	3.12	0.151
2	0.044	0.058	1.670	272	1.14	0.007
3	0.306	0.374	3.576	84	2.06	0.254
4	0.026	0.043	0.610	274	0.72	0.001
5 – S1	2.561	2.824	3.800	318	3.20	0.254
5 – S2	0.854	0.970	2.600	346	2.49	0.091
5 – S3	0.603	0.719	1.000	316	2.61	0.070
6	1.444	1.530	3.620	115	2.84	0.011

The vertical component of the snowfall is typically larger than the horizontal component. Therefore, the measurement protocol accuracy is better tested by considering the smaller horizontal component.

It is important to emphasize that the main assumption that makes this comparison possible is that the snowflakes are closely following the wind dynamics. In addition to velocity, PTV measurements include the diameter of the individual snowflake particles. PTV also provides estimates of the velocity and snowflake concentration as instantaneous values. By taking the product of the two quantities, one can estimate the snowfall flux by correlating the measured wind velocity with the observed resultant motion of the snowflakes. The results for the x-direction velocity calculated based on EDPIV (V_X) and the Vaisala anemometer (V_{X1}) show a strong relationship. This result basically validates the proposed image-based method to measure particle velocity. The PTV velocity measurements are slightly smaller than those obtained using the anemometer due to some uncertainties. Overall, the comparison between the two methods shows that the non-intrusive measurement protocols developed for measuring snowflake velocities are in agreement with independent direct measurement of wind velocity using a standard instrument (anemometer).

5.2 Snow Drift Measures

5.2.1   In Situ Measurements

The snow drift measurements can only be quantified in the context of the boundary layer transport processes, as described in Chapter 2. In terms of the horizontal flux of snow, the region of interest for snow fence design is situated between the ground and a distance of 6 to 8 ft above it (Weather Online). Measurements performed along the vertical direction within this region combine the effect of wind acting on the falling snowflakes with the effect of the suspension of the snowflakes entrained from the bed by wind currents. Unfortunately, it is not possible to split the flux into two components associated with these two effects. Therefore, taking measurements in the absence of snowfall is the best approach for quantifying snow drift because, in this case, only the second effect is present. Moreover, most of the snow transport contributing to the formation of the snow dunes is associated with the movement of "snow sheets" that slowly advance over the stationary layer of deposited and compacted snow.

The intertwined nature of snow transport processes necessitates separate measurement strategies for snowfall and the snow drift. In summary, for snowfall, measurements should be taken above the boundary layer (at least 6 to 8 ft above the ground), while for the snow drift, measurements should be acquired at less than 6 to 8 ft from the ground, preferably after the snowfall stops and the snow moves only via entrainment from the deposited snow on the ground. For a quick estimation of the snow drift flux, a good surrogate measurement is the movement of the snow sheets advancing over the stationary layer of deposited snow.

Sample in situ snow drift measurements were obtained using the PTV and LSPIV techniques during a snow drift event on December 16, 2016. The presented results are only marginally relevant because they were acquired during the development of the protocols for the in situ

measurement of snow drift leading to experimental arrangement EA6 described in Chapter 4.2.1. The mild snow storms that took place during the 2016–2017 winter season did not offer more opportunities to perform in situ measurements at the location where the PTV-LSPIV setup was installed. The alternative of mobilizing the recording and illumination equipment using forecasted storms at various locations where snow drifting occurs is feasible for the developed measurement protocols. However, the limited resources available for this research did not allow us to pursue this alternative. Based on the previous arguments, the results reported in this section only discuss the dynamics of snow dune movement. The full protocol for snow drift measurement is presented in the next section.

The protocol for measuring snow movement above the bed utilizes the PTV approach for estimating the velocity of the individual snowflakes moving near the bed, as illustrated on the right side of Figure 5.3(a).
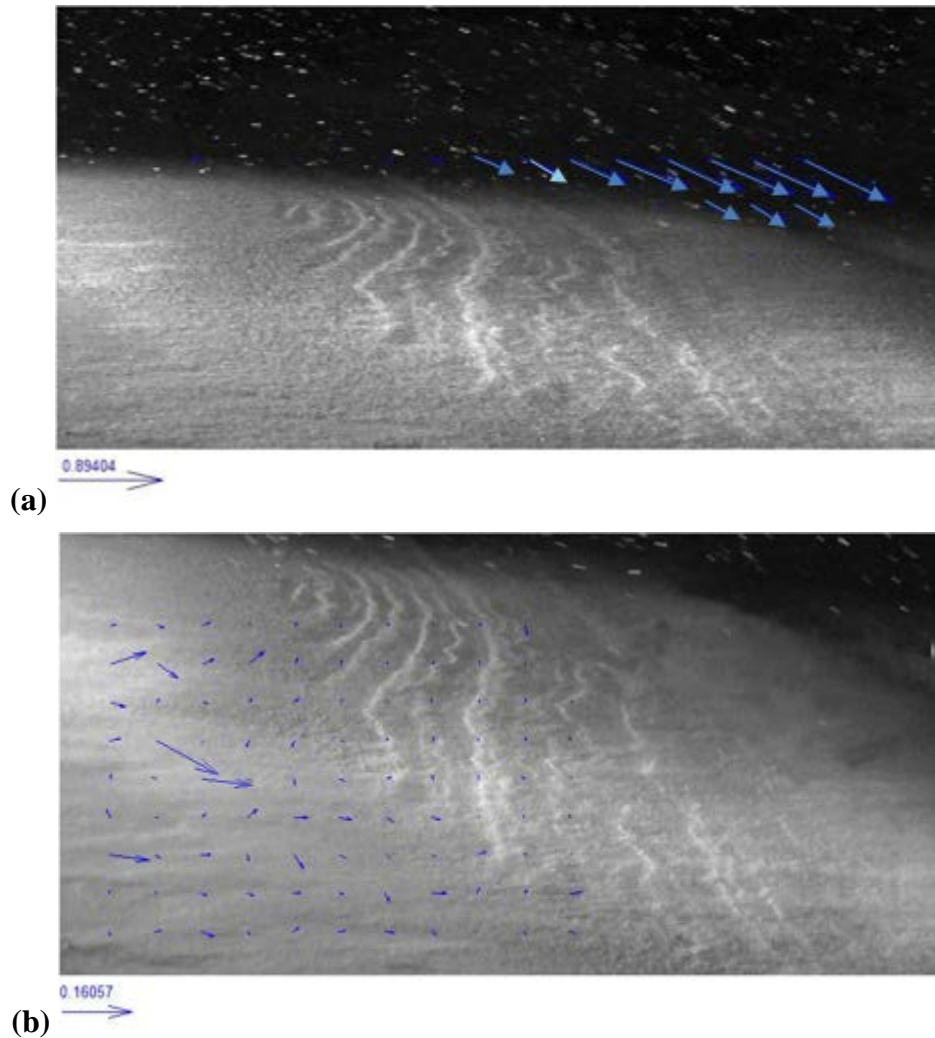
Figure 5.3. Illustration of measurement results used to quantify snow movement above the top of the layer of compacted snow: (a) velocity of snowflake particles moving near the bed and (b) velocity field over the snow bedforms

The movement of the snow dunes as they migrate over the layer of compacted snow is more accurately quantified by LSPIV than PTV. This is because LSPIV is based on gray-level pattern recognition while PTV is more accurate when the goal is to capture the movement of individual particles.

For cases when a high concentration of tracked particles is present, which is the case for snow particles moving as bedforms (see ripple-like bedforms in Figures 5.3[a] and 5.3[b]), the PTV technique has some limitations. The snowflake velocities obtained from PTV measurements using images taken at the same time are approximately one order of magnitude higher than the velocity of the snow bedforms migrating over the fixed layer of snow. It is the latter component of the total snow flux that must be accurately quantified for the design of snow fences.

5.2.2 Laboratory Measurements

The facility and measurement protocols for estimating snow drift in laboratory conditions were described in Chapters 4.2.1 and 4.2.2. Preliminary experiments were performed to evaluate several possible arrangements for the camera and lighting assembly. Several preliminary arrangements were tested before the EA6 arrangement was reliably replicated in the experimental setup. The movements of the melamine plastic particles modeling the snow drift in laboratory conditions were first mapped using photogrammetry. Their dynamics were then studied based on LSPIV data. LSPIV was applied to six bedform maps, as illustrated in Figure 5.4.

T = 0 min	**T = 1 min**	**T = 2 min**
T = 3 min	**T = 4 min**	**T = 5 min**
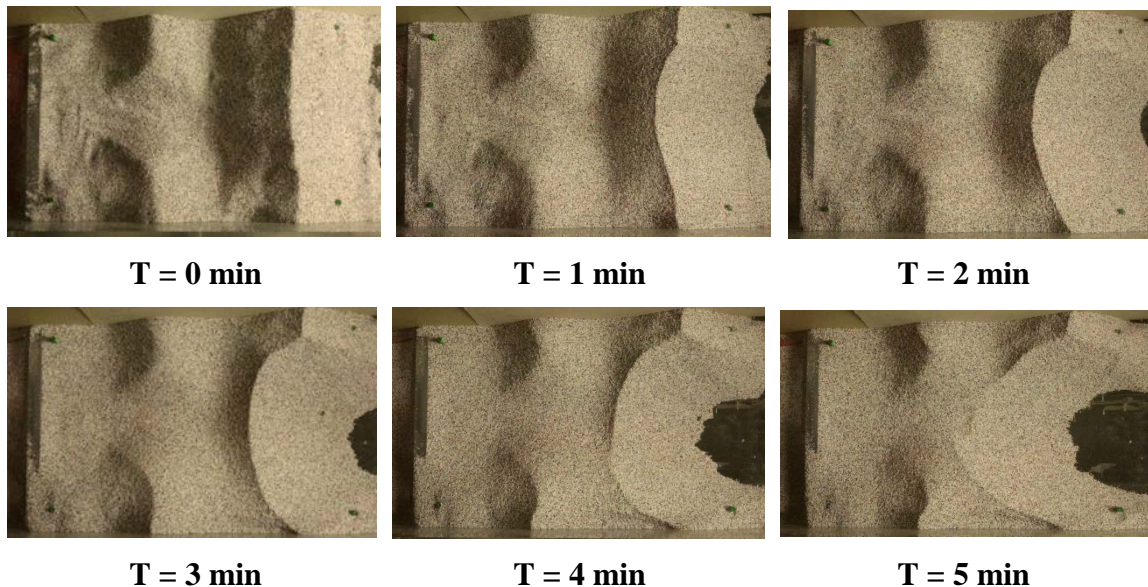
Figure 5.4. Visualization of the temporal evolution of the bedforms over a period of 5 minutes in the snow drift experiment

The time interval between the maps was 1 minute. Bedform migration was induced using a blower that covered the whole test section in the spanwise and streamwise directions. The

velocity magnitude in the streamwise direction was found to rapidly decay when the planar air jet was not confined, as is the case in standard wind tunnel experiments.

One of the procedures available to map snow deposition is photogrammetry (see Chapter 3.2.3). On average, six images were taken from various angles. Four ground reference points were used for scaling and image correction purposes. The present study used the Agisoft PhotoScan software to process the images and obtain the coordinates of each photo. Then, the overlapped GRPs were observed. Four steps were needed to reconstruct the 3D model using this photogrammetric approach: (1) align photos, (2) build a dense cloud, (3) build a mesh, and (4) apply texture to the image. The sequence of the steps and their output, as applied to the laboratory validation test, are illustrated in Figure 5.5.
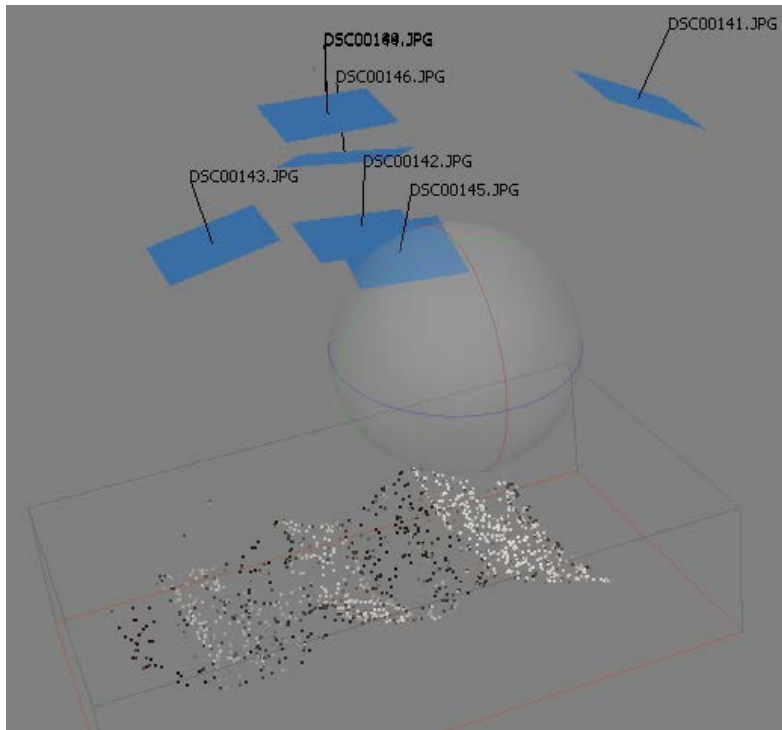
(1) Align photos and build dense clouds
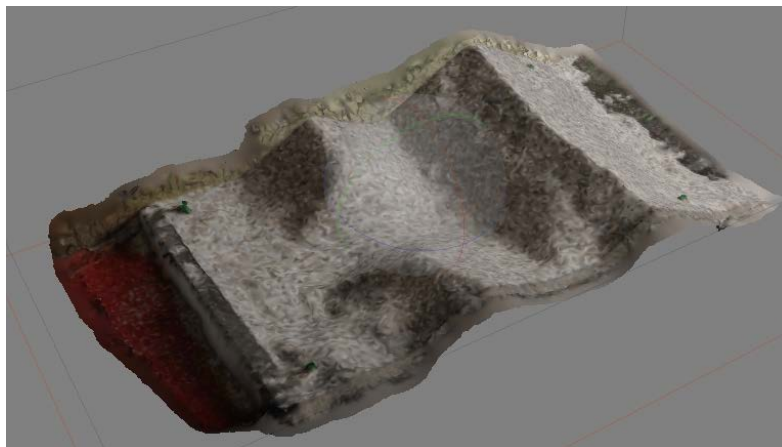
(2) Build mesh
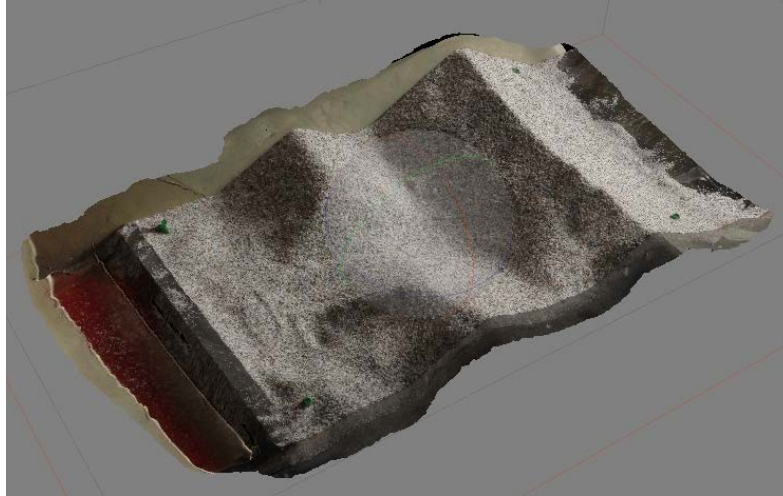
(3) Build texture
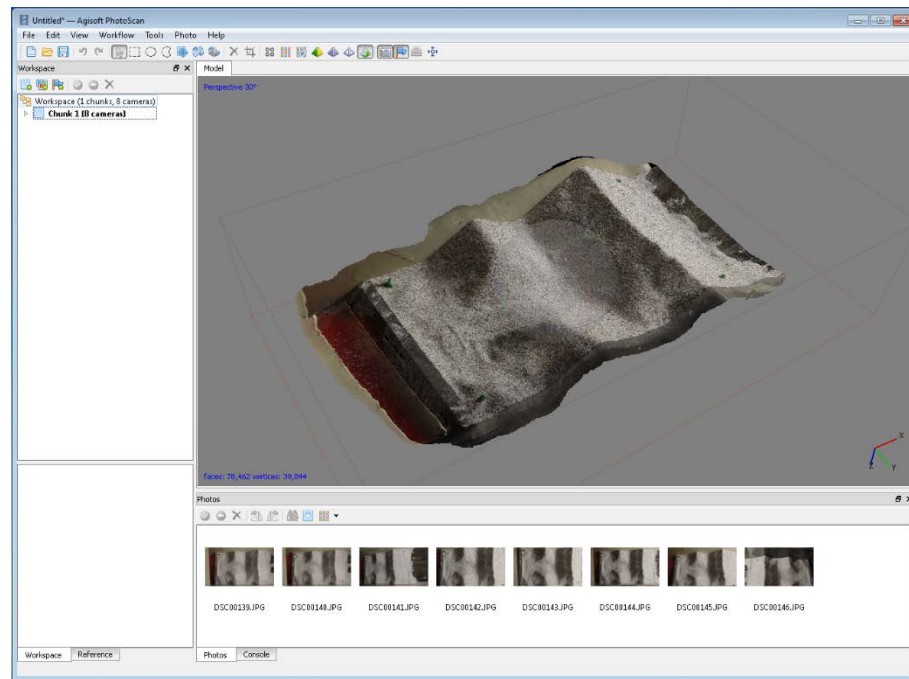
(4) Agisoft interface

Figure 5.5. Main steps of the procedure used to reconstruct the 3D model using the Agisoft software

In the first step, the images from various angles are stitched. Using the ground reference points set in the experimental test section, the proper photo alignment is carried out across all of the acquired images. Software workflows are available to subsequently create a rough layout of the mapped area. In the rare case where the camera falls short of recording the coordinates, the software has the ability to locate all the reference points using the known locations of the successive camera shots.

In the second step, the software generates a dense point cloud. The main purpose of this step is to generate and gather all of the points and use this information to advance the design process and obtain points acquired from raw information. The relatively smaller scale and simple structure of this experiment allowed the majority of the points to be generated without any problems. However, some studies (Maiwald et al. 2017) have noted that building dense clouds may not be sufficient to complete a detailed reconstruction of the model. For the field measurement protocols reported in Chapter 4.3.2, the building of the tie points was facilitated by spreading leaves over the textureless snow surface. In general, to improve the resolution and accuracy of the photogrammetry modeling, it is recommended that several images be taken of the area to be surveyed. The higher the quality of the original image, the better the constructed 3D model.

The main goal of the third step is to create a smaller mesh between all of the tie points generated from the dense clouds and to form a layer that links all of the points to create a smooth surface.

In the last step, the Agisoft PhotoScan software identifies the surface textures and colors in order to transfer and apply the texture layer on the top of the mesh layer. This step matches the 3D model with the actual object, giving the user final control over the surface's appearance.

The results generated by the Agisoft PhotoScan software were organized and compared side by side with the physical measurements, as shown in Figure 5.6.

Physical Measurements   **Agisoft PhotoScan**

T=0 min

T = 1 min

T = 2 min

T = 3 min

T = 4 min
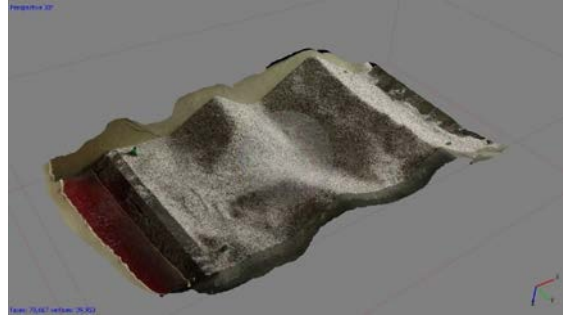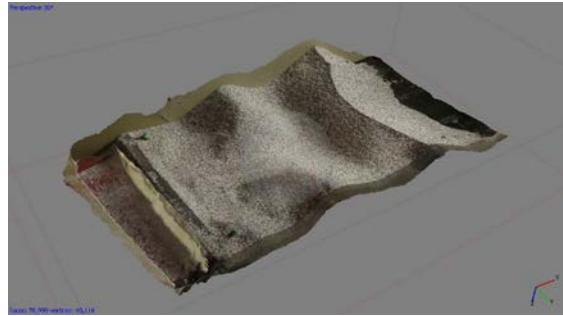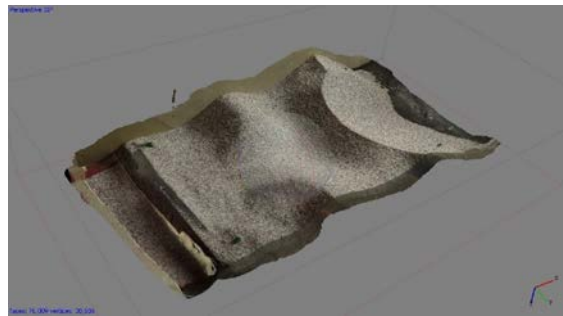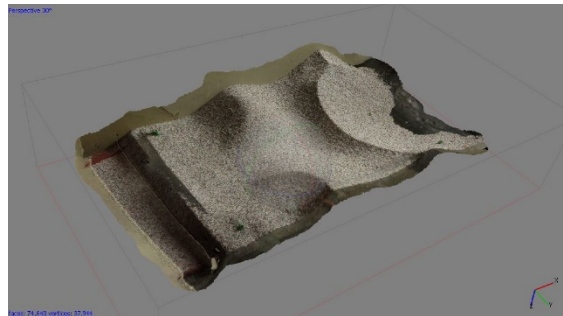
T = 5 min
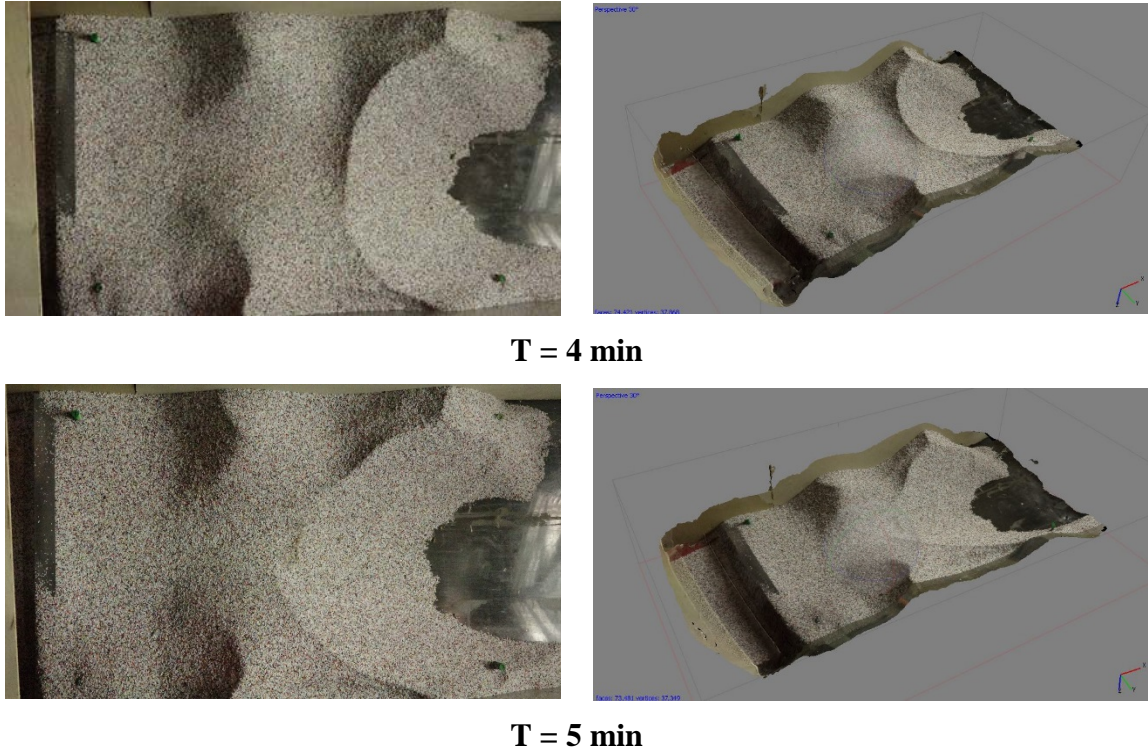
Figure 5.6. Comparison between Agisoft software 3D maps output and physical measurements

The results demonstrate the software's high capability of reconstructing the 3D model and its relevant details using only six images. The obtained photogrammetry maps can be used as standalone three-dimensional representations of the snow deposited at any location in situ, including the snow volumes developed upwind and downwind of the snow fence. Using successively generated photogrammetry maps, the rate of volume change can be tracked and then used to characterize the dynamics of the bedform movement, an essential factor in documenting snow drift dynamics.

In general, photogrammetry techniques have the ability to create an accurate 3D model of an object. Several studies (Skarlatos and Kiparissi 2012, Kersten 2006) have concluded that such techniques are relatively cost-efficient compared to techniques using laser scanning. Although the resolution and quality of the output might not be as precise as one obtained using laser scanning, the Agisoft PhotoScan software results are suitable for the present research. A main advantage of this technique is the relatively rapid processing time of the data to obtain the photogrammetry maps.

The series of repeated maps obtained using the photogrammetry technique is further used in conjunction with LSPIV to quantify the snow drift velocity. With this capability and an estimation of the snowfall velocity/flux, as described in Chapter 5.1, direct estimation of the snow relocation coefficient is possible. After inputting the six images into the LSPIV software, a searching area and an interrogation area were selected commensurate with the size of the identifiable patterns and the patterns' speed of movement between successive images.

Several different combinations of SA and IA parameters were tested to obtain the best results in terms of capturing the bedform velocity migration. Using images rather than different sensor outputs (acoustic or LIDAR) is advantageous in that an acceptable flow field can be determined quickly because visual observation is intuitive and does not require special training. Figure 5.7 shows the dune velocity vectors generated in the preliminary tests using different sets of SA and IA parameters.
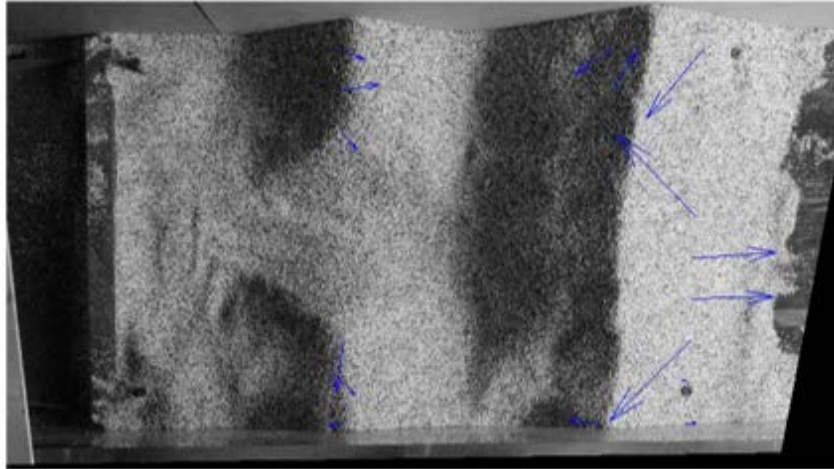
0.0074256

IA 128 SA 32
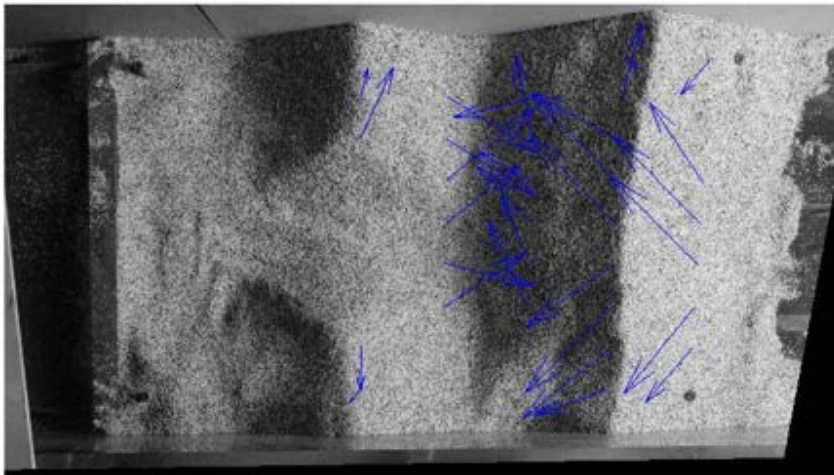
0.014968

IA 256 SA 64

0.028203
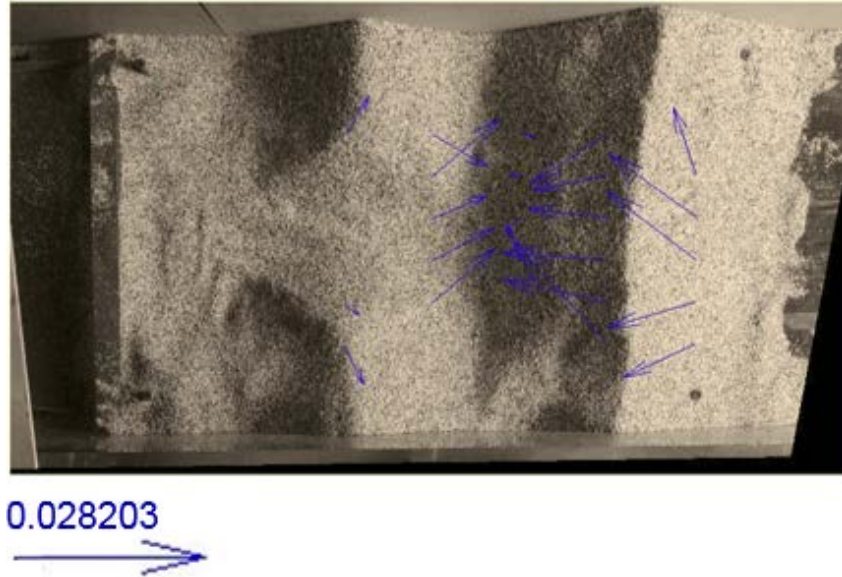
IA 512 SA 128

Figure 5.7. Dune propagation velocity vectors obtained using the LSPIV technique for different values of the main processing parameters: (a) IA: 128 pixels, SA: 32 pixels; (b) IA: 256 pixels, SA: 64 pixels; (c) IA: 512 pixels, SA: 128 pixels

All of the other processing parameters (i.e., minimum acceptable correlation coefficient of 60% and exposure time of 0.01667 s [1/60 seconds]) were kept the same to isolate the impact of the targeted parameters.

Visual observation of the actual video recordings and bedform dynamics estimated using LSPIV indicates that the setup with IA: 128 pixels and SA: 32 pixels falls short of capturing the full motion of the simulated snowflakes and dunes. The high uncertainty in the velocity vectors' magnitudes affects the results. The other two cases using relatively larger values of the IA and SA parameters successfully demonstrated the capability of tracking snowdrift movement. Both results agree with the direct observations of the velocity magnitudes and directions of the dunes' movement.

As part of this study, three separate cases with varying parameters were evaluated. Only 6 images were used to track the movement. Due to the large displacement within the 6 images, the estimated average displacement was chosen to have larger parameter values. One additional case was examined using a much longer series of images (approximately 600 images) cut from a 10-second recording to test this procedure. Because of the relatively small displacement observed between frames collected every 1/60 second, the estimated average displacements were selected using an IA value of 64 pixels and an SA value of 16 pixels. This was sufficient to track the propagating limbs of the individual dunes. Figure 5.8(a) shows the estimated pixels for a value of IA equal to 64 (blue) and a value of SA equal to 16 (red). This can provide a good first guess for the searching range and interrogation areas. The final result is presented in Figure 5.8(b).

93
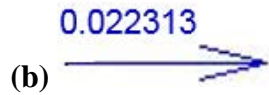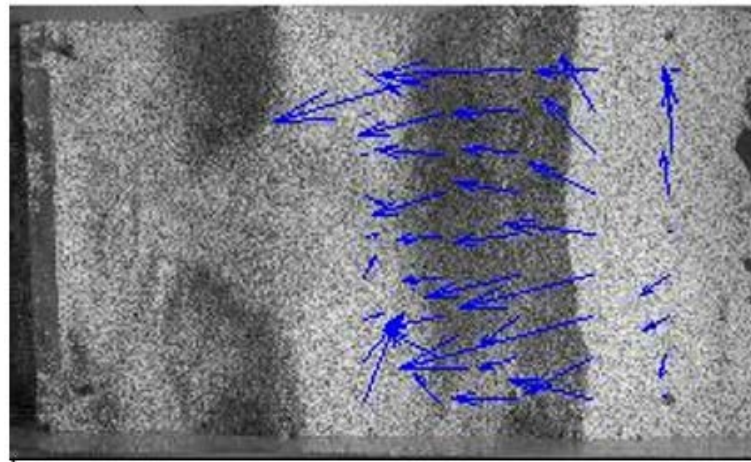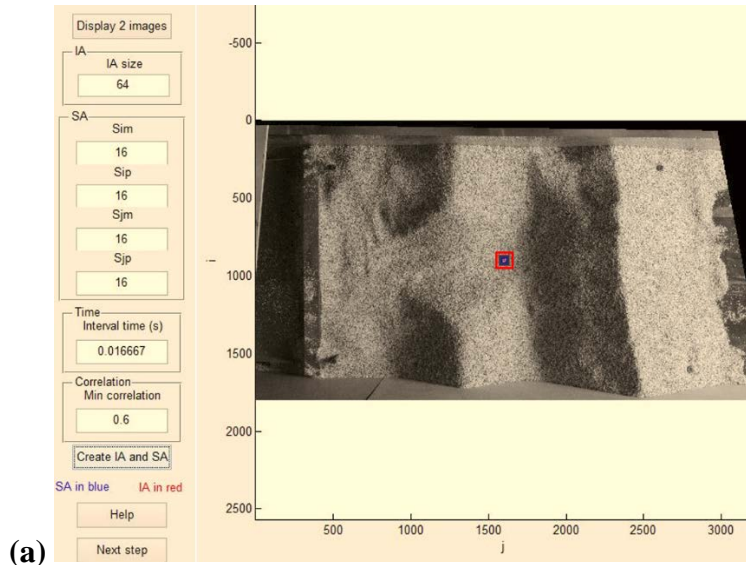
Figure 5.8. LSPIV velocity predictions obtained from a series of images: (a) SA and IA in pixels and (b) dune propagation velocity vectors

5.3 In Situ Mapping of the Snow Deposits at Fences during Storm Events

The measurements reported in this section were obtained during the 2016–2017 winter season at the Shueyville site, where two fences were deployed at the beginning of the winter season, as illustrated in Figure 4.25. The wind and temperature characteristics during the winter season are illustrated in Figure 5.9.
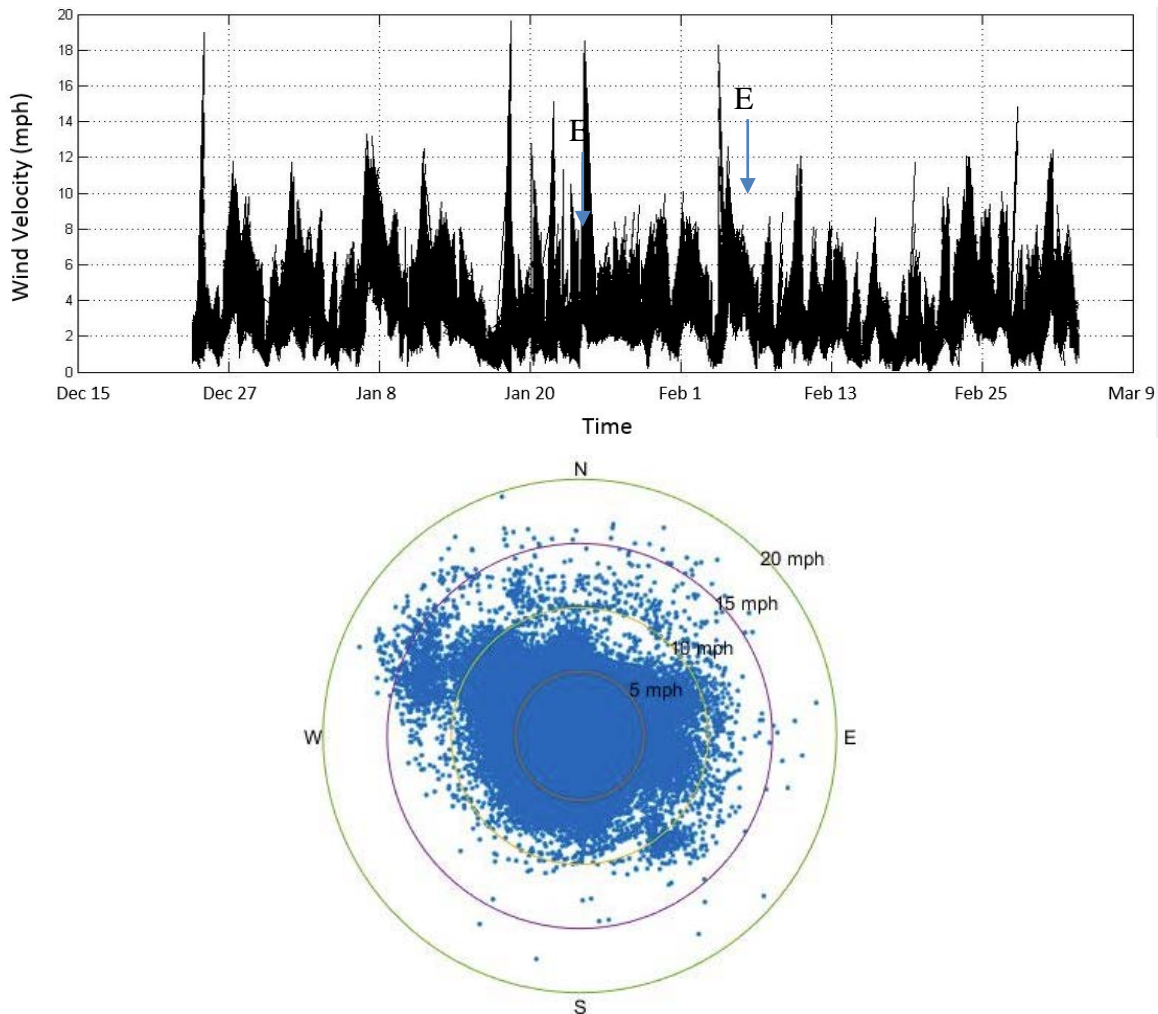
Figure 5.9. Sample of wind velocity and wind direction time series during the 2016–2017 winter season

Four larger storm events were monitored, and measurements were performed at the Shueyville site. The first event occurred on December 15–16, 2016; the second one (much milder) occurred on January 25–26, 2017; the third one occurred on February 8, 2017; and the fourth one occurred on March 12–13, 2017. The fourth event corresponded to the strongest storm. From the wind data presented in Figure 5.9, it can be seen that at most times the dominant wind was oriented along the northwest/southeast direction. For these conditions, the two snow fences were active. When the wind speed was below 15 mph, no major snow deposition at the two fences was observed during the 2016–2017 winter season. A detailed analysis of the wind velocity and wind direction recorded by the Vaisala anemometer was performed for all four snow storm events. The meteorological data for the March 12–13, 2017 storm is provided in Figure 5.10.
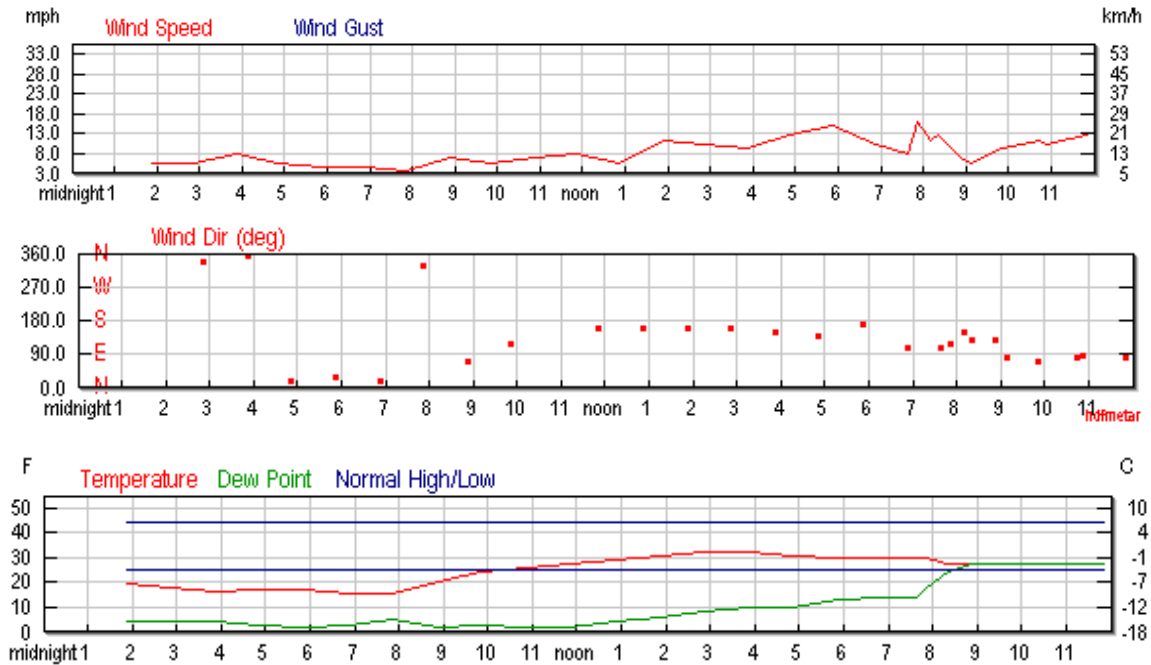
(a) March 12, 2017
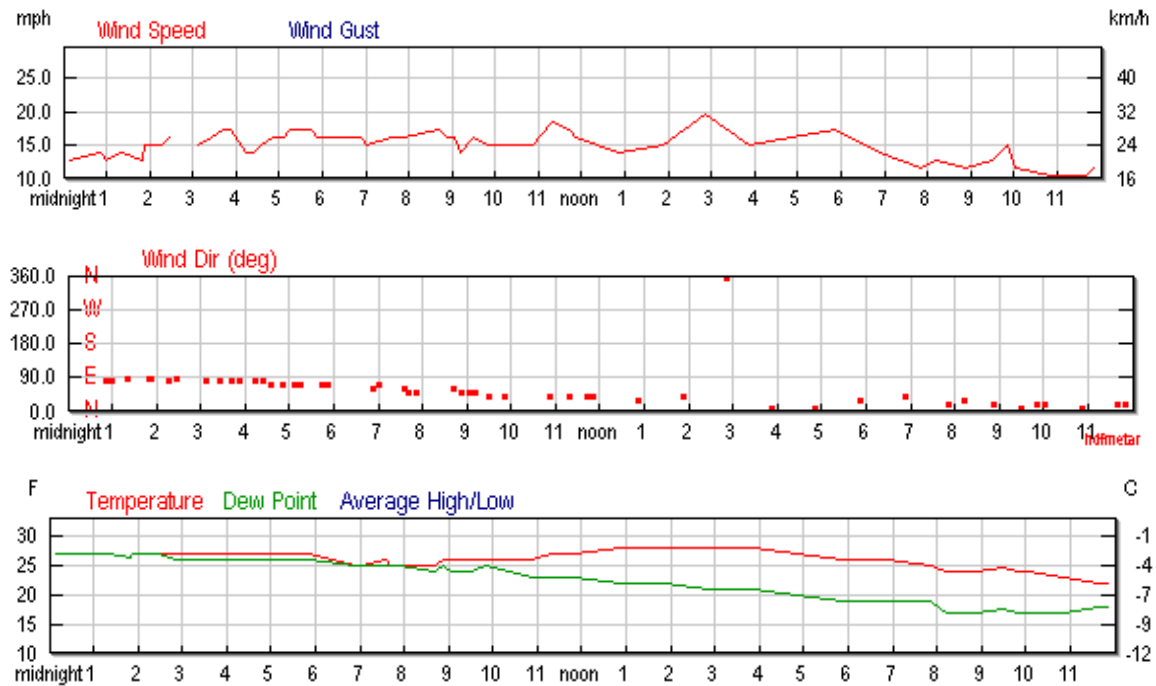
(b) March 13, 2017

Figure 5.10. Wind intensity (mph), wind direction (degree), and temperature: (a) March 12, 2017 event and (b) March 13, 2017 event

The wind intensity and direction measurements were conducted at the Eastern Iowa Airport situated six miles north of the Shueyville experimental site. This was done because the Vaisala anemometer server was down from March 4–16.

A series of images was also taken on both sides of the snow fences after the end of each storm to document the site conditions. Figure 5.11 shows such images for the March 14, 2017 storm.

During this event, the amount of snow deposited on the downwind side of the two fences was relatively small. The other snow events that were monitored during the 2016–2017 winter season are documented in Appendix B.

West fence, facing upwind (on the left of the school driveway)

West fence, facing downwind

East fence, facing upwind (on the right of the school driveway)

East fence, facing downwind

Figure 5.11. Event monitoring during the March 14, 2017 snow storm

CHAPTER 6: CONCLUSIONS AND RECOMMENDATIONS FOR FUTURE WORK

Snow drifting and blowing are common phenomena in four-season areas exposed to intense snowfalls and winds during the winter season. Preventive actions against snow drifting and blowing are conducted both during the road design stage (by choosing suitable road alignment alternatives) and after road construction (through snow-retention infrastructure deployed at the site or maintenance activities applied when needed). Development of an effective snow-retention solution is preferred to maintenance activities because the latter can become a large component of winter maintenance costs for states or local agencies. One of the most often used and reliable solutions for controlling snow drift is the deployment of snow fences along roads in regions where severe snow drifting is reported. The cost of the snow fences, including their installation costs, is about one order of magnitude lower than that of mechanical snow removal.

The design of snow fences is based on a set of local or regional weather conditions estimated over a long period and in consideration of the topology of the site where the snow fences are installed. This characterization is typically conducted through site surveys followed by the establishment of the orientation and geometry (e.g., height, bottom gap, porosity) of the fence and other design parameters needed to ensure the structural integrity of the snow fence. Among the most challenging tasks for the proper design of snow fences is the thorough characterization of the meteorological conditions at the snow fence site. In the absence of this local characterization, an efficient design for the snow fence is practically impossible because snow drifting is a process that is highly variable from location to location, even within the same climatologic area, and is also highly variable over time at the same location.

The present research addressed three critical aspects of snow fence design: estimation of the snowfall and snow drift fluxes and mapping of the snow volumes accumulated at the snow fence after its deployment at the site. The estimated snowfall and snow drift fluxes are used as input data in the software used for snow fence design, while the snow volume is used to evaluate the efficiency of the fence after its deployment. Conventional methods for estimating these three variables are outdated. Most of these methods are intrusive, requiring the deployment of instrumentation and personnel at the site for extended periods of time in harsh winter environments.

The first important contribution of this research was to develop a number of non-intrusive measurement techniques that work independently or in combination to provide quantitative and accurate estimations of these three variables. The proposed measurement methods do not require permanent installation of equipment, are mobile, and can be quickly performed to produce a wealth of qualitative and quantitative information readily usable in the design of snow fences. Their non-intrusive characteristics preclude extended exposure to frigid, windy conditions that could pose significant safety and health risks for the personnel conducting the measurements.

The snowfall measurements can be obtained continuously (day or night), with minimum preparation, using image-based techniques. The short-time video recordings acquired with off-the-shelf instrumentation do not interfere with the natural process of snow blowing in the vicinity of the ground. Locally adapted strategies are needed to provide adequate illumination, set the

camera parameters, and process the raw information using commercially available software. These types of methodologies are in sharp contrast to and are more accurate than the traditional ways of obtaining snowfall estimates using the intrusive measurement techniques currently in use at the majority of meteorological stations (snow boards, anemometer arrays, etc). Moreover, the remote nature of image-based measurements does not interfere in any way with the plane where the image acquisition is made. The images collected with a video camera are processed to provide individual snowflake velocity and size. Subsequent post-procesing provides two-dimensional fluxes of snow passing the imaged plane. The image size is considerably larger than the size of the snow boards currently used for the measurement of snowfall; therefore, image-based measurements can fully characterize the dynamics of the snowfall instantaneously or over a certain time interval. In contrast, when using classic methods, information on snowflake velocity and size are obtained using separate instruments.

The snow drift measurement protocols proposed as part of the present research also rely on image-based technologies (hardware and software). Concepts adopted from modern technology such as structure-from-motion (Westoby et al. 2012) and image velocimetry (Muste et al. 2004) have been assembled to propose, for the first time, a reliable, non-intrusive method for estimating the drifted snow velocity and snow fluxes over the top of the fixed layer of compacted snow. The methodologies and protocols assembled for characterizing the snow drift at a site provide multiple variables such as the velocity of snow sheets (ripples) moving along the bed (top of the fixed layer of snow), mean direction of motion over short and long time intervals, and characterization of the wind-fetch distance. Obtaining quantitative information on the snow drift is even more challenging than measuring the snowfall. The snow drift flux is rarely directly measured using intrusive methods (e.g., such measurements are usually performed using snow traps). Given the complexity of in situ measurements of the snow drift flux, several empirical and semi-empirical relationships have been developed. These relationships are site-dependent, and therefore they are not usable in geo-climatological areas other than those where they were determined.

Accurate estimation of the snowfall and snow drift fluxes is critical in defining the SRC, a variable that is of great importance in snow fence design (Tabler 1994). Conventional SRC estimation is based on empirical relationships derived from regression models applied to snow mass flux and wind intensity measured intrusively at various heights above the surface bed. These empirical relationships are typically site-dependent and strongly correlated with local meteorological and topological conditions. Therefore, the direct use of these relationships to predict the SRC at sites with different conditions is highly questionable. No corrections have been proposed to easily adapt these relationships for use at sites with different conditions. The ability to more efficiently measure the main variables involved in estimating the SRC using a mobile measurement platform consisting mainly of a portable camera and illumination devices is a considerable advantage over conventional approaches. Such conventional approaches for estimating the SRC require extensive labor and deployment time.

The SRC is also one of the main input parameters used in snow fence design software used by state agencies. Snow fence design is highly dependent on this variable. Therefore, accurate information about the value of the SRC at a given site is critical for correct design of the snow fence that will be deployed at the site. Currently, design engineers at state agencies generally use

a constant value for all cases based on Tabler's (2003) methodology developed for Wyoming conditions. Snow fence designers agree that this value is not always the correct one. The problem is that simple engineering judgement cannot predict the impact of the multiple variables involved in the snow drift process. Therefore, snow fence designers cannot develop a more accurate estimate of the SRC for a given site location and conditions.

Moreover, the methodology used for designing a snow fence generally assumes a one-storm event occurring at the fence site. In principle, however, a snow fence should have a sufficiently high snow-retention capacity to function well over a whole winter season when successive snow storms occur at a site. Additionally, multiple thermal processes are acting on the snow trapped by fences during and between successive storms. Such cases are not accounted for in the current design methodology. Moreover, the variability of weather conditions from storm to storm is not a parameter considered in standard the snow fence design methodology used by state agencies. Further complicating the estimation of the SRC is its dependence on snow type and the characteristics of the ground surface at the time of the snow storm event (e.g., the presence of tall vegetation, which results in a lower value of the SRC than if bare, flat ground were present at the same site).

Overall, it can be concluded that the availability of direct measurements for the SRC via the approaches and methodologies proposed in this research should result in significant improvements in the accuracy of the estimated SRC values. Direct measurement should also result in more accurate predictions of the volume of snow retained by the snow fence and estimates of the risk that the fence will be overtopped during a given storm event. The proposed methods to estimate the snowfall and snow drift fluxes are not only useful for snow fence design, but can be equally useful for a range of meteorological applications.

The technologies and protocols developed for mapping the snow deposition at a snow fence are part of a series of non-intrusive measurement approaches that can not only efficiently support decisions in the design stage relative to the type of snow fence selected, the size of the fence, and the position of the fence, but can also be used to evaluate the design efficiency of the snow fence. Quantification of snow accumulation at the fence site is the ultimate qualifier of the efficiency of the snow fence design and its operational performance. Direct observations of the capacity of the snow fence to retain snow during a whole winter season provide critical feedback for continually improving design guidelines for snow fences. Conventional methods for the quantification of snow accumulation are tedious, expensive, and, given the harsh winter environment, risky at times.

The present research further refines the use of close-range photogrammetry developed through previous work (Basnet et al. 2016) by providing a general methodology for non-intrusive remote estimation of the volume of snow retained by the snow fence using automated data acquisition protocols. The implementation of photogrammetry protocols for snow deposition mapping required the development of new means to deal with the "visualization" of the snow volumetric features. This was needed because, in the absence of visible patterns contained in the image recordings, the reconstruction of the imaged area is difficult and of low accuracy because the

pattern recognition performed by the software requires the presence of distinct, contrasting features captured in the images acquired for mapping.

The proof-of concept experimental methodologies and protocols developed to estimate critical variables for snow fence design have not been fully demonstrated because of the absence of snow drift conditions at the monitored sites over the two winter seasons in which this reasearch was conducted. This limitation led to the use of artificial means for some of the experiments and stretched the capabilities of the proposed methods into areas where they are prone to errors. Despite these limitations, the preliminary results for estimating snowfall fluxes and mapping snow deposits are promising. The snow drift measurement results are better substantiated but were only demonstrated in laboratory conditions with modeled snow particles.

The results of this research can be used as a solid basis for a thorough step-by-step verification and validation of the proposed methodologies through a systematically planned program. The following tasks are suggested:

- Use the proposed methodologies and protocols for measurements of snowfall during extreme snow storm events in areas where the wind is not obstructed (i.e., open fields with low ground cover over which the wind velocity is high enough to initiate drifting and a fetch distance that is sufficiently large that the supply of driftable snow is practically unlimited). These measurements should be acquired at a minum of 1.5 m above the ground.

- Use the prescribed methodologies and protocols for measurements of snow drift during strong events in areas of unobstructed wind. The snow drift measurements should be confined to a layer extending up to 1 m above the ground. This is needed because saltation of snow particles from the layer of deposited snow is the main contributor to snow drift flux.

- Repeat the above measurements to confirm the robustness of the proposed techniques and consolidate the results in a set of data that can be compared with available reference results (i.e., Tabler 1994). The processing of the experimental data should substantiate the variability of the snow drift and snowfall measurements over the event duration at a site. Ideally such measurements should be conducted at several sites to capture the spatio-temporal variability of the snow transport processes.

- Perform the whole chain of measurements to generate the data required by snow fence design software. Evaluate the design performance and compare the evaluations obtained using data collected directly at the snow fence site by employing the proposed methodologies and protocols with the design solutions obtained from the current methodologies used by state agencies.

- Develop standardized protocols for the implementation of the proposed methodologies in current practice. Reevaluate the available design standards and provide specific corrections that account for site characteristics and meteorological conditions.

REFERENCES

Adams, C. E. and G. L. Weatherly. 1981. Some Effects of Suspended Sediment Stratification on an Oceanic Bottom Boundary Layer. *Journal of Geophysical Research*. Vol. 86, No. C5, pp. 4161–4172.

Admiraal, D. 2017. Section 3.7.3. Particle Tracking Velocimetry. In *Experimental Hydraulics Volume II: Instrumentation and Measurement Techniques*. J. Aberle, C. D. Rennie, D. M. Admiraal, and M. Muste (Eds). Taylor & Francis, New York, NY.

Adrian, R. J. 1991. Particle-Imaging Techniques for Experimental Fluid Mechanics. *Annual Review of Fluid Mechanics*. Vol. 23, No. 1, pp. 261–304.

Adrian, R. J. 2005. Twenty Years of Particle Image Velocimetry. *Experiments in Fluids*. Vol. 39, No. 2, pp. 159–169.

Andreescu, M. P. and D. B. Frost. 1998. Weather and Traffic Accidents in Montreal, Canada. *Climate Research*. Vol. 9, No. 3, pp. 293–303.

Andrey, J. and R. Olley. 1990. The Relationship between Weather and Road Safety: Past and Future Research Directions. *Climatological Bulletin*. Vol. 24, No. 3, pp. 123–137.

Baker, H. A. and C. J. Williams. 1990. *Guidelines for Controlling Snowdrifting on Canadian Highways*. Transport Canada, Montreal, Quebec.

Basnet, K., M. Muste, G. Constantinescu, H. Ho, and H. Xu. 2016. Close Range Photogrammetry for Dynamically Tracking Drifted Snow Deposition. *Cold Regions Science and Technology*. Vol. 121, pp. 141–153

Bintanja, R. 2001. Modification of the Wind Speed Profile Caused by Snowdrift: Results from Observations. *Quarterly Journal of the Royal Meteorological Society*. Vol. 127, No. 577, pp. 2417–2434.

Budd, W. F. 1966. The Drifting of Nonuniform Snow Particles. In *Studies in Antarctic Meteorology*. M. J. Rubin (Ed.) American Geophysical Union, Washington, DC.

Constantinescu, G. and M. Muste. 2015. *Optimization of Snow Drifting Mitigation and Control Methods for Iowa Conditions*. Department of Civil and Environmental Engineering, The University of Iowa, Iowa City, IA.

Cooper, M. A. R. and S. Robson. 1996. Theory of Close Range Photogrammetry. In *Close Range Photogrammetry and Machine Vision*. K. B. Atkinson (Ed.) Whittles Publishing, Scotland, UK.

Dyer, K. R. 1986. *Coastal and Estuarine Sediment Dynamics*. Wiley and Sons Ltd., Chichester, Sussex, UK.

Elgobashi, S. E. and T. W. Abou-Arab. 1983. A Two-Equation Turbulence Model for Two-Phase Flows. *The Physics of Fluids*. Vol. 26, No. 4, pp. 931–938.

Fincham, A. M. and G. R. Spedding. 1997. Low-Cost, High-Resolution DPIV for Measurement of Turbulent Fluid Flows. *Experiments in Fluids*. Vol. 23, No. 6, pp. 449–462.

Fujita, I. and S. Komura. 1994. Application of Video Image Analysis for Measurements of River-Surface Flows. *Proceedings of Hydraulic Engineering*. Vol. 38, pp. 733–738.

Fujita, I., M. Muste, and A. Kruger. 1998. Large-Scale Particle Image Velocimetry for Flow Analysis in Hydraulic Applications. *Journal of Hydraulic Research*. Vol. 36, No. 3, pp. 397–414.

Garrett, T. J., C. Fallgatter, K. Shkurko, and D. Howlett. 2012. Fall Speed Measurement and High-Resolution Multi-Angle Photography of Hydrometeors in Freefall. *Atmospheric Measurement Techniques*. Vol. 5, pp. 4827–4850.

Iowa DOT. 2005. *Iowa's Cooperative Snow Fence Program*. Iowa Department of
Transportation. Last accessed August 21, 2017.
www.iowadot.gov/maintenance/pdf/snowfencebooklet.pdf.

Kaneko, M., T. Watanabe, M. Matsuzawa, and Y. Ito. 2012. Revision of Highway Snowstorm
Countermeasure Manual: Focus on Snowbreak Woods. International Conference on
Winter Maintenance and Surface Transportation Weather. Coralville, IA., April 30–
May 3.

Kathlein, C. 2009. Physics of Snow Drift. Report presented for the graduate course *AT-301:
Infrastructure in a Changing Climate*. University Centre, Svalbard, Norway, Sept. 10.

Kersten, T. P. 2006. Combination and Comparison of Digital Photogrammetry and Terrestrial
Laser Scanning for the Generation of Virtual Models in Cultural Heritage Applications.
In *7th International Symposium on Virtual Reality, Archaeology and Cultural Heritage*.
M. Ioannides, D. Arnold, F. Niccolucci, K. Mania (Eds.), pp. 207–214, Nicosia, Cyprus,
Oct. 30–Nov. 4.

Kobayashi, S. 1978. Snow Transport by Katabatic Winds in Mizuho Camp Area, East
Antarctica. *Journal of the Meteorological Society of Japan*. Vol. 56, No. 3, pp. 130–139.

Kobayashi, P. 1979. Studies on Interaction between Wind and Dry Snow Surface. *Contributions
of the Institute of Low Temperature Science*. Series A., No. 29, Hokkaido University,
Sapporo, Japan.

Kunapo, J. 2005. Spatial Data Integration for Classification of 3D Point Clouds from Digital
Photogrammetry. *Applied GIS*. Vol. 1, No. 3, pp. 26.1–26.15.

Kraus, K. 1993 *Photogrammetry, Vol. I. Fundamentals and Standard Processes*. Fourth Revised
and Enlarged Edition. Dümmlers, Bonn, Germany.

Lee, S. J. 2001. *PIV/PTV Velocity Field Measurement Technique – Theory and Practice*. Pohang
University of Science and Technology, Pohang, South Korea.

Liang, S., M. Xiangxian, and H. Zhang. 2010. Numerical Simulation of Snow Drifting Disaster
on Embankment Project. *Journal of Computers*. Vol. 5, No. 1, pp. 139–143.

Lloyd, M. P., D. J. Ball, and P. K. Stansby. 1995. Unsteady Surface Velocity Field Measurement
Using Particle Tracking Velocimetry. *Journal of Hydraulic Research*. Vol. 33, No. 4, pp.
519–534.

Lourenco, L. M., S. P. Gogineni, and R. T. LaSalle. 1994. On-Line Particle-Image Velocimeter:
An Integrated Approach. *Applied Optics*. Vol. 33, No. 13, pp. 2465–2470.

Maiwald, F., T. Vietze, D. Schneider, F. Henze, S. Münster, and F. Niebling. 2017.
Photogrammetric Analysis of Historical Image Repositories for Virtual Reconstruction in
the Field of Digital Humanities. *ISPRS - International Archives of the Photogrammetry,
Remote Sensing and Spatial Information Sciences*. Vol. XLII-2, No. W3, pp. 447–452.

Matthews, N. A. 2008. *Aerial and Close-Range Photogrammetric Technology: Providing
Resource Documentation, Interpretation, and Preservation*. Technical Note 428. Bureau
of Land Management, National Operations Center, Denver, CO.

McClung, D. and P. Schaerer. 1993. *The Avalanche Handbook*. Mountaineers Books, Seattle,
WA.

Mellor, M. and G. Fellers. 1986. *Concentration and Flux of Wind-Blown Snow*. Special Report
86-11. U.S. Army Corps of Engineers, Cold Regions Research and Engineering
Laboratory, Hanover, NH.

Muramoto, K-I., K. Matsuura, and T. Shiina. 1995. Measuring the Density of Snow Particles and Snowfall Rate. *Electronics and Communications in Japan*, *Part III.* Vol. 78, No. 11, pp. 71–79.

Muste, M., Z. Xiong, K. Kruger, and I Fujita. 1999. Error Estimation in PIV Applied to Large-Scale Flows. *Proceedings of the 3rd International Workshop on Particle Image Velocimetry.* September 16–18, Santa Barbara, CA, pp. 619–624.

Muste, M., Z. Xiong, J. Schöne, and Z. Li. 2004. Validation and Extension of Image Velocimetry Capabilities for Flow Diagnostic in Hydraulic Modeling Using Image Velocimetry. *Journal of Hydraulic Engineering.* Vol. 130, No. 3, pp. 175–185.

Muste, M., I. Fujita, and A. Hauet. 2008. Large-Scale Particle Image Velocimetry for Measurements in Riverine Environments. *Water Resources Research.* Vol. 44, No. 4.

Muste, M., A. Hauet, I. Fujita, C. Legout, and H-C. Ho. 2014. Capabilities of Large-Scale Particle Image Velocimetry to Characterize Shallow Free-Surface Flows. *Advances in Water Resources.* Vol. 70, pp. 160–171.

Muste, M., S. Baranya, R. Tsubaki, D. Kim, H-C. Ho, H-W. Tsai, and D. Law. 2015. Acoustic Mapping Velocimetry Proof-of-Concept Experiment. *E-Proceedings of the 36th IAHR World Congress.* June 28–July 3, The Hague, the Netherlands.

Muste, M., S. Baranya, R. Tsubaki, D. Kim, H-C. Ho, H-W. Tsai, and D. Law. 2016. Acoustic Mapping Velocimetry. *Water Resources Research.* Vol. 52, No. 5, pp. 4132–4150.

Naaim, M., F. Naaim-Bouvet, and H. Martinez. 1998. Numerical Simulation of Drifting Snow: Erosion and Deposition Models. *Annals of Glaciology. Vol.* 26, pp. 191–196.

Nixon, W. A., M. Davison, and G. Kochumman. 2006. *Living Snow Fences.* Hydroscience and Engineering, College of Engineering, University of Iowa, Iowa City, IA.

NOAA. 2013. *Snow Measurement Guidelines for National Weather Service Surface Observing Programs.* NOAA National Weather Service, Office of Climate, Water and Weather Services, Silver Spring, MD.

Osborne, L.F. Jr., B. W. Hershey, and J. J. Mewes. 2012. Operational Blowing Snow Modeling: Benefits for the End User. *International Conference on Winter Maintenance and Surface Transportation Weather.* Coralville, IA., April 30 – May 3.

Peel, T., Ahmed, M., and N. Ohara. 2017. Investigating the Safety Effectiveness of Wyoming Snow Fence Implementations along a Rural Mountainous Freeway. *Transportation Research Record: Journal of the Transportation Research Board.* Vol. 2613, pp. 8–15.

Perchanok, M. and A. Bacchus. 1993. Cost Analysis of Snow Control Structures in Ontario. In *Proceedings of the 61st Annual Western Snow Conference.* Quebec City, Quebec, Canada. June 9–11.

Perchanok, M. 1998. *Design and Maintenance Procedures to Minimize Impacts from Drifting on Highways.* Research and Development Branch, Ministry of Transportation, Ontario, Canada.

Pomeroy, J. W. and D. M. Gray. 1990. Saltation of Snow. *Water Resources Research.* Vol. 26, No. 7, pp. 1583–1594.

Pomeroy, J. W. and D. M. Gray. 1995. *Snowcover: Accumulation, Relocation and Management.* National Hydrology Research Institute, Saskatoon, Saskatchewan, Canada.

Raffel M., C. E. Willert, and J. Kompenhans. 1998. *Particle Image Velocimetry, A Practical Guide.* Springer-Verlag Berlin Heidelberg, Berlin, Germany.

Raffel, M., C. E. Willert, S. Wereley, and J. Kompenhans. 2007. *Particle Image Velocimetry: A Practical Guide.* Second Edition. Springer-Verlag Berlin Heidelberg, Berlin, Germany.

Sañudo-Fontaned, L. A., D. Castro-Fresno, J. J. del Coz-Díaz, and J. Rodriguez-Hernandez. 2011. Classification and Comparison of Snow Fences for the Protection of Transport Infrastructures. *Journal of Cold Regions Engineering*. Vol. 25, No. 4, pp. 162–181.

Schaerer, P. A. 1972. Control of Snow Drifting About Buildings. *Canadian Building Digest.* February 1.

Schmidt, R. A. 1986. Transport Rate of Drifting Snow and the Mean Wind Speed Profile. *Boundary Layer Meteorology*. Vol. 34, No. 2, pp. 13–24.

Skarlatos, D. and S. Kiparissi. 2012. Comparison of Laser Scanning, Photogrammetry and SfM-MVS Pipeline Applied in Structures and Artificial Surfaces. In: *ISPRS Annals of the Photogrammetry, Remote Sensing and Spatial Information Sciences*. XXII ISPRS Congress. Melbourne, Australia, Aug. 25–Sept. 1.

Tabler, R. D. 1986. *Snow Fence Handbook (Release 1.0).* Tabler & Associates, Laramie, WY.

Tabler, R. D. 1991. *SHRP-W/FR-91-106: Snow Fence Guide*. Tabler & Associates.

Tabler, R. D. 1994. *SHRP-H-381: Design Guidelines for the Control of Blowing and Drifting Snow*. Tabler & Associates, Longmont, CO.

Tabler, R. D. 2003. *Controlling Blowing and Drifting Snow with Snow Fences and Road Design.* NCHRP Project 20-7(147). Tabler and Associates, Niwot, CO.

Tabler, R. D., N. H. Berg, D. Trabant, H. Santeford, and P. A. Rechard. 1990. Measurement and evaluation of winter precipitation. *Cold Regions Hydrology and Hydraulics, ASCE Technical Council on Cold Regions Engineering Monograph*. American Society of Civil Engineers, Reston, VA.

Takeuchi, M. 1980. Vertical Profiles and Horizontal Increase of Drift Snow Transport. *Journal of Glaciology.* Vol. 26, No. 94, pp. 481–492.

Tang, Z-Z., J. Liang, C. Guo, and Y-X. Wang. 2012. Photogrammetry-Based Two-Dimensional Digital Image Correlation with Non-Perpendicular Camera Alignment. *Optical Engineering.* Vol. 51, No. 2.

Vanoni, A. V. 2006. Editor. *Sedimentation Engineering*. American Society of Civil Engineers, Reston, VA.

Westerweel J., G. E. Elsinga, and R. J. Adrian. 2013. Particle Image Velocimetry for Complex and Turbulent Flows. *Annual Review of Fluid Mechanics.* Vol. 45, pp. 409–36

Westoby, M., J. Brasington, N. F. Glasser, M. J. Hambrey, and J. M. Reynolds. 2012. "Structure-From-Motion" Photogrammetry: A Low-Cost, Effective Tool for Geoscience Applications. *Geomorphology*. Vol. 179, pp. 300–314.

Wolf, P. R. and B. A. Dewitt. 2000. *Elements of Photogrammetry with GIS Applications.* Third Edition. The McGraw-Hill Companies, New York, NY.

APPENDIX A: OBSERVED SNOW STORM EVENTS DURING MEASUREMENT CAMPAIGN

Event 1: January 19, 2016 – 2 hours

S1_Start: 239 images, 149 snowflakes

S1_Middle: 240 images, 184 snowflakes

S1_end: 245 images, 115 snowflakes

Total snow velocity for the three PIV samples

Total snowfall velocity during Event 1

Event 1					
	V_x (m/s)	V_y (m/s)	Total Velocity (m/s)	Avg. Particle Snow Flake (pix)	Concentration (%)
E1_S1_Start	-0.242	1.053	1.080	25.73	0.144
E1_S1_Middle	-0.208	0.972	0.994	29.04	0.178
E1_S1_End	-0.158	0.874	0.888	22.28	0.131
E1_S1_Average	**-0.202**	**0.966**	**0.987**	**25.68**	**0.151**

25.68 pixels snowflake size = 3.12 mm in snowflake diameter

Event 1	Angle from North is 97°		
	V_{x1} (m/s)	V_{x2} (m/s)	Total Wind Velocity (m/s)
E1_Wind	-0.246	-1.976	1.991

Event 2: January 25, 2016 – 2.5 hours
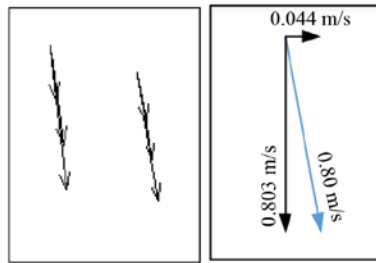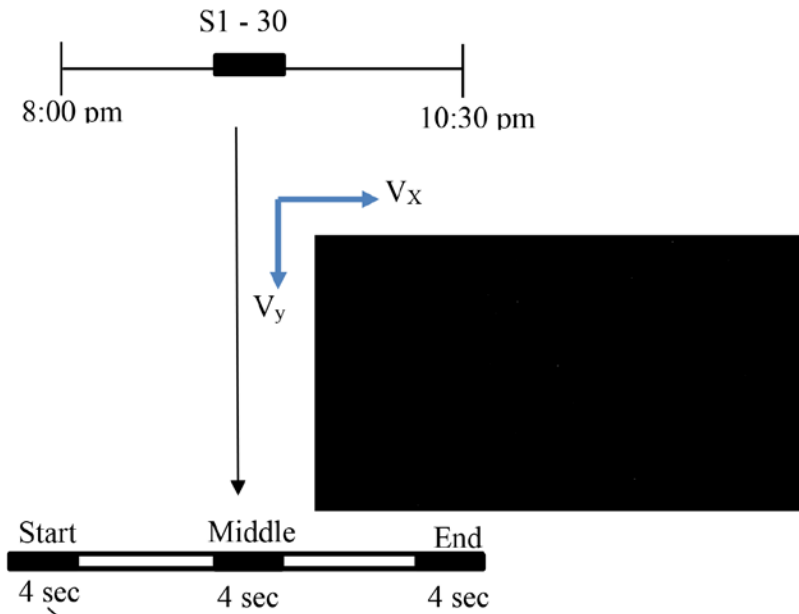
S1_Start: 239 images, 20 snowflakes

Event 2					
	V_x (m/s)	V_y (m/s)	Total Velocity (m/s)	Avg. Particle Snow Flake (pix)	Concentration (%)
E2_S1_Start	0.044	0.802	0.803	7.53	0.007

7.53 pixels snowflake size = 1.14 mm in snowflake diameter

Event 2	Angle from North is 272°		
	V_{x1} (m/s)	V_{x2} (m/s)	Total Wind Velocity (m/s)
E2_Wind	0.058	1.669	1.670

Event 3: February 2, 2016 – 1 hour

S1 - 30

8:30 am   9:30 am

V_X

V_y

Start   Middle   End

4 sec   4 sec   4 sec

0.31 m/s

2.64 m/s   2.66 m/s

S1_Start: 240 images, 360 snowflakes
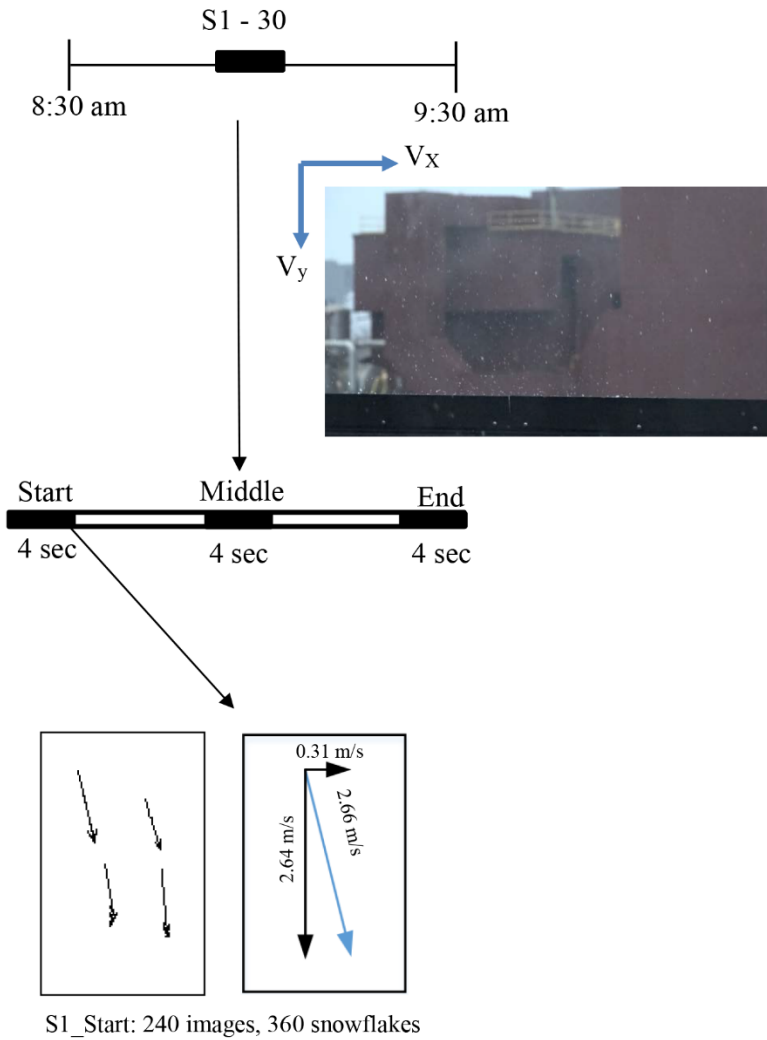
Event 3					
	V_x (m/s)	V_y (m/s)	Total Velocity (m/s)	Avg. Particle Snow Flake (pix)	Concentration (%)
E3_S1_Start	0.306	2.644	2.661	28.34	0.254

28.34 pixels snowflake size = 2.06 mm in snowflake diameter

Event 3	Angle from North is 84°		
	V_{x1} (m/s)	V_{x2} (m/s)	Total Wind Velocity (m/s)
E3_Wind	0.374	3.557	3.576

Event 4: February 7, 2016 – 0.5 hours

S1_Start: 290 images, 9 snowflakes

S1_Middle: 227 images, 13 snowflakes

S1_end: 239 images, 10 snowflakes
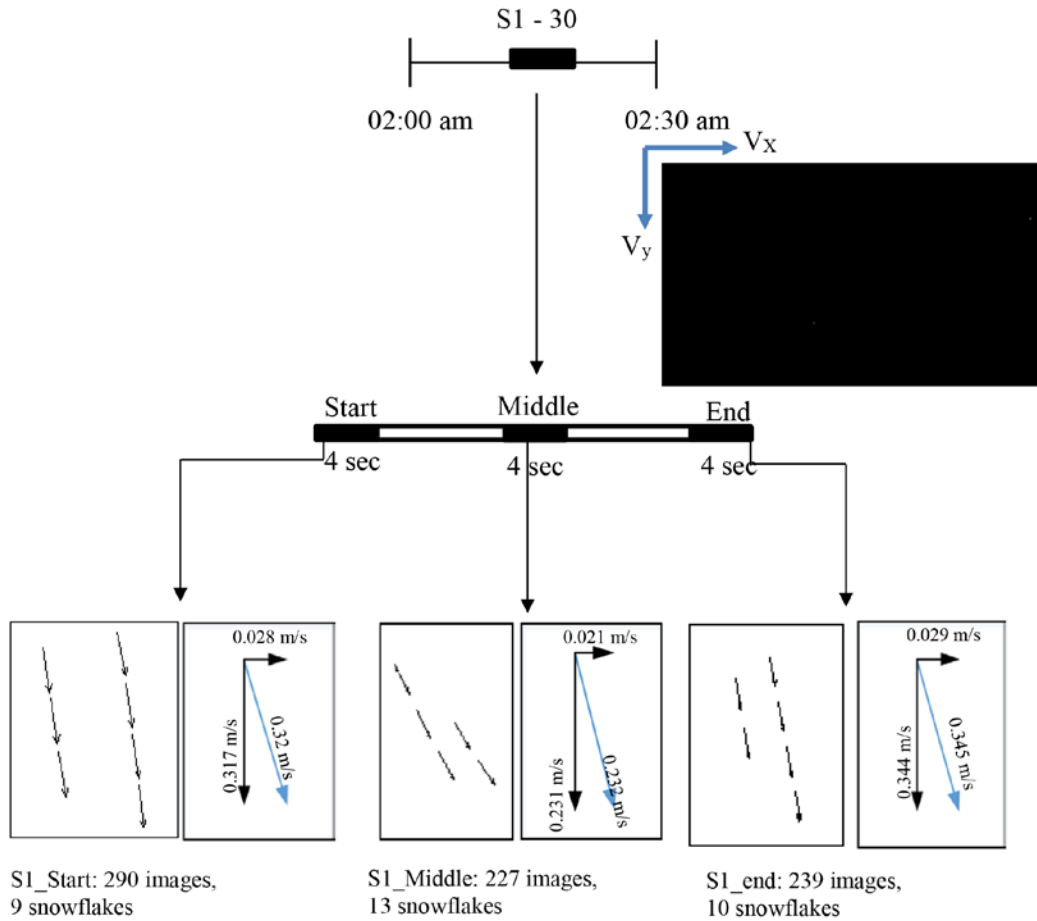
| Event 4					
	Vx (m/s)	Vy (m/s)	Total Velocity (m/s)	Avg. Particle Snow Flake (pix)	Concentration (%)
E4_S1_Start	0.028	0.317	0.319	3.68	0.001
E4_S1_Middle	0.021	0.231	0.232	3.66	0.001
E4_S1_End	0.029	0.344	0.345	2.90	0.001
E4_S1_Average	**0.026**	**0.297**	**0.299**	**3.41**	**0.001**

3.41 pixels snowflake size = 0.72 mm in snowflake diameter

Event 4	Angle from North is 274°		
	Vx1 (m/s)	Vx2 (m/s)	Total Wind Velocity (m/s)
E4_Wind	0.043	0.609	0.610

Event 5 – S1: February 8, 2016 – 8 hours

E5_S1_Start: 221 images, 155 snowflakes

E5_S1_Middle: 241 images, 159 snowflakes

E5_S1_End: 240 images, 133 snowflakes
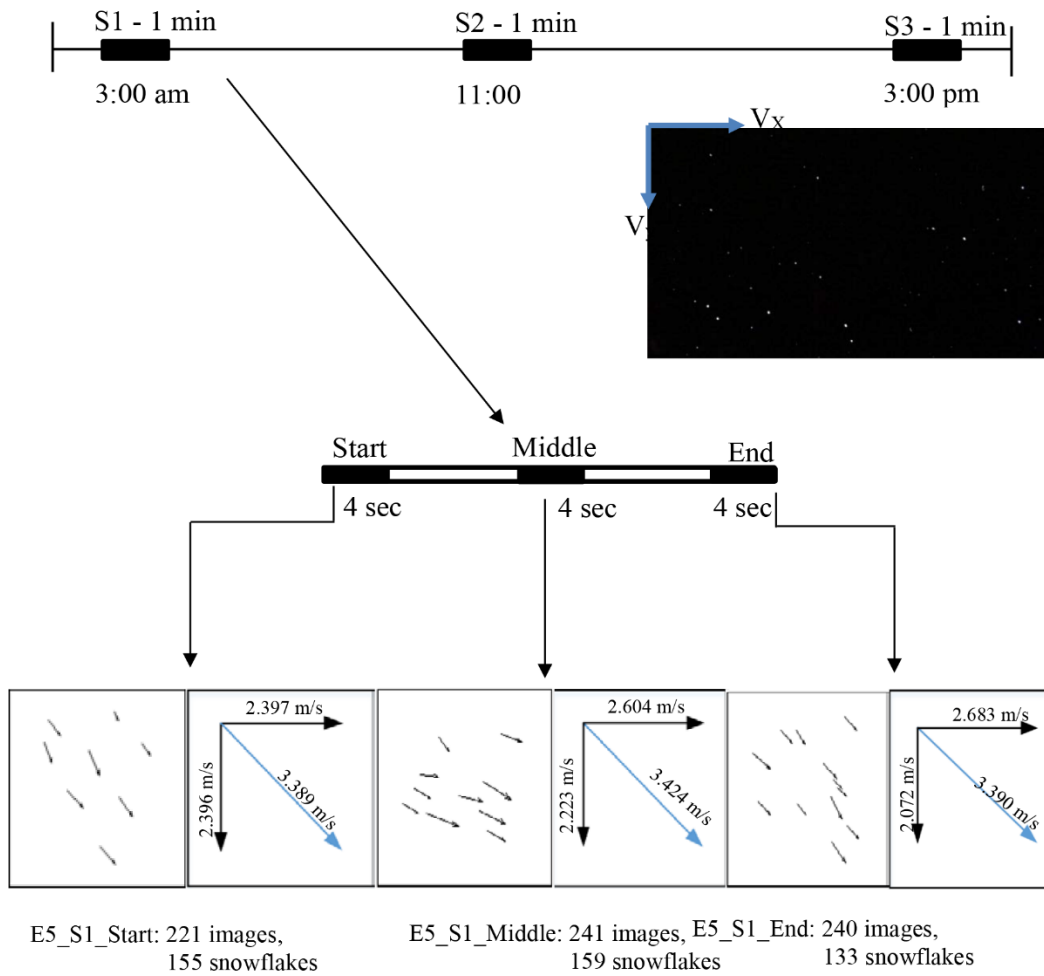
| Event 5					
	Vx (m/s)	Vy (m/s)	Total Velocity (m/s)	Avg. Particle Snow Flake (pix)	Concentration (%)
E5_S1_Start	2.397	2.396	3.389	30.76	0.35
E5_S1_Middle	2.604	2.223	3.424	26.01	0.222
E5_S1_End	2.683	2.072	3.390	24.96	0.190
E5_S1_Average	**2.561**	**2.230**	**3.401**	**27.24**	**0.254**

27.24 pixels snowflake size = 3.20 mm in snowflake diameter

Event 5	Angle from North is 318°		
	Vx1 (m/s)	Vx2 (m/s)	Total Wind Velocity (m/s)
E5_S1_Wind	2.824	2.543	3.8

114

Event 5 – S2: February 8, 2016 – 8 hours
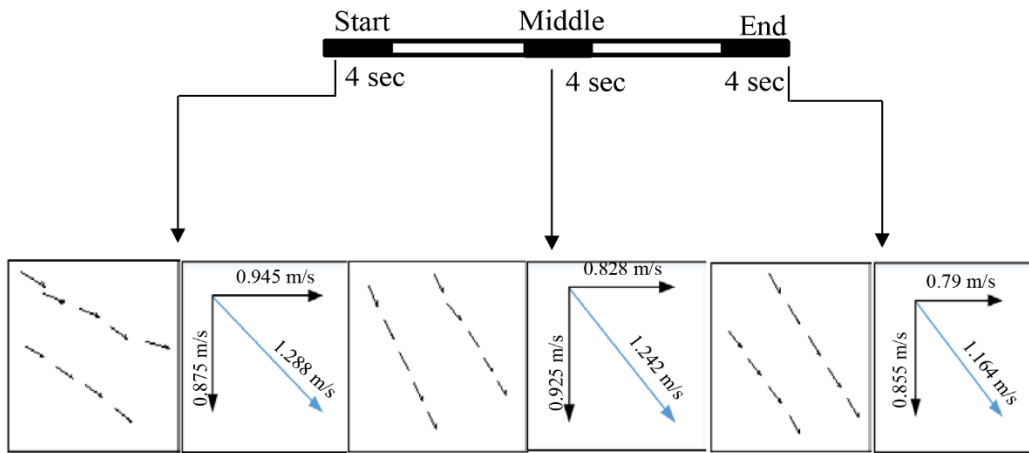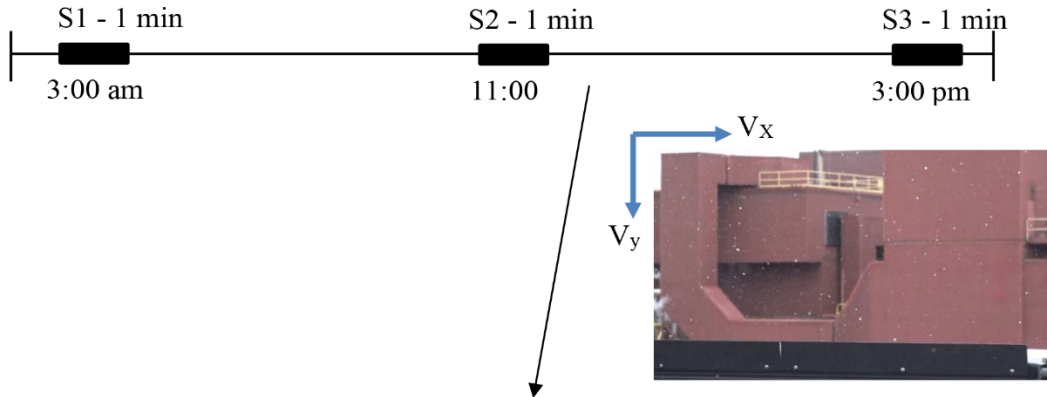
E5_S2_Start: 337 images, 145 snowflakes

E5_S2_Middle: 290 images, 79 snowflakes

E5_S2_End: 297 images, 66 snowflakes

Event 5					
	V_x (m/s)	V_y (m/s)	Total Velocity (m/s)	Avg. Particle Snow Flake (pix)	Concentration (%)
E5_S2_Start	0.945	0.875	1.288	24.05	0.13
E5_S2_Middle	0.828	0.925	1.242	20.83	0.075
E5_S2_End	0.790	0.855	1.164	18.65	0.067
E5_S2_Average	**0.854**	**0.885**	**1.231**	**21.18**	**0.091**

21.18 pixels snowflake size = 2.49 mm in snowflake diameter

Event 5	Angle from North is 346°		
	V_{x1} (m/s)	V_{x2} (m/s)	Total Wind Velocity (m/s)
E5_S2_Wind	0.970	2.419	2.6

Event 5 – S3: February 8, 2016 – 8 hours

E5_S3_Start: 244 images, 146 snowflakes

E5_S3_Middle: 234 images, 69 snowflakes

E5_S3_End: 205 images, 90 snowflakes
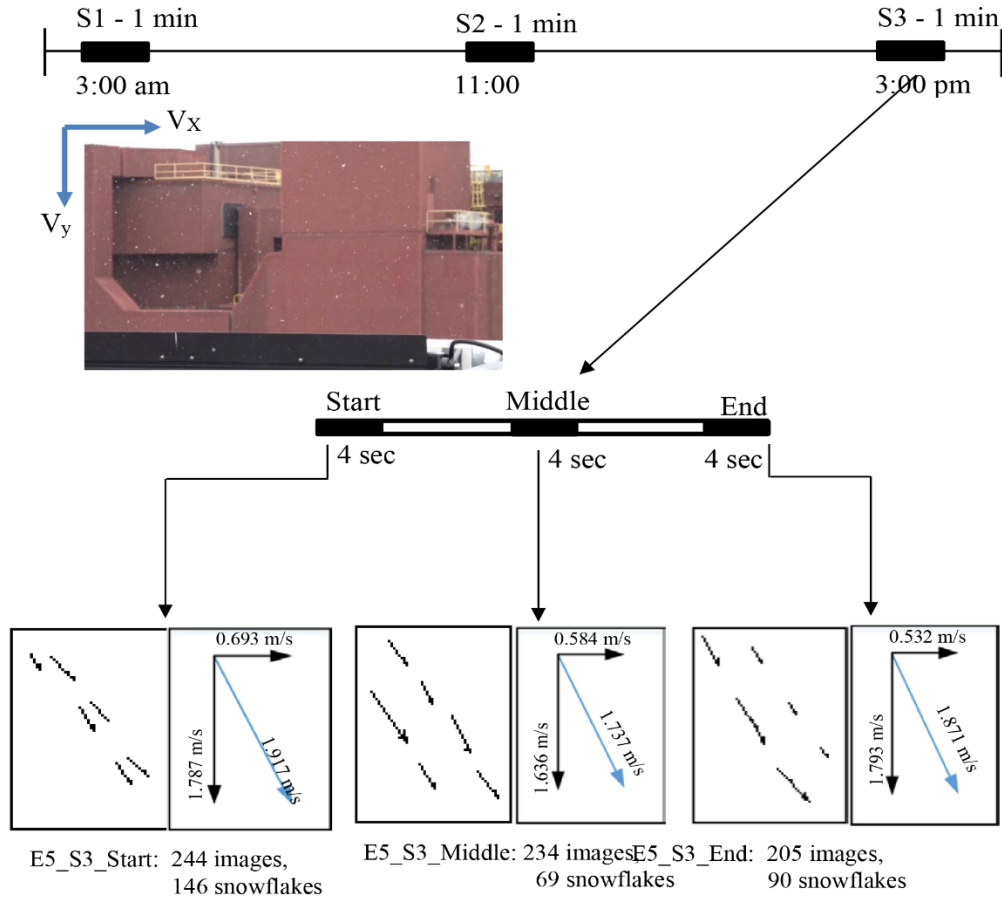
Event 5					
	V_x (m/s)	V_y (m/s)	Total Velocity (m/s)	Avg. Particle Snow Flake (pix)	Concentration (%)
E5_S3_Start	0.693	1.787	1.917	19.09	0.082
E5_S3_Middle	0.584	1.636	1.737	14.80	0.043
E5_S3_End	0.532	1.793	1.871	20.92	0.086
E5_S3_Average	**0.603**	**1.739**	**1.842**	**18.27**	**0.070**

18.27 pixels snowflake size = 2.61 mm in snowflake diameter

Event 5	Angle from North is 316°		
	V_{x1} (m/s)	V_{x2} (m/s)	Total Wind Velocity (m/s)
E5_S3_Wind	0.719	0.695	1.0

116

Event 6: February 14, 2016 – 4.5 hours
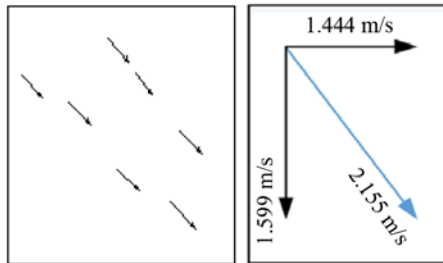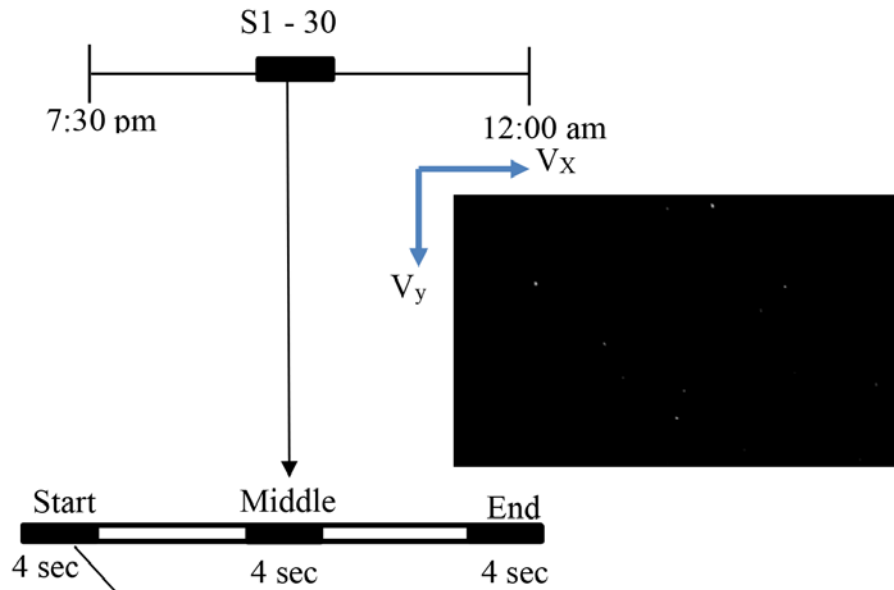
S1_Start: 302 images, 86 snowflakes

Event 6					
	Vx (m/s)	Vy (m/s)	Total Velocity (m/s)	Avg. Particle Snow Flake (pix)	Concentration (%)
E6_S1_Start	1.444	1.599	2.155	20.11	0.0107

20.11 pixels snowflake size = 2.84 mm in snowflake diameter

Event 6	Angle from North is 115°		
	Vx1 (m/s)	Vx2 (m/s)	Total Wind Velocity (m/s)
E6_Wind	1.530	3.281	3.620

APPENDIX B: MONITORING OF SNOW FENCE SITE DURING MAIN SNOW STORMS IN THE 2016–2017 WINTER SEASON

Snow Storm I: December 15–16, 2016 (no equipment as per the approval to use the site)

WEST FENCE – Looking upwind (on the left of the school driveway)

EAST FENCE – Looking upwind (on the right of the school driveway)

Snow Storm II: January 25–26, 2017

WEST FENCE – Looking upwind (on the left of the school driveway)

Looking downwind

EAST FENCE – Looking upwind (on the right of the school driveway)

Looking downwind

Snow Storm III: February 8, 2017 (from 2 am to 4 am)

WEST FENCE – Looking upwind (on the left of the school driveway)

Looking downwind

EAST FENCE – Looking upwind (on the right of the school driveway)

Looking downwind

Snow Storm IV: March 12–13, 2017

WEST FENCE – Looking upwind (on the left of the school driveway)

Looking downwind

EAST FENCE – Looking upwind (on the right of the school driveway)

Looking downwind